

Boundary-Driven XXZ Spin- $\frac{1}{2}$ Chain

Simon Essink

Masterarbeit in Physik
angefertigt im Helmholtz-Institut für Strahlen- und
Kernphysik

vorgelegt der
Mathematisch-Naturwissenschaftlichen Fakultät
der
Rheinischen Friedrich-Wilhelms-Universität
Bonn

April 2018

I hereby declare that this thesis was formulated by myself and that no sources or tools other than those cited were used.

Bonn,

Date

.....

Signature

1. Gutachterin: Prof. Dr. Corinna Kollath
2. Gutachter: Dr. Vladislav Popkov

Contents

1	Introduction	1
2	Boundary-Driven XXZ Spin-$\frac{1}{2}$ Chain	5
2.1	Open Quantum Systems	5
2.1.1	Density Matrix Formalism	5
2.1.2	Lindblad Master Equation	8
2.2	The XXZ Spin- $\frac{1}{2}$ Chain	9
2.3	The Boundary-Driven XXZ Chain in 1D	10
2.3.1	Quantum Zeno limit	12
2.3.2	Spin Helix States	13
2.3.3	Uniqueness of the Non-Equilibrium Steady State	14
2.3.4	Symmetries of the Model	15
3	Exact Diagonalization	17
3.1	Exact Diagonalization of the Lindblad Superoperator	17
3.1.1	Definition of a Basis for Spin Systems	18
3.1.2	Setting up the XXZ Hamiltonian	18
3.1.3	Reshaping the Lindblad Master Equation	19
3.1.4	Exemplary Eigenspectrum of a Liouvillian for our Model	21
3.1.5	Time Evolution and Steady State	23
3.2	Physical Observables	23
3.3	Limitations of Exact Diagonalization	25
4	Perturbation Theory	27
4.1	Stationary Perturbation Theory	27
4.1.1	Secular Condition	28
4.1.2	General Ansatz	31

4.1.3	Interpretation of the Stochastic Matrix F	35
4.1.4	Heuristic Guess for the Dynamics	39
4.2	Time-Dependent Perturbation Theory	40
4.2.1	Dyson Expansion of the Semigroup	41
5	Results	47
5.1	Exploring the Parameter Space	47
5.1.1	Case Study I: Fixed Boundaries, Changing Anisotropy	48
5.1.2	γ -Dependence	52
5.1.3	Analytical Results for Small Systems $N = 3, 4, 5$	54
5.1.4	Breakdown of Pure Description	58
5.2	Rank 2 Hypothesis	63
5.2.1	Numerical Evidence	65
5.2.2	Analytical Evidence	66
5.3	Time evolution: Relaxation Towards Spin Helix State	76
5.3.1	Identification of Time Scales	76
5.3.2	Validity of Stochastic Prediction for Finite Γ	80
6	Conclusion	83
	Bibliography	87
A	Code	93
B	Details on Perturbative Calculation	109
B.1	Definitions of Subhamiltonians	109
B.2	Calculation of the Commutator and the Secular Condition at First Order	110
B.3	Diagonal Elements of $\text{Tr}_{1,N}([H, \rho^{(1)}]) = 0$	112
C	Analytical Results for $N = 5$	115
C.1	Steady State Density Matrix for $N = 5$ and Unnormalized Eigenvectors of h_{00}	116
C.2	Auxiliary Matrices $N = 5$ and Parallel Boundaries	118
	List of Figures	119
	List of Tables	121

Introduction

In the past few decades, advances in the development of quantum optical tools enabled the physics community to investigate a broad range of phenomena in the context of light-matter interaction. With the increased control of atomic motion, it became possible to create and control quantum mechanical systems. A major breakthrough was the realization of Bose-Einstein Condensation in an atomic vapor [1–3]. In particular, ultracold atoms in optical lattices, which are artificial crystals of light, enabled experimentalists to simulate condensed matter systems in a highly controllable way. A variety of theoretical models such as the Bose-Hubbard model [4, 5] and the Fermi-Hubbard model [6] could be engineered experimentally and paradigmatic theoretical predictions could be investigated. A striking example is the observation of the superfluid to Mott-insulator transition for bosons trapped in an optical lattice [4, 5]. Several propositions [7–12] suggest that the physics of the paradigmatic XXZ model can be realized in either Bose-Bose or Fermi-Bose mixtures. In all such experimental setups it is, however, inevitable that the system interacts with its environment, which leads to dissipation.

The Lindblad master equation was introduced to describe such dissipative open quantum systems [13, 14] and has proven to be valid under the conditions present in atomic, molecular and optical systems [15]. In those settings, the coupling of the environment onto the system is small compared to the energy scales in either bath and system (Born approximation), the energy non-conserving terms in the interaction Hamiltonian can be neglected (Rotating Wave Approximation) and the action of the bath onto the system is fast compared to other time scales in the system and thus adiabaticity is given (Markov Approximation). Dissipative systems give rise to exotic non-equilibrium dynamics. Decoherence may lead to a loss of quantumness,

however, it could be shown that even under strong dissipation unitary dynamics can be preserved on certain time scales [16, 17]. The dissipation can be engineered such that a desired steady state is the attractor of the dynamics, e.g. enabling robust entangled state generation [18]. The vast amount of unexplored physics in dissipative open quantum systems makes it a vibrant research field in both experiment and theory.

From a theoretical point of view, it is interesting to look at models of reduced complexity, which are well-understood in the isolated case at equilibrium and build upon this knowledge to investigate the emerging physics in dissipative setups. In this manner the Lindblad master equation is taken as a phenomenological equation, whose properties reveal information about the system's behavior. Following this line of argumentation, much progress has been made to improve our understanding of one-dimensional XXZ chains of spin- $\frac{1}{2}$ subject to a boundary-drive. The XXZ model is a paradigmatic theoretical model to describe magnetic materials. Exact analytical methods [19–21] were used to yield exact solutions for the non-equilibrium steady state as a matrix product state.

A more general boundary drive, which allows to target arbitrary polarizations of the left and right spins was proposed by Popkov et al. [22–27]. For fine-tuned parameters of the dissipation and the system, intriguing non-equilibrium steady states with helical structure were found to appear. For certain configurations these states are predicted, but fail to converge [25]. The aim of this work is to uncover the conditions under which the predictions fail and understand the physics of the occurring non-equilibrium steady states.

The present thesis is structured as follows. In Chapter 2, we familiarize the reader with the language of open quantum systems and give details on the Lindblad master equation. We introduce the XXZ model as an isolated system and define the boundary-driven XXZ chain. We review known properties as the uniqueness of the steady state, symmetries and the emergence of the spin helix states.

In Chapter 3, we present the numerical method of exact diagonalization, which is used to solve the behavior of small systems, discuss the characteristics of the Liouvillian, the generator of the Lindblad dynamics, and introduce the used physical observables.

In Chapter 4, we study the stationary perturbation theory in the limit of strong coupling. We present the formalism that, to a large part, was developed in previous publications [24–27] and calculate perturbative corrections starting from a general ansatz for the steady state in the limit of infinite strong dissipation (Zeno limit). Subsequently, we make use of these findings to guess the dynamics and validate it via time-dependent perturbation theory.

In Chapter 5 we look at the results. In a first section, we investigate the parameter space and discover the underlying physics of the non-equilibrium steady state. After that, we identify the

particular points for which pure states are expected, but do not occur. We then focus on the situations for which a mixed state, composed of two helical states with opposite windings, seems to be generated as steady state. We hypothesize this formally using the findings of stationary perturbation theory and give evidence to support this hypothesis from different angles. In the last section we confirm the three predicted time-scales of the time-dependent perturbation theory using a case study via numerical time evolution.

In the end we will conclude, put the results in the broader context and discuss limitations as well as possible implications for future research.

Boundary-Driven XXZ Spin- $\frac{1}{2}$ Chain

In the first section of this chapter, the concept of open quantum systems and the density matrix formalism are introduced. Furthermore, a short introduction to the Lindblad formalism is given. The second section presents the XXZ model as an isolated model. The focus lies on the final section, in which the boundary-driven anisotropic Heisenberg chain is defined and some of its important properties are discussed. This model will be thoroughly investigated throughout this thesis.

2.1 Open Quantum Systems

Consider the following situation: A quantum mechanical system S living in the Hilbert space \mathcal{H}_S is in contact with a bath B living in \mathcal{H}_B . We shall call the combined system an *open quantum system* with Hilbert space $\mathcal{H} = \mathcal{H}_S \otimes \mathcal{H}_B$ where \otimes denotes a tensor product (cf. 2.1).

2.1.1 Density Matrix Formalism

A system's state is most generally described by its density matrix

$$\rho = \sum_{\alpha} \omega_{\alpha} P_{\alpha} \tag{2.1}$$

$$= \sum_{\alpha} \omega_{\alpha} |\psi_{\alpha}\rangle \langle \psi_{\alpha}|, \tag{2.2}$$

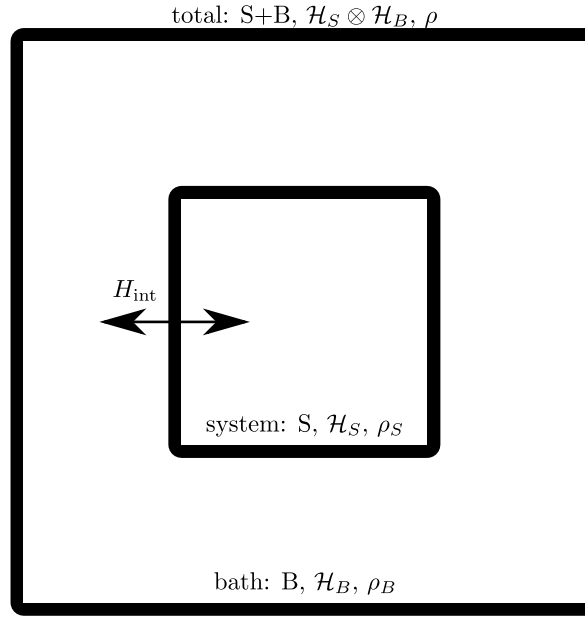


Figure 2.1: Sketch of an open quantum system. A system S with Hilbert space \mathcal{H}_S interacts with an environment B with Hilbert space \mathcal{H}_B via an interaction Hamiltonian H_{int} .

where ω_α are the weights of the *projectors* $P_\alpha = |\psi_\alpha\rangle\langle\psi_\alpha|$. The weights ω_α can be interpreted as probabilities of the state $|\psi_\alpha\rangle$ to be occupied. They are positive and satisfy the normalization condition $\sum_\alpha \omega_\alpha = 1$. The density matrix is a positive semi-definite, hermitian matrix with trace 1:

$$\rho \geq 0 \quad \rho^\dagger = \rho \quad \text{Tr}(\rho) = 1, \quad (2.3)$$

where $A^\dagger = (A^*)^T$ denotes the conjugate transpose. As a hermitian matrix, ρ can be diagonalized yielding a set of eigenvalues p_i , which due to semi-definiteness $\rho \geq 0$ are bigger or equal to zero, and corresponding orthogonal eigenstates $|\phi_i\rangle$. In its spectral decomposition, the density matrix can be written as

$$\rho = \sum_i p_i |\phi_i\rangle\langle\phi_i|, \quad (2.4)$$

with a normalization condition $\text{Tr}(\rho) = \sum_i p_i = 1$.

The density matrix is often referred to as *statistical operator*. The purity of a statistical

ensemble can be tested with the quantity

$$\text{Tr}(\rho^2) \leq 1. \quad (2.5)$$

The equal sign holds only for a *pure state*, or more precisely, a density matrix consisting only of one projector with weight 1

$$\rho = |\psi\rangle\langle\psi|. \quad (2.6)$$

For $\text{Tr}(\rho^2) < 1$ the state consists of a *statistical mixture*.

The calculation of the expectation value of an observable \hat{A} is given by the trace of the product between density matrix and operator

$$\langle\hat{A}\rangle = \text{Tr}(\hat{A}\rho). \quad (2.7)$$

It will be convenient to remember that the most general density matrix of a spin- $\frac{1}{2}$ system can be given in terms of the Pauli matrices as

$$\rho = A\sigma^x + B\sigma^y + C\sigma^z + D\mathbb{1}, \quad (2.8)$$

where

$$\begin{aligned} \sigma^x &= \begin{pmatrix} 0 & 1 \\ 1 & 0 \end{pmatrix} & \sigma^y &= \begin{pmatrix} 0 & -i \\ i & 0 \end{pmatrix} \\ \sigma^z &= \begin{pmatrix} 1 & 0 \\ 0 & -1 \end{pmatrix} & \mathbb{1} &= \begin{pmatrix} 1 & 0 \\ 0 & 1 \end{pmatrix}. \end{aligned} \quad (2.9)$$

The density matrix is particularly useful to describe composite systems [28] such as the system-bath setting mentioned previously: Consider the total density matrix of $\mathcal{H}_S \otimes \mathcal{H}_B$. Let us denote a basis of \mathcal{H}_S by $\{\psi_k\}$ and a basis of \mathcal{H}_B as $\{\phi_l\}$. Then, one can define the *reduced density matrix* of the system as

$$\langle\psi_k|\rho_S|\psi_{k'}\rangle = \sum_l \langle\psi_k;\phi_l|\rho|\psi_{k'};\phi_l\rangle \quad (2.10)$$

and similarly for the bath-reduced density matrix. By taking the partial trace over one subsystem, the reduced density matrix can be obtained from the full density matrix

$$\rho_S = \text{Tr}_B(\rho_{\text{total}}). \quad (2.11)$$

This can be of interest if the bath is intractable and only information of the system is of interest.

Having established the density matrix formalism, we can introduce a phenomenological equation for the time evolution of the density matrix of the system S in contact with a bath B .

2.1.2 Lindblad Master Equation

In 1976, Lindblad derived a Markovian master equation, the so-called *Lindblad master equation* (LME), [13, 14]

$$\begin{aligned} \frac{d\rho}{dt} &= -i[H, \rho] + \mathcal{D}[\rho] \\ &= \mathcal{L}[\rho]. \end{aligned} \quad (2.12)$$

where H denotes the Hamiltonian of the system S . \mathcal{D} and \mathcal{L} are functionals called *dissipator* and *Liouvillian* (sometimes named Lindbladian), respectively. The Liouvillian consists of two terms: The first term is known from quantum mechanics as the unitary part of the dynamics generated by the Hamiltonian (often called Liouville-von Neumann equation). The second term, called *dissipator*, describes the action of the bath onto the system.

The Lindbladian can be understood as a mapping of the density matrix at time $\rho(t)$ to a later time $\rho(t + dt)$ and, as such, must preserve the key properties of the density matrix: hermiticity, trace and positivity. This requirement sets restrictions onto the form of the dissipator. In its most general form, it is given by

$$\mathcal{D}[\rho] = \sum_j \Gamma_j \left(L_j \rho L_j^\dagger - \frac{1}{2} \{L_j^\dagger L_j, \rho\} \right), \quad (2.13)$$

where L_j are *Lindblad operators* (or jump operators), which represent the action of the bath onto the system that is parametrized by a *coupling strength* (or dissipation strength) Γ_j . It is important to mention that the Lindblad master equation is Markovian and thus time-local by construction.

As mentioned in the introduction, microscopic derivations of the Lindblad master equation make use of certain approximations on the system, the bath and its interactions. It has been demonstrated in [15] that these approximations hold in atomic, molecular and optical (AMO) settings. For more details regarding possible derivations, the reader is referred to [29]. In this thesis, we use this equation as a phenomenological equation and assume validity.

Stationary Lindblad Master Equation The full dynamical problem is often difficult to solve, while solutions of the stationary Lindblad master equation for the non-equilibrium steady states are attainable and give interesting insights into the underlying physics. The non-equilibrium steady state solves the stationary Lindblad master equation

$$\mathcal{L}\rho_\infty = 0 \quad (2.14)$$

where $\rho_\infty = \rho(t \rightarrow \infty)$. In principle, the solution does not have to be unique.

The next section reviews the isolated XXZ chain. This section should serve as a basis for the boundary-driven version that will be treated thereafter.

2.2 The XXZ Spin- $\frac{1}{2}$ Chain

The XXZ spin- $\frac{1}{2}$ chain or (anisotropic Heisenberg chain) is a model which describes spins in magnetic materials in one dimension. As a low-dimensional model, it has been studied extensively during the last century and allowed for many exact theoretical results [30]. The Hamiltonian of this one-dimensional model is given by

$$\begin{aligned} H &= J \sum_{j=1}^{N-1} \left((S_j^x S_{j+1}^x + S_j^y S_{j+1}^y) + \Delta S_j^z S_{j+1}^z \right) \\ &= J \sum_{j=1}^{N-1} \left(\frac{1}{2} (S_j^+ S_{j+1}^- + S_j^- S_{j+1}^+) + \Delta S_j^z S_{j+1}^z \right) \end{aligned} \quad (2.15)$$

where j is a spatial index denoting the site of the chain and $S_j^\alpha = \frac{\hbar}{2} \sigma_j^\alpha$ with $\alpha = x, y, z$ the spin operators, which only act non-trivially on the corresponding site j . In the second line, the transverse interaction was rewritten in terms of the raising and lowering operators $S_j^\pm = S_j^x \pm iS_j^y$. The *coupling constant* (or exchange constant) J is chosen to be positive and set to unity in this work. The *anisotropy* Δ governs the interaction behavior of the Z-components of the spins and makes this model a realistic candidate to describe magnetism in solid state materials [30].

The XXZ model in 1D exhibits three groundstate phases (cf. Figure 2.2). For $\Delta < -1$, the Z-components of the spins align either in positive or negative Z-direction; the chain is said to be in a ferromagnetic regime (FM). The excitation spectrum of this phase is gapped. The transverse interaction dominates the behavior for $-1 < \Delta < 1$. This regime is gapless and called the Luttinger liquid (or XY-phase). Furthermore, in the gapped antiferromagnetic phase

(or Néel phase, AFM) $\Delta > 1$, the interaction is such that Z-components of the spins misalign. These groundstate phases intuitive make sense, since, depending on whether $\Delta < -1$ or $\Delta > 1$, neighboring spins minimize their energy by being aligned (FM) or misaligned (AFM). For those cases in which $|\Delta| > J$, the spin flip term can be neglected.

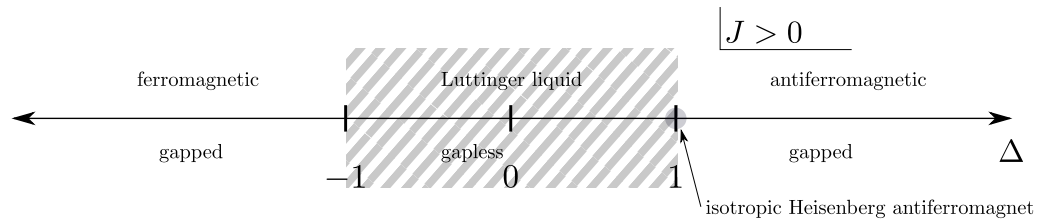


Figure 2.2: Sketch of the groundstate phase diagram of the XXZ chain in 1D for positive coupling constant J as a function of anisotropy Δ .

At this point, it is worth mentioning a few particular points on this axis: At $\Delta = 0$ the XXZ model reduces to the XX model, which can be mapped to non-interacting spinless fermions via a Jordan-Wigner transformation. The XXZ model becomes isotropic for $\Delta = 1$. For the limit $|\Delta| \rightarrow \infty$, the Z-component dominates and one recovers the (anti)ferromagnetic Ising model. The XXZ model for spin- $\frac{1}{2}$ is an integrable model and exactly solvable via Bethe Ansatz techniques (as reviewed in [31]).

In the preceding sections, the formalism to investigate open quantum systems was introduced and the closed system model was discussed. All is set to finally define the open quantum system that we will discuss throughout this thesis.

2.3 The Boundary-Driven XXZ Chain in 1D

The boundary-driven XXZ chain (or anisotropic Heisenberg chain) consists of a XXZ chain coupled to polarization baths at the boundaries as illustrated in Figure 2.3. The polarization baths polarize the boundary spins into certain directions parameterized by the azimuthal angle φ and the polar angle θ (see Figure 2.4).

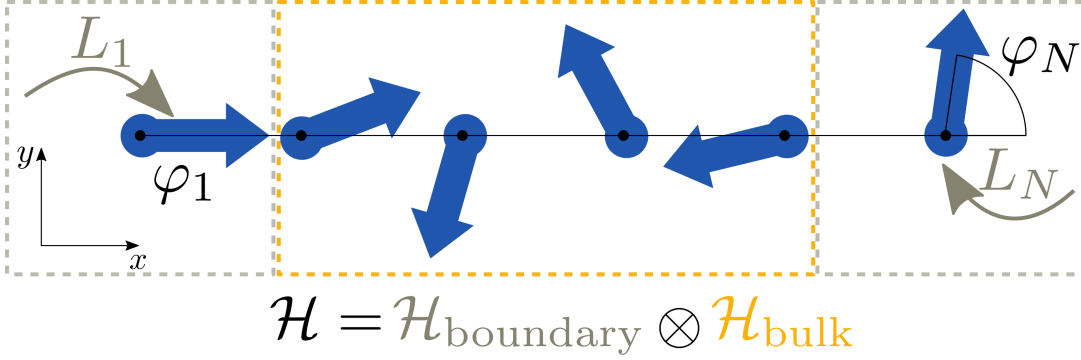


Figure 2.3: Sketch of a boundary-driven spin chain restricted onto the XY-plane for simplified visualization. The boundary polarization bath acts through the Lindblad operators L_1, L_N onto the first and last spins of the chain. The Hilbert space can be formally split into a boundary part (gray box) and a bulk part (yellow box).

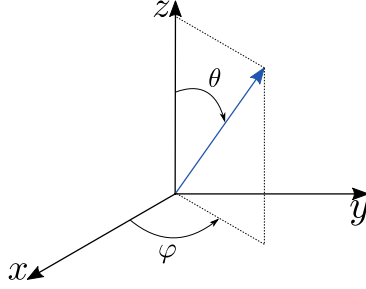


Figure 2.4: A coordinate system in 3D that illustrates the definition of azimuthal (φ) and polar (θ) angle.

The Lindblad master equation for this model is given by

$$\dot{\rho} = -i[H, \rho] + \Gamma \mathcal{D}[\rho] = \mathcal{L}[\rho], \quad (2.16)$$

$$\mathcal{D}[\rho] = \sum_{j=\{1, N\}} \left(L_j \rho L_j^\dagger - \frac{1}{2} \{L_j^\dagger L_j, \rho\} \right), \quad (2.17)$$

with specified Lindblad operators

$$L_1(\theta_L, \varphi_L) = \frac{1}{2} \left(-\sin \theta_L \sigma_1^z + (1 + \cos \theta_L) e^{-i\varphi_L} \sigma_1^+ - (1 - \cos \theta_L) e^{i\varphi_L} \sigma_1^- \right), \quad (2.18)$$

$$L_N(\theta_R, \varphi_R) = \frac{1}{2} \left(-\sin \theta_R \sigma_N^z + (1 + \cos \theta_R) e^{-i\varphi_R} \sigma_N^+ - (1 - \cos \theta_R) e^{i\varphi_R} \sigma_N^- \right), \quad (2.19)$$

where we made use of $\sigma_j^\pm = \frac{1}{2} (\sigma_j^x \pm i\sigma_j^y)$.

The coupling of the two baths has been chosen to be of equal strength. Thus, the dissipation strength Γ can be pulled out of the dissipator. To understand the action of these Lindblad

operators, consider the most general spin state and a state perpendicular to it

$$|\Sigma(\theta, \varphi)\rangle = e^{-i\varphi/2} \cos \frac{\theta}{2} |+\rangle + e^{i\varphi/2} \sin \frac{\theta}{2} |-\rangle, \quad (2.20)$$

$$|\Pi(\theta, \varphi)\rangle = e^{-i\varphi/2} \sin \frac{\theta}{2} |+\rangle - e^{i\varphi/2} \cos \frac{\theta}{2} |-\rangle, \quad (2.21)$$

where $|\pm\rangle$ denote spin up/down state. Acting on it with the Lindblad operators, one obtains

$$L_{1/N}(\theta, \varphi) |\Sigma(\theta, \varphi)\rangle = 0, \quad (2.22)$$

$$L_{1/N}(\theta, \varphi) |\Pi(\theta, \varphi)\rangle = -|\Sigma(\theta, \varphi)\rangle. \quad (2.23)$$

A spin state polarized in the direction of θ and φ is a dark state of the Lindblad operator, which targets this direction. That also means that once the boundary spins point into the targeted direction, the dissipator is zero and no dissipation acts on the system. Any arbitrary state can be decomposed into components along $|\Sigma(\theta, \varphi)\rangle$ and $|\Pi(\theta, \varphi)\rangle$ resulting in $|\Psi(\theta, \varphi)\rangle = a|\Sigma(\theta, \varphi)\rangle + b|\Pi(\theta, \varphi)\rangle$. As the Lindblad operator acts on the arbitrary state

$$L_{1/N}(\theta, \varphi) |\Psi(\theta, \varphi)\rangle = -b|\Sigma(\theta, \varphi)\rangle \quad (2.24)$$

it gets kicked into the dark, targeted state.

2.3.1 Quantum Zeno limit

In many cases, we will restrict the discussion to the so-called *Quantum Zeno limit*. In this limit, the dissipation strength Γ tends to infinity. The boundary spins are fixed into certain polarizations by the boundary baths. The behavior of the bulk part of the chain is governed by the anisotropy Δ as sketched in Figure 2.5.

Physically, this limit is equivalent to a continuous measurement of the quantum state of the boundary spins: Consider a single measurement of an observable. The quantum state will collapse onto an eigenstate of the eigenbasis of the observable. After the measurement, the state will continue to evolve and, therefore, transition into other states. If, however, a second measurement takes place at an infinitesimal small time step after the first, the state has no time to evolve. It can be shown that transitions to other states have a vanishingly small probability and the state will collapse into the same eigenstate as before. The state of the system is virtually frozen. The argument can be extended to continuous measurements [32]. Furthermore, the Zeno limit is not merely a theoretical concept, but an experimentally realizable situation [33]. For

the boundary-driven system in Zeno limit, it is tempting to think of it as a closed system with fixed boundary conditions. However, the crucial difference lies in the dynamics: While a closed system would evolve unitarily, in the Zeno limit, the unitary evolution decays over time due to dissipation.

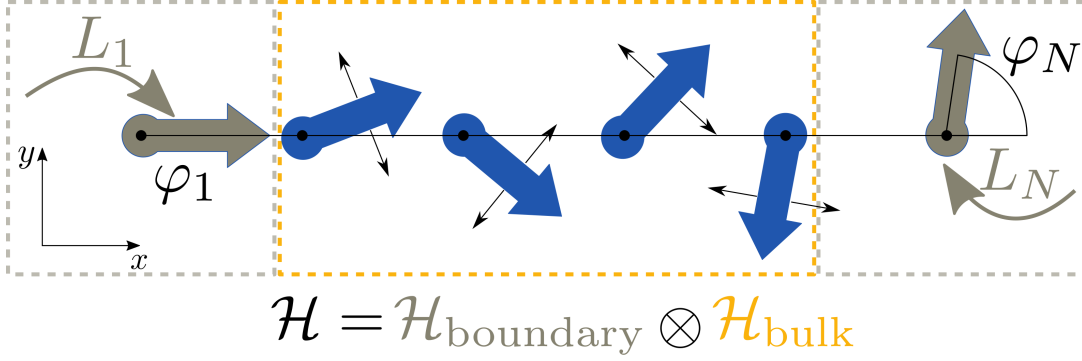


Figure 2.5: Sketch of a boundary-driven spin chain restricted onto the XY-plane in Zeno limit. The boundary spins (gray) have fixed polarizations, whereas the bulk spins can move according to the anisotropy Δ .

2.3.2 Spin Helix States

As has been shown in previous works [24–27] on the boundary-driven XXZ chain that the interplay of a fine-tuned Hamiltonian and dissipation leads to the formation of a non-equilibrium steady state with a helical structure (see Figures 2.6 and 2.7). Spin helix states occur precisely, if

$$\theta_L = \theta_R = \theta \quad (2.25)$$

$$\Phi = \varphi_R - \varphi_L \neq 0 \quad (2.26)$$

$$\gamma = \frac{\Phi + 2\pi m}{N - 1} \quad (2.27)$$

$$\Delta = \cos \gamma \quad (2.28)$$

$$\Gamma = \infty \quad (2.29)$$

where the difference of azimuthal angles of left and right boundary spin is called *boundary gradient* Φ . This boundary gradient can be reached if starting from the left boundary, the remaining $(N - 1)$ spins are turned incrementally by an angle γ (see Figure 2.6). In doing so, the spin chain makes $m = 0, 1, \dots, N - 2$ *windings* (or revolutions) around the Z-axis.

If all of the above conditions are fulfilled, the non-equilibrium steady state can be expressed in a simple factorized form

$$|\Psi_{\text{helix}}\rangle = \bigotimes_{k=1}^N \left(\cos \frac{\theta}{2} e^{-iy(k-1)/2} \right) \left(\sin \frac{\theta}{2} e^{iy(k-1)/2} \right) \quad (2.30)$$

$$\lim_{\Gamma \rightarrow \infty} \rho_{\text{helix}}(\Gamma) = |\Psi_{\text{helix}}\rangle \langle \Psi_{\text{helix}}| \quad (2.31)$$

This state describes the precession of a spin around the Z-axis, with a constantly increasing azimuthal angle.

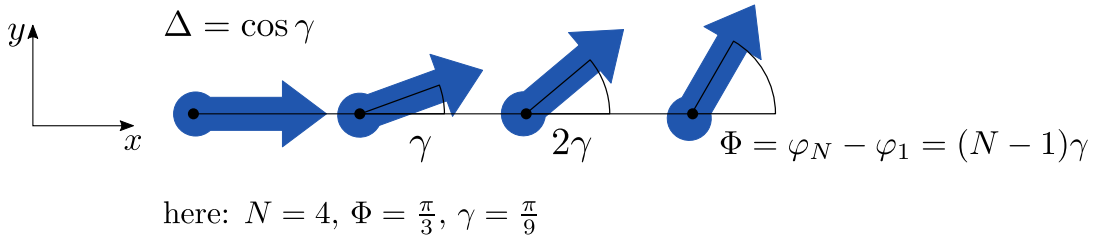


Figure 2.6: Sketch of a spin helix state in the XY-plane. The first spin is aligned with X-axis, while the boundary gradient is $\Phi = \frac{\pi}{3}$. The anisotropy Δ is chosen such that the intermediate spins turn by an angle $\gamma = \frac{\pi}{9}$.

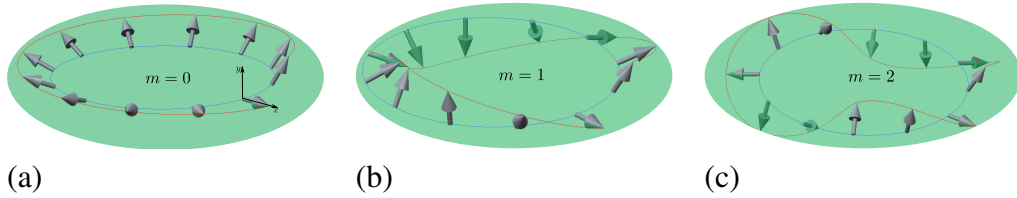


Figure 2.7: Illustration of spin helix states for $N = 11$ spins with a boundary gradient $\Phi = \frac{\pi}{3}$ and winding (a) $m = 0$, (b) $m = 1$ and (c) $m = 2$.

2.3.3 Uniqueness of the Non-Equilibrium Steady State

For our particular choice of Lindblad operators, it can be shown that the Lindblad master equation has a unique non-equilibrium steady state. The argumentation follows a theorem by Evans [21, 34], stating that the steady state is unique, if and only if the set of operators $\mathcal{M} = \{H, L_1, L_N\}$ generate, under multiplication and addition, the entire algebra in \mathcal{H} , which in our case consists of the Pauli algebra. In [21], the proof is sketched for Lindblad operators which correspond to $\theta_L = \theta_R = 0, \pi$ and $\varphi_L = \varphi_R = 0$.

The uniqueness of ρ_∞ underlines the fact that it is independent of the initial condition and makes the non-equilibrium steady state an attractor of the dynamics. The formation of the steady state in the long time limit is somehow robust.

2.3.4 Symmetries of the Model

We can make use of this uniqueness to find symmetries of the non-equilibrium steady state: Every global transformation that leaves the stationary Lindblad master equation invariant, results in a respective symmetry of ρ_∞ .

For instance, for N even, the unitary transformation $U_{\text{even}} = (I \otimes \sigma^z)^{\otimes \frac{N}{2}}$ leaves the Lindblad master equation invariant, i.e. $\mathcal{L}[\rho_\infty] = 0$ becomes $\mathcal{L}[\tilde{\rho}_\infty] = 0$. It follows that $\rho_\infty = \tilde{\rho}_\infty$ since the non-equilibrium steady state is unique. Introducing the explicit dependence on the parameters we can write

$$\rho_\infty \equiv \rho_\infty(\gamma, \theta, \Delta) \quad (2.32)$$

$$\rho_\infty(\gamma, \theta, \Delta) = U_{\text{even}} \rho_\infty^*(\pi - \gamma, \theta, -\Delta) U_{\text{even}} \quad \text{for even N} \quad (2.33)$$

where ρ_∞^* denotes the complex conjugate of the density matrix. This transformation allows to map the steady state for positive Δ to the steady state of negative Δ . In the same manner, the transformation $U_{\text{odd}} = (I \otimes \sigma^z)^{\otimes \frac{N}{2}} \otimes I$ leads to

$$\rho_\infty(\gamma, \theta, \Delta) = U_{\text{odd}} \rho_\infty^*(\gamma, \theta, -\Delta) U_{\text{odd}} \quad \text{for odd N.} \quad (2.34)$$

There is a symmetry, which can be thought of as a reversing transformation of the spin chain given by

$$\rho(\gamma, \theta, \Delta) = \Sigma_x V R(\rho(\gamma, \pi - \theta, \Delta)) R V \Sigma_x \quad (2.35)$$

with $\Sigma_x = (\sigma^x)^{\otimes N}$, $V = (e^{i\frac{\phi_R}{2}\sigma^z})^{\otimes N}$ and $R(A \otimes B \dots W \otimes Z)R = Z \otimes W \dots B \otimes A$. For two sites, R reduces to the permutation operator P_{12} has the explicit form

$$P_{12} = \begin{pmatrix} 1 & 0 & 0 & 0 \\ 0 & 0 & 1 & 0 \\ 0 & 1 & 0 & 0 \\ 0 & 0 & 0 & 1 \end{pmatrix}. \quad (2.36)$$

For more sites, R can be obtained using $(P_{12})^2 = 1$ and $P_{12}P_{13} = P_{23}P_{12}$, where P_{12} is pulled to the right. Let us discuss a minimal example for this: Take a chain of two spins, whose first spin is polarized with a polar angle θ_1 and whose second spin is polarized with a polar angle θ_2 . The transformation maps this onto a chain, whose first spin is polarized with a polar angle $\pi - \theta_2$ and whose second spin is polarized with a polar angle $\pi - \theta_1$. This can be understood as a mirroring in the middle of the chain and a mirroring with respect to XY-plane. Note, that for $\theta = \frac{\pi}{2}$ Equation (2.35) is a mapping onto itself.

To summarize, this chapter presented basic knowledge on density matrices, open quantum systems, its treatment within Lindblad master equation formalism, the isolated and boundary-driven XXZ model. In the next chapter, we will introduce the numerical techniques to investigate the physics of the boundary-driven XXZ model.

Exact Diagonalization

In the previous chapters, we have established the research question (Chapter 1) and understood the basic properties of the model (Chapter 2). This chapter deals with the methods that we use to analyze the model. The first section on exact diagonalization explains how the XXZ model and its corresponding Lindblad equation are implemented and solved for steady states, as well as for the time evolution. The second section discusses perturbation approaches for the stationary and the dynamical problem.

3.1 Exact Diagonalization of the Lindblad Superoperator

At the beginning of this section, the main concept of the exact diagonalization will be introduced, followed by a sketch of the implementation with references to the code in Appendix A. After that, we discuss how to obtain the steady state and the dynamic solution of the Lindblad master equation.

Originally, exact diagonalization is a numerical method to solve the Schrödinger equation of a quantum system. It is a practical technique to explore the relevant physics of small systems and is often used to benchmark more elaborate algorithms. The exceptional advantage of the method is, that no approximations are needed. For small systems, one can get the full information of the energy spectrum and the full set of eigenstates. Due to the exponentially increasing dimension of the Hilbert space of the problem, the method reaches its limits quite fast. Often one is restricted to solving just for the groundstate or the lowest lying eigenstates.

The exact diagonalization can also be applied to solve the Lindblad master equation. In

general, this is a dynamical problem, that is governed by the time evolution operator. For our case, this operator can be formally written as $e^{\mathcal{L}t}$. We seek to represent the Liouvillian \mathcal{L} , which governs the time evolution operator, in an appropriate basis, such that we can diagonalize it and determine its complete eigensystem.

In practice, one has to carry out the following steps: First, one defines a basis, in which one can represent the Liouvillian as a matrix. Then, its eigenvalues and eigenvectors are determined using appropriate algorithms. That is enough to solve the Lindblad equation.

In this chapter, we detail the steps in solving the Lindblad superoperator via exact diagonalization and by doing so, briefly explain the Python code that was used (see Appendix A). We first set up the Hamiltonian of the system, which is given by Equation (2.16) and choose a basis for its representation.

3.1.1 Definition of a Basis for Spin Systems

The following derivation follows the notation of [35]. For a spin- $\frac{1}{2}$ system each spin can occupy $M_S = 2$ different spin states: either spin at site j is down ($s_j = 0$) or spin is up ($s_j = 1$) in the S^z -eigenbasis. We can formulate a basis by assigning a value to each possible spin configuration

$$|K\rangle = |s_1, s_2, \dots, s_N\rangle \quad (3.1)$$

with

$$K = \sum_{j=1}^N s_j M_s^{j-1} \quad (3.2)$$

where N denotes the number of sites in the chain. This corresponds to converting a state given by a binary list $[s_N, s_{N-1}, \dots, s_1]$, containing the values $s_j = \{0, 1\}$ for spin at site j down or up respectively, to an integer number K .

3.1.2 Setting up the XXZ Hamiltonian

Having defined the basis, there are various ways to create the Hamiltonian. In this thesis, we first set up the operators and subsequently construct the Hamiltonian out of the operators. In order to find the operators in a given basis, one can exploit the information on the coupling of different basis states through the operators. From now on we will set the reduced Planck's constant $\hbar = 1$.

Let us focus on the example of the S^+ operator. We know the action of this operator onto

spin up and down

$$S^+ |\uparrow\rangle = 0 \quad S^+ |\downarrow\rangle = |\uparrow\rangle; \quad (3.3)$$

thus, to obtain the spin up operator S_i^+ for site i , one can loop over all basis states and determine, whether the action of the operator connects the state to another basis state. By doing so, the operator is obtained element by element. The same procedure can be applied to the other spin operators having in mind their actions

$$S^- |\uparrow\rangle = |\downarrow\rangle \quad S^- |\downarrow\rangle = 0 \quad (3.4)$$

$$S^z |\uparrow\rangle = +\frac{1}{2} |\uparrow\rangle \quad S^z |\downarrow\rangle = -\frac{1}{2} |\downarrow\rangle \quad (3.5)$$

where S^z , obviously, is diagonal and the remaining two

$$S^x = \frac{1}{2} (S^+ + S^-) \quad S^y = \frac{-i}{2} (S^+ - S^-) \quad (3.6)$$

can be obtained via combinations of S^+ and S^- .

In the Python code (Appendix A), the above two steps are combined in a class object called `HeisenbergBasis`, which requires the spin chain length N as an argument. Within this class, functions are defined to generate the operators (e.g. `sigma_x`) and the Hamiltonian matrix (e.g. via Pauli operators `hamiltonian_pauliop`) using the basis proposed above.

Since we want to treat the boundary-driven system and, hence, want to solve the Lindblad master equation, another trick has to be applied. The Lindblad master equation is a matrix equation and can be represented in a more tractable way by transforming it into so-called *superspace* by reshaping (or vectorization). This has the side-effect of reducing computational cost.

3.1.3 Reshaping the Lindblad Master Equation

There are two different ways to reshape a matrix (compare [36, 37]). In the code given in the Appendix A, we chose to reshape the density matrix in the Fortran way using the Python function `np.reshape(A, (N,M), order='F')` where A is the input matrix and (N,M) is the

desired shape. The following minimal example illustrates the reshaping:

$$\rho = \begin{pmatrix} \rho_{11} & \rho_{12} \\ \rho_{21} & \rho_{22} \end{pmatrix} \rightarrow |\rho\rangle = \begin{pmatrix} \rho_{11} \\ \rho_{21} \\ \rho_{12} \\ \rho_{22} \end{pmatrix}. \quad (3.7)$$

The above corresponds to reordering the matrix, such that one column is appended below the next column

$$|\alpha\rangle\langle\beta| \rightarrow |\beta\rangle \otimes |\alpha\rangle. \quad (3.8)$$

It was realized at a later stage of the work, that the standard way of reshaping is different, namely row below row

$$|\alpha\rangle\langle\beta| \rightarrow |\alpha\rangle \otimes |\beta\rangle. \quad (3.9)$$

The Lindblad equation, using the reshaping in (3.8), can be brought into the form

$$\frac{d}{dt} |\rho\rangle = \mathcal{L} |\rho\rangle, \quad (3.10)$$

where the individual terms of the Lindblad master equation transform as follows (cf. [37])

$$-i[H, \rho] \rightarrow -i(\mathbb{1} \otimes H - H^T \otimes \mathbb{1}) \cdot |\rho\rangle \quad (3.11)$$

$$L_j \rho L_j^\dagger \rightarrow \left((L_j^\dagger)^T \otimes L_j \right) \cdot |\rho\rangle \quad (3.12)$$

$$L_j^\dagger L_j \rho \rightarrow \left(\mathbb{1} \otimes L_j^\dagger L_j \right) \cdot |\rho\rangle \quad (3.13)$$

$$\rho L_j^\dagger L_j \rightarrow \left((L_j^\dagger L_j)^T \otimes \mathbb{1} \right) \cdot |\rho\rangle. \quad (3.14)$$

These operations are implemented in the functions `unitary_lindblad`, which creates the unitary part, and `dissipative_lindblad`, which sets up the dissipator. `dissipative_lindblad` takes as input a nested list containing all the parameters for the left and right Lindblad operators. The Hilbert space and, thus, the Hamiltonian for a 1D spin chain has dimension $\dim(H_{\text{spin}}) \sim 2^N$, whereas the Liouvillian in superspace has dimension $\dim(\mathcal{L}_{\text{spin}}) \sim (2^N)^2$.

At this point, we have set up the Hamilton matrix in a well-defined basis and constructed the Liouvillian as a matrix in superspace. This matrix can now be diagonalized using standard

algorithms to obtain its eigenvalues and eigenstates.

3.1.4 Exemplary Eigenspectrum of a Liouvillian for our Model

Especially for the dynamics of the system it is important to take into account the structure of the spectrum. For the diagonalization, we used the Python function `np.linalg.eig`, which returns two arrays with the eigenvalues and the eigenvectors. In Figure 3.1 an exemplary spectrum is shown, which is representative and reflects the generic case.

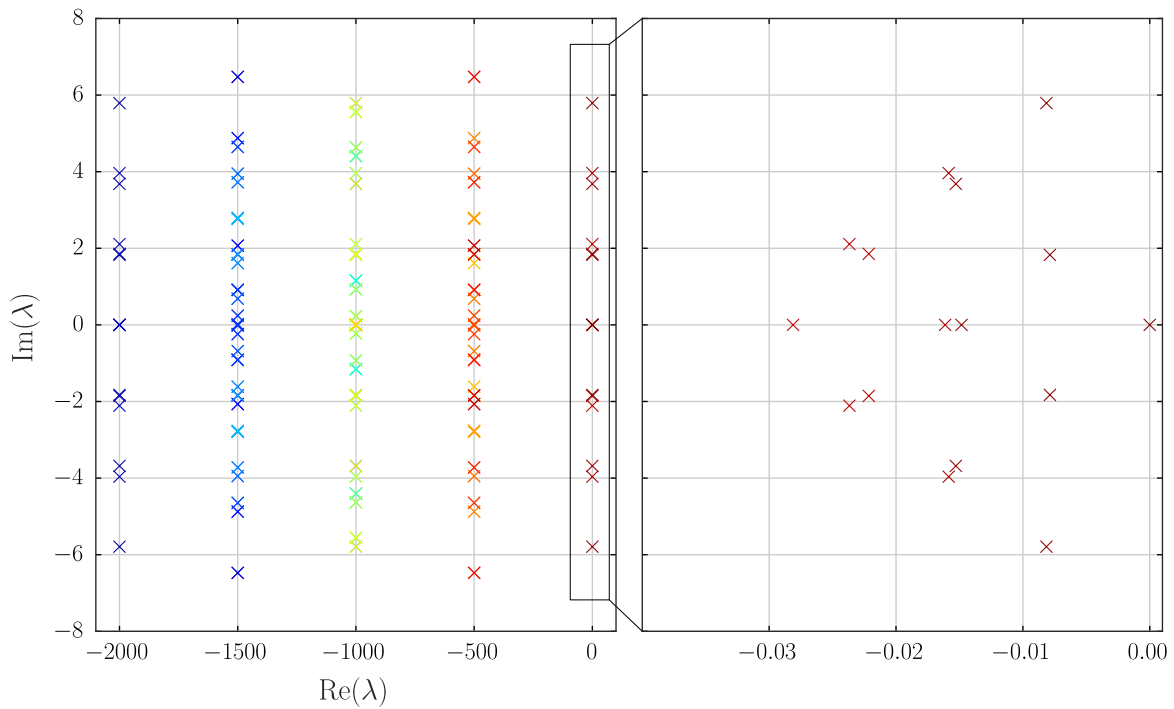


Figure 3.1: Exemplary spectrum of the Liouvillian. This spectrum was created using $N = 4$, $\Gamma = 1000$ and randomly sampled values for the other parameters $\theta_L = 0.546$, $\theta_R = 0.963$, $\varphi_L = 0.608$, $\varphi_R = 0.876$, $\Delta = 0.905$. On the left-hand side, the full spectrum is shown, whereas on the right-hand side, we zoomed into the band at $\text{Re}(\lambda_i) \leq 0$. The real part of the eigenvalues of the Lindbladian is smaller or equal to zero ($\text{Re}(\lambda_i) \leq 0$).

The diagonalization of the Liouvillian reveals a generic pattern. The real part of the eigenvalues of the Lindbladian is always smaller or equal to zero ($\text{Re}(\lambda_i) \leq 0$), where the $\lambda_0 = 0$ is unique (2.3.3). The condition $\text{Re}(\lambda_i) \leq 0$ reflects the trace-preserving property of the Liouvillian, which eliminates unphysical states. If the eigenvalues were larger than zero, the time evolution operator would diverge. For a large dissipation strength $\Gamma \gg 1$, the limit considered throughout this thesis, the eigenvalues λ are organized in equidistant bands. The distance can be understood

in terms of the eigenvalues of the dissipator \mathcal{D}

$$\mathcal{D}[\bullet] = \sum_{j=\{1,N\}} L_j \bullet L_j^\dagger - \frac{1}{2} L_j^\dagger L_j \bullet - \frac{1}{2} \bullet L_j^\dagger L_j. \quad (3.15)$$

where \bullet serves as a placeholder. In our model, the Lindblad operators L_j are acting locally on the first and the last spin. Thus, we can split the dissipator in the corresponding two superoperators $\mathcal{D}[\bullet] = \mathcal{D}_1[\bullet] + \mathcal{D}_N[\bullet]$. For each of them, we can introduce a complete orthonormal basis, $\{\phi_L^\alpha\}$ with $\alpha = 1, \dots, 4$ for the first and $\{\phi_R^\beta\}$ with $\beta = 1, \dots, 4$ for the last spin, which solves the associated eigenequations

$$\begin{aligned} \mathcal{D}_1[\phi_L^\alpha] &= \lambda_\alpha \phi_L^\alpha \\ \mathcal{D}_N[\phi_R^\beta] &= \mu_\beta \phi_R^\beta. \end{aligned} \quad (3.16)$$

For simplicity, we restrict this discussion to Lindblad operators of the form $L_1 = \sigma^+$ and $L_2 = \sigma^-$. The general solution of the problem can be obtained by rotating the system in the appropriate way and can be found in [24]. The eigenoperators and eigenvalues for the proposed simplified Lindblad operators are summarized in Table 3.1.

ϕ_L^α	λ_α	ϕ_R^β	μ_β
$\phi_L^1 = \sigma_1^+ \sigma^-$	$\lambda_1 = 0$	$\phi_R^1 = \sigma_N^- \sigma^+$	$\mu_1 = 0$
$\phi_L^2 = \sigma_1^+$	$\lambda_2 = -\frac{1}{2}$	$\phi_R^2 = \sigma_N^+$	$\mu_2 = -\frac{1}{2}$
$\phi_L^3 = \sigma_1^-$	$\lambda_3 = -\frac{1}{2}$	$\phi_R^3 = \sigma_N^-$	$\mu_3 = -\frac{1}{2}$
$\phi_L^4 = \sigma_1^z$	$\lambda_4 = -1$	$\phi_R^4 = \sigma_N^z$	$\mu_4 = -1$

(a)
(b)

Table 3.1: Exemplary eigensystems for (a) the left and (b) the right (a) the left and (b) the right with Lindblad operators $L_1 = \sigma^+$ and $L_N = \sigma^-$.

The eigenvalues of the full dissipator $\mathcal{D}[\bullet] = \mathcal{D}_1[\bullet] + \mathcal{D}_N[\bullet]$, thus, are given by the following set of five (degenerate) numbers

$$\mathcal{E} = \{0, -\frac{1}{2}, -1, -\frac{3}{2}, -2\}, \quad (3.17)$$

which multiplied by Γ return the positions of the main bands on the real axis. The spread around the real and imaginary axes depends on the Hamiltonian parameters. The real part of the stripes has been found to have a width of the order $\frac{1}{\Gamma}$. The spread of the imaginary part, however, is related to the eigenvalues of the dissipation-projected Hamiltonian, an object which will be

introduced later.

We denote the absolute value of the first eigenvalue $|\lambda_1| = |\lambda_1 - \lambda_0|$ with non-zero real part as the *gap*. Its inverse gives the decay rate towards the steady states and, thus, defines the slowest time scale in the system. Generally, we found that it scales like $\sim \frac{1}{L}$, but, in certain situations, it was found to scale like $\sim \frac{1}{L^3}$. This will be specified further in the results.

3.1.5 Time Evolution and Steady State

The dynamics of our system is governed by the time-dependent Lindblad equation. We can rotate the initial state into the eigenbasis of \mathcal{L} , apply the time evolution operator $e^{\mathcal{L}t}$ and rotate back to the original basis

$$|\rho(t)\rangle = \left(\sum_i |\rho_i\rangle \langle \rho_i| \right)^{-1} \left(\sum_i e^{\lambda_i t} |\rho_i\rangle \langle \rho_i| \right) |\rho(0)\rangle \quad (3.18)$$

Consequently, by a full diagonalization, we can obtain the time evolution starting from an arbitrary initial state. Due to the fact that $\text{Re}(\lambda_i) \leq 0$, it immediately becomes clear that a unique steady state (cf. Chapter 2.3.3) is reached for the long-time limit. The non-equilibrium steady state can alternatively be obtained by solving the stationary Lindblad equation

$$\mathcal{L}\rho = 0, \quad (3.19)$$

which can be treated as an eigenequation. The above equation is then trivially solved by the eigenstate corresponding to the eigenvalue that is equal to zero $\lambda = 0 \rightarrow \rho_{\text{steady state}}$. In contrast to the time evolution, we directly identify the corresponding eigenstate to be the solution.

At this point, we have defined the model and know how to solve the governing equations of motion. Next, we will introduce the quantities that will be used to characterize the states of the chain.

3.2 Physical Observables

The purity of a density matrix, as mentioned above, can be calculated by $\text{Tr}\rho$. A more versatile notion, however, is the concept of the *von Neumann entropy*. It is defined by

$$S_{\text{VNE}} = - \sum_i p_i \log_2(p_i) \quad \text{with} \quad \rho = \sum_i p_i |\phi_i\rangle \langle \phi_i|, \quad (3.20)$$

where p_i are the eigenvalues of the density matrix ρ . Since we defined the von Neumann entropy using the binary logarithm, it has convenient properties:

- It vanishes for a pure state ($\log_2(1) = 0$).
- Consider a chain of spins with $N = 3$, whose first and last spin are fixed via Zeno limit Lindblad action. If the middle spin is totally mixed, its density matrix will have two-fold degenerated eigenvalue at $\frac{1}{2}$; therefore, the maximal entropy will be at 1. Analogously, for $N = 4$, $S_{max} = 2$ etc.

Since we observe an open non-equilibrium system, it is interesting to study its transport phenomena such as the magnetization current in Z-direction. We use the short notation $\hat{j}_k^z = \hat{J}_{k \rightarrow k+1}^z$ for the operator describing current flow from site k to site $k + 1$. It is defined by the lattice continuity equation

$$\frac{d}{dt}\sigma_k^z = \hat{J}_{k-1}^z - \hat{J}_k^z, \quad (3.21)$$

meaning that the change of magnetization at site k $\frac{d}{dt}\sigma_k^z$ equals the magnetization current in and out of this site. Additionally, we know from Heisenberg's equation of motion that

$$\frac{d}{dt}\sigma_k^z = i[H, \sigma_k^z]. \quad (3.22)$$

The current operator follows from (3.21) and (3.22) via Pauli algebra

$$\hat{J}_k^z = 2J(\sigma_k^x \sigma_{k+1}^y - \sigma_k^y \sigma_{k+1}^x) \quad (3.23)$$

$$= 2iJ(\sigma_k^+ \sigma_{k+1}^- - \sigma_k^- \sigma_{k+1}^+) \quad (3.24)$$

with J the coupling constant. Since the magnetization current is locally conserved, it is constant along the whole chain and

$$j^z = \langle \hat{J}_k^z \rangle. \quad (3.25)$$

The next quantity will help to understand the occurrence of states with a certain winding. We will look at the following generalized discrete Fourier transform

$$\hat{f}_m(\Phi) = \frac{1}{N-1} \sum_{k=0}^{N-2} f_k e^{-i\phi(m)k}. \quad (3.26)$$

where $m = 0, 1, \dots, N - 2$ denotes the winding number around Z-axis and

$$\begin{aligned}\phi(m) &= \frac{\Phi + 2\pi m}{N - 2} \\ f_k &= 2 \langle \sigma^+ \rangle.\end{aligned}$$

It cumulatively characterizes the polarization of the spins in xy-plane (recall that $\langle \sigma^+ \rangle = \langle \sigma^x \rangle + i \langle \sigma^y \rangle$) and the obtained $\hat{f}_m(\Phi)$ can be interpreted as weights for a winding m around the Z-axis. For parallel boundary spins, the boundary gradient Φ is zero and the usual discrete Fourier transform is recovered. We will refer to this quantity as winding weights.

It will turn out useful to gather analytical expressions for these physical observables for the spin helix states from earlier works [25]:

$$S_{\text{VNE}}(\rho_{\text{helix}}) = 0 \quad (3.27)$$

$$j^z(\rho_{\text{helix}}) = J \sin \theta \sin \gamma \quad (3.28)$$

$$\hat{f}_m(\Phi) = \sin \theta \delta_{m, m_0} \quad (3.29)$$

For a spin-helix state with winding number m_0 , corresponds to a $\gamma = \frac{\Phi + 2\pi m_0}{M}$, where Φ is the boundary gradient, we find $f_k = e^{i\varphi(m_0)k}$.

3.3 Limitations of Exact Diagonalization

The exact diagonalization of the Lindbladian is limited to small system sizes $N \leq 7$ due to exponentially growing matrix sizes. The limiting factors are the memory usage and the runtime, which usually scale cubically with the matrix dimension $\sim M^3$ (compare Table 3.2). However, it is advantageous to use exact diagonalization since no approximations are made and the full density matrix is obtained. This enables us to calculate a broad range of observables and to thoroughly investigate small system behavior.

In this work, we restrict ourselves to the brute force method. However, in principle more elaborate treatments can be chosen: Symmetries of the model are frequently exploited to write the Hamiltonian or Lindbladian in a block-diagonal form. If the desired solution lies in one of these symmetry sectors, the dimension of the matrix that is to be diagonalized can be significantly reduced.

For the solution of the stationary problem, as mentioned before, only the eigenstate corresponding to the eigenvalue $\lambda_0 = 0$ has to be found. In this case iterative numerical diagonalization

N	matrix size	memory [GB]
4	256	0.000
5	1024	0.002
6	4096	1.296
7	16384	20.503
8	65536	1281.210

Table 3.2: Scaling of matrix size and memory with system size. This table illustrates the limitations of exact diagonalization to small systems due to exponentially growing superspace. The memory estimation for a full diagonalization for $N = 8$ was obtained by fitting a power law $\sim M^3$ with M denoting the matrix dimension.

algorithms can be used (e.g. Lanczos). We tried this approach, but due to the limitations of our computational resource it wasn't practical: Starting from a random vector, too many Krylow vectors would have been needed to satisfy a reasonable convergence threshold, which increased runtime immensely.

Up to here, we have discussed the numerical methods that we use to obtain the exact stationary state and the time evolution for small systems. To gain deeper understanding of the physics, we employ perturbation theory.

Perturbation Theory

This chapter will give detailed calculations on both the time-independent and the time-dependent perturbation theory. We start with the stationary problem and introduce the tools, which are needed to comfortably calculate exact expressions for the specific case of the boundary-driven XXZ chain. This discussion brings together ideas of previous works [24–27], merges them and uses them to compute the perturbation theory for a general ansatz, leading to the discovery of an underlying stochastic process. The results of the stationary problem motivate a heuristic guess for the dynamics. This heuristic guess can then be validated by a formal time-dependent perturbation theory in the last part of this chapter.

4.1 Stationary Perturbation Theory

We start the discussion on perturbation theory by considering the stationary problem. The interesting limit in this problem is the strong coupling limit $\Gamma \gg 1$ limit, which contains the extreme case of infinite coupling (Zeno limit).

For such a situation, we use a series expansion of the density matrix in powers of $1/\Gamma$

$$\rho = \sum_{n=0}^{\infty} \frac{\rho^{(n)}}{\Gamma^n} \quad (4.1)$$

where the expansion order is indicated by bracketed superscripts, which are not to be confused with powers. We insert this series into the stationary Lindblad master equation and obtain an

equality, which needs to be fulfilled at each order of Γ .

$$-i[H, \rho] + \Gamma \mathcal{D}[\rho] = 0 \quad (4.2)$$

$$-i[H, \rho^{(0)}] - i \left[H, \frac{\rho^{(1)}}{\Gamma} \right] - \dots + \Gamma \mathcal{D}[\rho^{(0)}] + \Gamma \mathcal{D} \left[\frac{\rho^{(1)}}{\Gamma} \right] + \dots = 0. \quad (4.3)$$

At $\mathcal{O}(\Gamma)$, we find that the solution in Zeno limit has to be a dark state of the dissipator, therefore,

$$\mathcal{D}[\rho^{(0)}] = 0. \quad (4.4)$$

For orders $\mathcal{O}(1)$ to $\mathcal{O}(\frac{1}{\Gamma^n})$, we obtain a recurrence relation of the following form

$$\rho^{(n+1)} = i\mathcal{D}^{-1}[[H, \rho^{(n)}]] + M^{(n+1)}, \quad (4.5)$$

where, due to the formal inversion of the dissipator, an auxiliary matrix $M^{(n+1)} \in \text{Ker}\mathcal{D}$ has to be added as additional degree of freedom at each step. In principle this inversion is not trivial and it will be treated more carefully in the next section. Furthermore, the properties of the density matrix ρ have to be satisfied at all steps. For $\rho^{(0)}$ to be a physical state in Zeno limit, it has to have unit trace. Hence, all higher orders are traceless. It can be shown that $\mathcal{D}^{-1}[[H, \rho^{(n)}]]$ for $n = 1, 2$ is traceless and, consequently, the auxiliary matrix has to be traceless, $\text{Tr}M^{(m)} = 0$, as well.

The inversion of the dissipator is not trivial. In the following section, we will approach this issue and derive a condition for the dissipator to be invertible.

4.1.1 Secular Condition

At this point, it is necessary to have a closer look at the inversion of the dissipator. We follow the argumentation and notation used in [24]. In the previous chapter, we have introduced the concept of eigensystems for left and right dissipators (see Equation (3.16) and Table 3.1) which we will use here.

Any arbitrary matrix χ can be expressed in terms of two bases

$$\chi = \sum_{\alpha=1}^4 \sum_{\beta=1}^4 \phi_L^\alpha \otimes \chi_{\alpha\beta} \otimes \phi_R^\beta. \quad (4.6)$$

Since we know how the dissipator acts on the matrix χ ,

$$\mathcal{D}[\chi] = \sum_{\alpha=1}^4 \sum_{\beta=1}^4 \lambda_{\alpha} \phi_L^{\alpha} \otimes \chi_{\alpha\beta} \otimes \mu_{\beta} \phi_R^{\beta} \quad (4.7)$$

$$= \sum_{\alpha=1}^4 \sum_{\beta=1}^4 (\lambda_{\alpha} + \mu_{\beta}) \phi_L^{\alpha} \otimes \chi_{\alpha\beta} \otimes \phi_R^{\beta}, \quad (4.8)$$

we also know how the inverse dissipator will act on it:

$$\mathcal{D}^{-1}[\chi] = \sum_{\alpha=1}^4 \sum_{\beta=1}^4 \frac{1}{\lambda_{\alpha} + \mu_{\beta}} \phi_L^{\alpha} \otimes \chi_{\alpha\beta} \otimes \phi_R^{\beta}. \quad (4.9)$$

For our choice of basis vectors and, thus, eigenvalues (see Table 3.1) this expression for the inverse dissipator becomes singular, if $\alpha = \beta = 1$. To eliminate this singularity, we require $\chi_{11} = 0$.

In order to arrive at an expression for the expansion coefficient $\chi_{\alpha\beta}$, we introduce the complementary bases ($\{\psi_L^{\alpha}\}, \{\psi_R^{\beta}\}$) (see Table 4.1). These complementary bases are trace orthonormal ($\text{Tr}(\phi_L^{\alpha} \psi_L^{\gamma}) = \delta_{\alpha\gamma}$, $\text{Tr}(\phi_R^{\beta} \psi_R^{\delta}) = \delta_{\beta\delta}$) to the eigenbases ($\{\phi_L^{\alpha}\}, \{\phi_R^{\beta}\}$).

ψ_L^{α}	ψ_R^{β}
$\psi_L^1 = \mathbb{1}$	$\psi_R^1 = \mathbb{1}$
$\psi_L^2 = \sigma_1^{-}$	$\psi_R^2 = \sigma_N^{-}$
$\psi_L^3 = \sigma_1^{+}$	$\psi_R^3 = \sigma_N^{+}$
$\psi_L^4 = \frac{\sigma_1^z - \mathbb{1}}{2}$	$\psi_R^4 = \frac{\sigma_N^z - \mathbb{1}}{2}$
(a)	(b)

Table 4.1: Exemplary trace orthonormal basis for (a) the left and (b) the right boundary spin space with Lindblad operators $L_1 = \sigma^+$ and $L_N = \sigma^-$, which represents a rotated version of antiparallel boundaries.

We can now express the coefficients $\chi_{\alpha\beta}$ using these trace-orthonormal bases

$$\chi_{\alpha\beta} = \text{Tr}_{1,N} \left((\psi_L^{\alpha} \otimes \mathbb{1}^{\otimes N-1}) \chi (\mathbb{1}^{\otimes N-1} \otimes \psi_R^{\beta}) \right), \quad (4.10)$$

where $\text{Tr}_{1,N}$ is the partial trace over the subspace of the first and the last spin. We check, if this

is consistent with Equation (4.17) by

$$\chi_{\gamma\delta} = \text{Tr}_{1,N} \left((\psi_L^\gamma \otimes \mathbb{1}^{\otimes N-1}) \left[\sum_{\alpha=1}^4 \sum_{\beta=1}^4 \phi_L^\alpha \otimes \chi_{\alpha\beta} \otimes \phi_R^\beta \right] (\mathbb{1}^{\otimes N-1} \otimes \psi_R^\delta) \right) \quad (4.11)$$

$$= \sum_{\alpha=1}^4 \sum_{\beta=1}^4 \text{Tr}_{1,N} (\psi_L^\gamma \phi_L^\alpha \otimes \mathbb{1}^{\otimes N-1} \chi_{\alpha\beta} \mathbb{1}^{\otimes N-1} \otimes \phi_R^\beta \psi_R^\delta) \quad (4.12)$$

$$= \sum_{\alpha=1}^4 \sum_{\beta=1}^4 \delta_{\alpha\gamma} \chi_{\alpha\beta} \delta_{\beta\delta} \quad (4.13)$$

$$= \chi_{\gamma\delta}. \quad (4.14)$$

To ensure that no singularities are present, we check the element χ_{11} , which has to be equal to zero

$$\chi_{11} = \text{Tr}_{1,N} \left((\psi_L^1 \otimes \mathbb{1}^{\otimes N-1}) \chi (\mathbb{1}^{\otimes N-1} \otimes \psi_R^1) \right) \quad (4.15)$$

$$= \text{Tr}_{1,N} (\chi) \stackrel{!}{=} 0, \quad (4.16)$$

where we made use of the definition $\psi_L^1 = \psi_R^1 = \mathbb{1}$. In another check for consistency, we have a look at $\text{Tr}_{1,N} (\chi)$, which has to vanish

$$\text{Tr}_{1,N} (\chi) = \text{Tr}_{1,N} \left(\mathcal{D} \left[\mathcal{D}^{-1} [\chi] \right] \right) \quad (4.17)$$

$$= \text{Tr}_{1,N} \left(\mathcal{D} \left[\sum_{\alpha=1}^4 \sum_{\beta=1}^4 \frac{1}{\lambda_\alpha + \mu_\beta} \phi_L^\alpha \otimes \chi_{\alpha\beta} \otimes \phi_R^\beta \right] \right) \quad (4.18)$$

$$= \text{Tr}_{1,N} \left(\mathcal{D} \left[\sum_{\substack{j=1 \\ \text{excluding } j=k=1}}^4 \sum_{k=1}^4 \frac{1}{\lambda_\alpha + \mu_\beta} \phi_L^\alpha \otimes \chi_{\alpha\beta} \otimes \phi_R^\beta \right] \right) \quad (4.19)$$

$$= \sum_{\substack{j=1 \\ \text{excluding } j=k=1}}^4 \sum_{k=1}^4 \text{Tr}(\phi_L^\alpha) \otimes \chi_{\alpha\beta} \otimes \text{Tr}(\phi_R^\beta) \quad (4.20)$$

$$= 0, \quad (4.21)$$

where in the last step, we used the tracelessness of ϕ_L^α and ϕ_R^β .

Turning back to solving the recurrence equation (4.5), we can identify χ with the commutator

$[H, \rho^{(n)}]$ and arrive at the *secular condition*

$$\text{Tr}_{1,N}([H, \rho^{(n)}]) = \text{Tr}_{\mathcal{H}_{\text{boundary}}}([H, \rho^{(n)}]) = 0. \quad (4.22)$$

To summarize, \mathcal{D} has a non-zero kernel. This subspace consists of matrices of the form $\rho_1 \otimes A \otimes \rho_N$ with A being an arbitrary $2^{N-2} \times 2^{N-2}$ matrix. For $\rho^{(n+1)}$ to exist, we demand that there is no overlap between $[H, \rho^{(n)}]$ and this subspace (secular condition). At this point, we are all set to calculate higher order corrections in perturbation theory starting from a general ansatz for the zeroth order.

4.1.2 General Ansatz

Our goal here is to better understand the steady state of the boundary-driven XXZ chain in the limit of strong dissipation. In order to do so, we use the recurrence relation (4.5) and start from a general ansatz for the steady state

$$\rho^{(0)} = |e^0\rangle \langle e^0| \otimes R^{(0)}, \quad (4.23)$$

where we define

$$R^{(0)} = \sum_{\alpha=0}^{d_1-1} v_\alpha |\alpha\rangle \langle \alpha|, \quad (4.24)$$

with the properties

$$\sum_{\alpha=0}^{d_1-1} v_\alpha = 1 \quad (4.25)$$

$$|e^0\rangle \in \mathcal{H}_{\text{boundary}} \quad (4.26)$$

$$|\alpha\rangle \in \mathcal{H}_{\text{bulk}}. \quad (4.27)$$

This ansatz consists of the pure targeted boundary spin states in Zeno limit $|e^0\rangle = |\psi_1^{\text{Zeno}}\rangle \otimes |\psi_N^{\text{Zeno}}\rangle$ on the boundaries and an arbitrary mixture of states α weighted by v_α in the bulk of the chain. We denote by d_0 the dimension of $\mathcal{H}_{\text{boundary}}$ (in our case $\mathcal{H}_{\text{boundary}} = \mathbb{C}^2 \otimes \mathbb{C}^2$ and thus $d_0 = 4$) and d_1 the dimension of the bulk subspace. Previously, in investigations for the pure spin helix state solutions, a special case of the reduced bulk density matrix was chosen, where $R^{(0)} = |0\rangle \langle 0|$.

In the following, the above ansatz is inserted into the recurrence relation. At each order, the secular condition has to be fulfilled, which will effectively determine the restrictions on the state in the bulk. We will start by introducing a proper framework, which will simplify the calculations substantially.

Let us introduce a complete basis in the subspace of the boundary spins $\mathcal{H}_{\text{boundary}}$. Starting from the targeted boundary spin states in Zeno limit $|e^0\rangle$, three additional, mutually perpendicular states can be constructed in the following way

$$|e^0\rangle = |\psi(\theta_L, \varphi_L)\rangle \otimes |\psi(\theta_R, \varphi_R)\rangle, \quad (4.28)$$

$$|e^1\rangle = \cos w |\psi^\perp(\theta_L, \varphi_L)\rangle \otimes |\psi(\theta_R, \varphi_R)\rangle - \sin w |\psi(\theta_L, \varphi_L)\rangle \otimes |\psi^\perp(\theta_R, \varphi_R)\rangle, \quad (4.29)$$

$$|e^2\rangle = \sin w |\psi^\perp(\theta_L, \varphi_L)\rangle \otimes |\psi(\theta_R, \varphi_R)\rangle + \cos w |\psi(\theta_L, \varphi_L)\rangle \otimes |\psi^\perp(\theta_R, \varphi_R)\rangle, \quad (4.30)$$

$$|e^3\rangle = |\psi^\perp(\theta_L, \varphi_L)\rangle \otimes |\psi^\perp(\theta_R, \varphi_R)\rangle, \quad (4.31)$$

with the free parameter ω , which we fix for convenience to

$$w = \frac{\pi}{4}, \quad (4.32)$$

and definitions for the spin states

$$|\psi(\theta, \varphi)\rangle = \begin{pmatrix} \cos \frac{\theta}{2} e^{-i\varphi/2} \\ \sin \frac{\theta}{2} e^{i\varphi/2} \end{pmatrix}, \quad (4.33)$$

$$|\psi^\perp(\theta, \varphi)\rangle = \begin{pmatrix} \sin \frac{\theta}{2} e^{-i\varphi/2} \\ -\cos \frac{\theta}{2} e^{i\varphi/2} \end{pmatrix}. \quad (4.34)$$

In terms of this orthonormal basis, $\{|e^j\rangle\}$ with $j = 0, 1, 2, 3$, we can split the XXZ Hamiltonian in the following way:

$$H_{\text{XXZ}} = \sum_{j=0}^{d_0-1} \sum_{k=0}^{d_0-1} H_{jk} \quad (4.35)$$

$$= H_{00} + \sum_{j \neq 0} (H_{j0} + H_{0j}) + \sum_{j \neq 0} \sum_{k \neq 0} H_{jk}$$

$$= \sum_{j=0}^{d_0-1} \sum_{k=0}^{d_0-1} |e^j\rangle \langle e^k| \otimes h_{jk}, \quad (4.36)$$

where $h_{jk} = \langle e^j | H | e^k \rangle$. Explicit expressions for h_{jk} can be found in the Appendix B and were

derived in [25]. At this point, it is important to note the hermiticity of the sub-Hamiltonians $h_{jk} = h_{kj}^\dagger$ and that $h_{03} = 0$ for $N \geq 2$. The sum, thus, effectively runs from 0 to 2, if not otherwise defined.

With this in mind, we can start calculating the first correction in perturbation theory

$$\rho^{(1)} = i\mathcal{D}^{-1} [[H, \rho^{(0)}]] + M^{(1)}, \quad (4.37)$$

where $M^{(1)}$ is an object of the dissipation-free subspace and can be written as $|e^0\rangle\langle e^0| \otimes m^{(1)}$ with $m^{(1)} = \sum_{\alpha=0}^{d_1-1} \sum_{\beta=0}^{d_1-1} m_{\alpha\beta}^{(1)} |\alpha\rangle\langle\beta|$. We immediately notice that the secular condition $\text{Tr}_{1,N}([H, \rho^{(0)}]) = 0$ has to be checked. The commutator can be simplified by using the expressions (4.23), (4.35) and orthonormality of the basis $\{|e^j\rangle\}$ to yield

$$[H, \rho^{(0)}] = \left(H_{00} + \sum_{j \neq 0} (H_{j0} + H_{0j}) + \sum_{j \neq 0} \sum_{k \neq 0} H_{jk} \right) (|e^0\rangle\langle e^0| \otimes R^{(0)}) \quad (4.38)$$

$$- (|e^0\rangle\langle e^0| \otimes R^{(0)}) \left(H_{00} + \sum_{j \neq 0} (H_{j0} + H_{0j}) + \sum_{j \neq 0} \sum_{k \neq 0} H_{jk} \right) \quad (4.39)$$

$$= \left(|e^0\rangle\langle e^0| \otimes h_{00} + \sum_{j \neq 0} (|e^j\rangle\langle e^0| \otimes h_{j0}) \right) R^{(0)} \quad (4.40)$$

$$- R^{(0)} \left(|e^0\rangle\langle e^0| \otimes h_{00} + \sum_{j \neq 0} (|e^0\rangle\langle e^j| \otimes h_{0j}) \right) \quad (4.41)$$

$$= |e^0\rangle\langle e^0| \otimes [h_{00}, R^{(0)}] + \sum_{j \neq 0} (|e^j\rangle\langle e^0| \otimes h_{j0} R^{(0)} - |e^0\rangle\langle e^j| \otimes R^{(0)} h_{0j}). \quad (4.42)$$

For the secular condition, we now need to take the trace over the boundary space and realize that the second and third term of the expression vanish $\text{Tr}_{1,N}(|e^j\rangle\langle e^0|) = \text{Tr}_{1,N}(|e^0\rangle\langle e^j|) = 0$, which leaves us with

$$\text{Tr}_{1,N}(|e^0\rangle\langle e^0| \otimes [h_{00}, R^{(0)}]) = [h_{00}, R^{(0)}] \quad (4.43)$$

$$= \left[h_{00}, \sum_{\alpha} \nu_{\alpha} |\alpha\rangle\langle\alpha| \right] \quad (4.44)$$

$$= \sum_{\alpha} \nu_{\alpha} [h_{00}, |\alpha\rangle\langle\alpha|] \stackrel{!}{=} 0. \quad (4.45)$$

The trivial solution, $\nu_{\alpha} = 0 \quad \forall \alpha$, is not physical, hence, the condition can only be satisfied if

and only if $|\alpha\rangle$ are eigenstates of h_{00} from which follows that

$$h_{00} |\alpha\rangle = \lambda_\alpha |\alpha\rangle, \quad (4.46)$$

where λ_α are the corresponding eigenvalues. Furthermore, we notice that $H_{00} = |e^0\rangle\langle e^0| \otimes h_{00}$ lies in the kernel of the dissipator and, therefore, is an object of the dissipation-free subspace. In the following, we call $h_{00} = \langle e^0| H |e^0\rangle$ the *dissipation-projected Hamiltonian*. The total Hilbert space, thus, is spanned by the vectors $|e^k\rangle \otimes |\alpha\rangle$.

Approaching the first order correction, this result helps to simplify the commutator (4.42) to

$$[H, \rho^{(0)}] = \sum_{j \neq 0}^2 \left(|e^j\rangle\langle e^0| \otimes h_{j0} R^{(0)} - |e^0\rangle\langle e^j| \otimes R^{(0)} h_{0j} \right). \quad (4.47)$$

In the following, we discuss how to calculate the inverse dissipator, which in general is a non-trivial operation. However, in our case, the dissipator only affects the boundary subspace and, using the explicit form of \mathcal{D} and the basis states $\{|e^j\rangle\}$, one can show that:

$$\mathcal{D} \left[|e^1\rangle\langle e^0| \right] = -\frac{1}{2} |e^1\rangle\langle e^0|, \quad (4.48)$$

$$\mathcal{D} \left[|e^2\rangle\langle e^0| \right] = -\frac{1}{2} |e^2\rangle\langle e^0|, \quad (4.49)$$

$$\mathcal{D} \left[|e^3\rangle\langle e^0| \right] = -|e^3\rangle\langle e^0|, \quad (4.50)$$

which by simply inverting gives

$$\mathcal{D}^{-1} \left[|e^1\rangle\langle e^0| \right] = -2 |e^1\rangle\langle e^0|, \quad (4.51)$$

$$\mathcal{D}^{-1} \left[|e^2\rangle\langle e^0| \right] = -2 |e^2\rangle\langle e^0|, \quad (4.52)$$

$$\mathcal{D}^{-1} \left[|e^3\rangle\langle e^0| \right] = -|e^3\rangle\langle e^0|, \quad (4.53)$$

and enables us to write down the action of the inverse dissipator on the states we want to calculate. The first-order correction can then be given by

$$\rho^{(1)} = -2i \sum_{j \neq 0}^2 \left(|e^j\rangle\langle e^0| \otimes h_{j0} R^{(0)} - |e^0\rangle\langle e^j| \otimes R^{(0)} h_{0j} \right) + |e^0\rangle\langle e^0| \otimes m^{(1)}. \quad (4.54)$$

In a similar fashion, but a bit more lengthy and tedious, one can calculate the next order commutator $[H, \rho^{(1)}]$ and the corresponding secular condition $\text{Tr}_{1,N}([H, \rho^{(1)}]) = 0$. A detailed

calculation is given in Appendix B. By going through the calculation, one obtains the following condition

$$\text{Tr}_{1,N}([H, \rho^{(0)}]) = [h_{00}, m^{(1)}] + 4i \sum_{j \neq 0} \mathcal{D}_{h_{j0}} [R^{(0)}] \stackrel{!}{=} 0. \quad (4.55)$$

The equation obtained for the secular condition at first order (4.55) is a matrix equation of dimension $2^{N-2} \times 2^{N-2}$. In order to better understand its properties, we look at its diagonal and off-diagonal elements.

Let us now take into account the diagonal elements of this condition, which, with some algebra (see Appendix B), can be brought into the form:

$$\langle \gamma | \text{Tr}_{1,N}([H, \rho^{(0)}]) | \gamma \rangle = 4i \sum_{j \neq 0} \left(\sum_{\alpha \neq \gamma}^{d_1-1} v_\alpha \left(|\langle \gamma | h_{j0} | \alpha \rangle|^2 \right) - v_\gamma \sum_{\beta \neq \gamma}^{d_1-1} \left(|\langle \beta | h_{j0} | \gamma \rangle|^2 \right) \right) \stackrel{!}{=} 0. \quad (4.56)$$

These equations set the conditions for the eigenvalues v_α , as will be explained further in the next subsection.

In the same way, we can obtain a condition for the elements of the auxiliary matrix $m^{(1)}$ from the off-diagonal elements of (4.55), yielding

$$\langle \gamma | \text{Tr}_{\mathcal{H}_0}[H, \rho^{(1)}] | \delta \rangle = \langle \gamma | 4i \sum_{k \neq 0} \mathcal{D}_{h_{k0}} [R^{(0)}] | \delta \rangle + \langle \gamma | [h_{00}, m^{(1)}] | \delta \rangle \quad (4.57)$$

$$= \langle \gamma | 4i \sum_{k \neq 0} \mathcal{D}_{h_{k0}} [R^{(0)}] | \delta \rangle + (\lambda_\gamma - \lambda_\delta) \langle \gamma | m^{(1)} | \delta \rangle \stackrel{!}{=} 0. \quad (4.58)$$

In principle, we can now proceed to higher orders of the stationary perturbation theory, since the expressions necessary for $\rho^{(2)}$ and the subsequent secular condition at second order have been derived. However, they are not needed in the frame of this work.

4.1.3 Interpretation of the Stochastic Matrix F

We started from a general ansatz for the non-equilibrium steady state in Zeno limit and calculated perturbative corrections via a recurrence relation. At each order, the secular condition set restrictions on the general ansatz, that we have made. A thorough analysis of the diagonal condition (4.56) revealed that, combined with $\sum_{\alpha=0}^{d_1-1} v_\alpha = 1$, it completely determines the eigenvalues v_α for a non-degenerate h_{00} . Furthermore, one can proof that the rank can be predicted reliably even for a degenerate h_{00} .

To demonstrate this, let us define

$$Q_{\alpha\beta}(j) = |\langle \alpha | h_{j0} | \beta \rangle|^2 \quad (4.59)$$

and use this to reformulate (4.56) as

$$\sum_{\beta}^{d_0-1} F_{\alpha\beta} v_{\beta} = 0, \quad (4.60)$$

where matrix F is a matrix with non-diagonal elements being real non-negative $F_{\alpha\beta} = \sum_{j=1}^3 Q_{\alpha\beta}(j)$ and the diagonal F elements satisfying the stochastic matrix rule,

$$F_{\alpha\alpha} = - \sum_{\beta \neq \alpha}^{d_1-1} F_{\beta\alpha}. \quad (4.61)$$

The vector $|v\rangle$ contains all the eigenvalues, since

$$|v\rangle = \begin{pmatrix} v_0 \\ v_1 \\ \vdots \\ v_{(d_1-1)} \end{pmatrix}. \quad (4.62)$$

The stochastic matrix \hat{F} , thus, has the following form:

$$F = \sum_{j \neq 0}^{d_0-1} \begin{pmatrix} -\sum_{\beta \neq 0}^{d_1-1} Q_{\beta 0}(j) & Q_{01}(j) & \cdots & Q_{0(d_1-1)}(j) \\ Q_{10}(j) & -\sum_{\beta \neq 1}^{d_1-1} Q_{\beta 1}(j) & & \vdots \\ \vdots & & \ddots & \vdots \\ Q_{(d_1-1)0}(j) & Q_{(d_1-1)1}(j) & \cdots & -\sum_{\beta \neq d_1-1}^{d_1-1} Q_{(d_1-1)\beta}(j) \end{pmatrix} \quad (4.63)$$

Link to Markov Processes

The F matrix is said to be stochastic, as its column sum is zero [38]. This reminds us of classical stochastic processes (Markov processes). Discrete Markov processes are described by a transition matrix P . There can be right and left stochastic matrices depending on whether the column sum or the row sum is equal to 1. As our matrix F has zero column sum, we focus on left stochastic matrices. Such a transition matrix satisfies the eigensystem with eigenvalue one $\mathbf{1}P = \mathbf{1}$, where $\mathbf{1}$ is a row vector with all elements being ones. As for a square matrix left

and right eigenvalues are the same, the matrix also has a right column eigenvector $P|\pi\rangle = |\pi\rangle$ with eigenvalue one, which can be identified to be the stationary probability vector [39, 40]. Furthermore, demanding irreducibility of this transition matrix, one can show via Perron-Frobenius theorem, that this stationary vector with eigenvalue one has to be unique and it must have non-negative entries.

The irreducibility can be understood in terms of a Markov chain. If one can go from every site i to every site j and back, the chain is irreducible. On the contrary, there may be a decoupled set of state that, does not communicate with the rest of the system. In such a case the chain is reducible. The corresponding transition matrix would have a block structure.

Furthermore there may be absorbing states, that, once entered, cannot be left anymore. In terms of elements of the transition matrix, there would be non-zero element $P_{i \rightarrow j}$, but zero elements $P_{j \rightarrow i}$. We will encounter such a structure for situations, which lead to finite rank stationary states in the results.

This discussion is related to our stochastic matrix by a simple shift $F = P - \mathbb{1}$. The elements $F_{\alpha\alpha}$ can be interpreted as transition rates to go from state $|\beta\rangle$ to $|\alpha\rangle$

$$F_{\alpha\alpha} = \omega_{\beta \rightarrow \alpha}. \quad (4.64)$$

Thus, we can make use of the rich theoretical background of Markov transition matrices. The theorem of Perron-Frobenius, that states, that for non-negative matrices there exists a non-degenerate non-negative eigenvector of the form (4.62) exists. The normalization condition (4.25) in this case can be interpreted as probability conservation. This theorem is particularly useful to determine the number of non-zero values in the vector $|nu\rangle$ and thus of the rank of the non-equilibrium steady state. The following theorem and proof was proposed by Popkov [41].

Reliable Rank Prediction

Theorem 1 *Let $|\alpha\rangle$ be an eigenbasis of the dissipation-projected Hamiltonian h_{00} ((4.46)). Let, then, the matrix F defined through ((4.60)), to have the property*

$$\begin{aligned} F_{r+1,\alpha} = F_{r+2,\alpha} = \dots = F_{d_1-1,\alpha} &= 0 \\ \alpha &= 1, 2, \dots r. \end{aligned} \quad (4.65)$$

for some r . Then, the non-equilibrium steady state converges to a state with the rank r in the Zeno limit $\Gamma \rightarrow \infty$.

Proof 1 First, note that due to Perron-Frobenius theorem, a solution of ((4.60)) is unique. Let us show that a solution $|\pi^*\rangle = \{v_1, v_2, \dots, v_r, 0, 0, \dots\}$ of ((4.60)) exists. Indeed, $\sum_{\beta} F_{\alpha\beta} |\pi^*\rangle_{\beta} = 0$ for $\alpha \geq r + 1$ is satisfied trivially due to ((4.65)). For the remaining $\alpha = 1, 2 \dots r$, the equations $\sum_{\beta=1}^r F_{\alpha\beta} |\pi^*\rangle_{\beta} = 0$ have a unique solution (up to normalization) due to the fact that the submatrix of F of size $r \times r$ with elements $F_{\alpha\beta}$, $\alpha, \beta \leq r$ is a stochastic matrix as well, to which the Perron-Frobenius uniqueness property applies. From the global uniqueness property we deduce that $|\pi^*\rangle$ with r non-zero entries is a unique solution of ((4.60)). If the spectrum of h_{00} is non-degenerate, then ((4.24)) follows from the commutation property ((4.45)) and the rank of non-equilibrium steady state is equal to r . If the spectrum of h_{00} is degenerate, then due to degeneracies, instead of ((4.24)) we have from ((4.45))

$$R^{(0)} = \sum_{\alpha=0}^r v'_{\alpha} |\alpha'\rangle \langle \alpha'|, \quad (4.66)$$

where the set $\{|\alpha'\rangle\}$ are some linear combinations of the vectors $\{|\alpha\rangle\}$ in the degeneracy subspaces of h_{00} , and the set $\{v'_{\alpha}\}$ is generically different from the set $\{v_{\alpha}\}$ for this very reason. However, the rank of the non-equilibrium steady state $R^{(0)}$ is preserved under any linear operation on it's basis.

We conclude, that the non-equilibrium steady state rank is equal to r irrespectively of whether the spectrum of h_{00} is degenerate or not. Further treatment of the case when the spectrum of h_{00} is degenerate is given in the following section.

Degeneracies of h_{00}

For particular dissipation at the boundaries, the dissipation-projected Hamiltonian h_{00} has degeneracies. The expansion of the reduced density matrix $R^{(0)} = \sum_{\alpha=0}^{d_1-1} v_{\alpha} |\alpha\rangle \langle \alpha|$ is not unique for this case. In the degeneracy subspaces we can have any linear combination of eigenvectors which form an orthogonal set. In order to cope with this problem, we have to employ a perturbation, which lifts the degeneracy and which is continuous in the sense that $R^{(0)}(\epsilon) \xrightarrow{\lim_{\epsilon \rightarrow 0}} R^{(0)}$. The degeneracies occur due to symmetries. The perturbation that we choose has to break these underlying symmetries. For any generic system parameters this statement is correct, however for certain configurations (e.g. spin helix state situation) we have singular behavior and by perturbing the system in the wrong "direction", we can miss these singular points. In that sense we also have to preserve certain symmetries. Unfortunately, we were not able to clarify this issue further.

Discussion

The dimension of the dissipation-projected Hamiltonian is $\dim(h_{00}) \sim 2^{N-2} \times 2^{N-2}$, and therefore the diagonalization can be easily performed for up to 14 sites. However, the limiting procedure is solving the system of equations in Equation (4.60). As F is a stochastic matrix, it is singular $\text{Det}(F) = 0$, thus the matrix is not invertible and the system has no unique solution per se. The normalization condition $\sum_i v_i = 1$ fixes this problem.

In conclusion, the secular condition at zeroth order gives us the information that the non-equilibrium steady state in Zeno limit can be built of eigenvectors of the dissipation-projected Hamiltonian (see (4.46)), which can be analytically constructed via (B.1). Furthermore, the secular condition at first order determines the weights of these eigenvectors from a set of equations given by (4.60). Again, we have all the ingredients to construct the matrix F exactly. In this fashion, we can construct the non-equilibrium steady state in $\mathcal{H}_{\text{bulk}}$ Zeno limit. Before we start introducing the time-dependent perturbation theory, let us first guess the dynamics by heuristic argumentation.

4.1.4 Heuristic Guess for the Dynamics

We have discussed the spectrum of the Liouvillian in some detail in Section 3.1.4 and seen that the eigenvalues are organized in stripes. The distance between these stripes is of the order of Γ . We have identified the eigenvalue equal to zero as the non-equilibrium steady state, towards which excitations (states in higher strings) decay exponentially fast $\propto e^{-\Gamma t}$ (see Figure 3.1).

According to this, for large Γ the effective dynamics only takes place in the dissipation-free subspace obtained by $\text{Tr}_{\mathcal{H}_0}(H) = h_{00}$ (string around $\text{Re}(\lambda) = 0$). At $t = 0$, the density matrix can be written as

$$\rho(t = 0) = \rho_1 \otimes R(t = 0) \otimes \rho_N \quad (4.67)$$

$$= |e^0\rangle \langle e^0| \otimes R(t = 0) \quad (4.68)$$

$$h_{00} |\alpha\rangle = \lambda_\alpha |\alpha\rangle \quad (4.69)$$

$$R(t = 0) = \sum_{\alpha\beta} \rho_{\alpha\beta}(t = 0) |\alpha\rangle \langle\beta|, \quad (4.70)$$

with the bulk density matrix, which can be represented by eigenvectors of h_{00} . As h_{00} is hermitian, the eigenvalues λ_α are real. The time evolution of this bulk density matrix, neglecting the decaying part entering due to the Lindblad operators, for a fast time scale is simply unitary

and thus, given by the von Neumann equation yields

$$\frac{\partial R(t_{\text{fast}})}{\partial t_{\text{fast}}} = -i[h_{00}, R] \quad (4.71)$$

$$\Leftrightarrow \langle \alpha | \frac{\partial R(t_{\text{fast}})}{\partial t_{\text{fast}}} | \beta \rangle = -i \langle \alpha | [h_{00}, R] | \beta \rangle \quad (4.72)$$

$$\Leftrightarrow \frac{\partial R_{\alpha\beta}(t_{\text{fast}})}{\partial t_{\text{fast}}} = -i (\langle \alpha | h_{00} R - R h_{00} | \beta \rangle) \quad (4.73)$$

$$\Leftrightarrow \frac{\partial R_{\alpha\beta}(t_{\text{fast}})}{\partial t_{\text{fast}}} = -i (\lambda_{\alpha} - \lambda_{\beta}) \langle \alpha | R | \beta \rangle. \quad (4.74)$$

The solution of the above differential equation is given by

$$R(t_{\text{fast}}) = \sum_{\alpha, \beta} \rho_{\alpha\beta}(t=0) e^{i(\lambda_{\beta} - \lambda_{\alpha})t} |\alpha\rangle \langle \beta|, \quad (4.75)$$

where the diagonal elements of this matrix can be expressed as

$$\langle \alpha | R(t_{\text{fast}}) | \alpha \rangle = \rho_{\alpha\alpha}(t_{\text{fast}}) = \rho_{\alpha\alpha}(t_{\text{fast}}=0) \equiv v_{\alpha}(t_{\text{fast}}). \quad (4.76)$$

Eventually, the unitarily oscillating off-diagonal elements will decay due to the dissipation. According to what we have seen in the previous chapter for longer times, the dynamics is governed by a stochastic process. The continuous-time Markov process can be written as

$$\frac{\partial v_{\alpha}(t_{\text{slow}})}{\partial t_{\text{slow}}} = \sum_{\beta \neq \alpha} v_{\beta} \omega_{\beta \rightarrow \alpha} - v_{\alpha} \sum_{\beta \neq \alpha} \omega_{\alpha \rightarrow \beta} \quad (4.77)$$

$$= F_{\alpha\beta} v_{\beta}. \quad (4.78)$$

4.2 Time-Dependent Perturbation Theory

As we have seen in the preceding section, the solution for the stationary Lindblad master equation in Zeno limit for the boundary-driven XXZ model is in principle determined by an underlying Markov process in the dissipation-free subspace. In this chapter, we want to see whether we recover such a process in the time-dependent perturbation theory.

4.2.1 Dyson Expansion of the Semigroup

The behavior above was, more or less, guessed from the results obtained through time-independent perturbation theory. In principle, it is possible to use time-dependent perturbation theory to clarify at which time scales these processes occur.

The derivation follows [16, 17] and uses a similar notation. We start with the time-dependent Lindblad equation,

$$\frac{\partial \rho}{\partial t} = -i[H, \rho] + \Gamma \mathcal{D}[\rho] = \mathcal{L}\rho, \quad (4.79)$$

and divide it by Γ . By rescaling time as $\Gamma t \rightarrow t$, we obtain an equation with a perturbative term in the limit of strong dissipation $\Gamma \gg 1$:

$$\frac{\partial \rho}{\partial t} = \underbrace{-\frac{i}{\Gamma} [H, \rho]}_{K\rho} + \underbrace{\mathcal{D}[\rho]}_{\mathcal{L}_0\rho} = (\mathcal{L}_0 + K)\rho = \mathcal{L}\rho, \quad (4.80)$$

where the linear operator \mathcal{L}_0 denotes the dissipator and $K = -\frac{i}{\Gamma} [H, \bullet]$ is the commutator with the Hamiltonian. It is instructive to think of these operators as living in the superspace. This time-dependent Lindblad equation has a formal solution,

$$\rho(t) = \underbrace{e^{\mathcal{L}t}}_{\mathcal{E}(t)} \rho(0) = \mathcal{E}(t)\rho(0), \quad (4.81)$$

for which the time evolution operator $\mathcal{E}(t)$ can be expanded as

$$\mathcal{E}(t) = e^{\mathcal{L}_0 t} + \int_0^t e^{\mathcal{L}_0 t_1} K \mathcal{E}(t_1) dt_1. \quad (4.82)$$

We confirm this to be true up to a constant, by comparing the derivatives of (4.81) and (4.82):

$$\frac{\partial \mathcal{E}(t)}{\partial t} \stackrel{(4.81)}{=} \mathcal{L}\mathcal{E}(t) = (\mathcal{L}_0 + K)\mathcal{E}(t) \quad (4.83)$$

$$\stackrel{(4.82)}{=} \mathcal{L}_0 \mathcal{E}(t) + \underbrace{e^{\mathcal{L}_0 t} e^{-\mathcal{L}_0 t}}_{=1} K \mathcal{E}(t) = (\mathcal{L}_0 + K)\mathcal{E}(t). \quad (4.84)$$

Now, we can iterate (4.82) to arrive at the standard Dyson expansion that is familiar from time-independent perturbation theory. Up to second order, we can then write the time evolution

operator as

$$\mathcal{E}(t) = e^{\mathcal{L}_0 t} \left(1 + \int_0^t dt_1 e^{-\mathcal{L}_0 t_1} K e^{\mathcal{L}_0 t_1} + \int_0^t dt_1 e^{-\mathcal{L}_0 t_1} K e^{\mathcal{L}_0 t_1} \int_0^{t_1} dt_2 e^{-\mathcal{L}_0 t_2} K e^{\mathcal{L}_0 t_2} + \dots \right). \quad (4.85)$$

Up to here, we just formally expanded the time evolution operator $\mathcal{E}(t)$. Now, we introduce the projector onto the kernel of the dissipator (kernel of \mathcal{L}_0) which in our specific case is $\mathcal{P}_0 = |e^0\rangle\langle e^0| \otimes \text{Tr}_{1,N}(\bullet)$, where \bullet serves as a placeholder. We define the projector onto the complementary subspace by $\mathcal{Q}_0 := \mathbb{1} - \mathcal{P}_0$. This results in a full spectral decomposition with the properties $\mathcal{P}_0 + \mathcal{Q}_0 = \mathbb{1}$ and $\mathcal{P}_0 \mathcal{Q}_0 = 0$. Let us see how this projector acts on the dissipator

$$\mathcal{L}_0 \mathcal{P}_0 = \mathcal{P}_0 \mathcal{L}_0 = 0 \quad (4.86)$$

and, consequently,

$$e^{\mathcal{L}_0 t} \mathcal{P}_0 = \mathcal{P}_0 e^{\mathcal{L}_0 t} = \mathcal{P}_0, \quad (4.87)$$

as only the zeroth order of the expansion of $e^{\mathcal{L}_0 t} = 1 + \mathcal{L}_0 t + \dots$ survives.

Similarly, we can ask how the time evolution operator $\mathcal{E}(t)$ behaves under a projection \mathcal{P}_0 . To do so, we use the properties explained above to write

$$\mathcal{E}(t) \mathcal{P}_0 = e^{\mathcal{L}_0 t} \left(1 + \int_0^t dt_1 e^{-\mathcal{L}_0 t_1} K e^{\mathcal{L}_0 t_1} + \int_0^t dt_1 e^{-\mathcal{L}_0 t_1} K e^{\mathcal{L}_0 t_1} \int_0^{t_1} dt_2 e^{-\mathcal{L}_0 t_2} K e^{\mathcal{L}_0 t_2} + \dots \right) \mathcal{P}_0 \quad (4.88)$$

$$= \mathcal{P}_0 + e^{\mathcal{L}_0 t} \int_0^t dt_1 e^{-\mathcal{L}_0 t_1} K e^{\mathcal{L}_0 t_1} \mathcal{P}_0 + e^{\mathcal{L}_0 t} \int_0^t dt_1 e^{-\mathcal{L}_0 t_1} K e^{\mathcal{L}_0 t_1} \int_0^{t_1} dt_2 e^{-\mathcal{L}_0 t_2} K e^{\mathcal{L}_0 t_2} \mathcal{P}_0. \quad (4.89)$$

Let us focus on the second term and insert the spectral decomposition:

$$e^{\mathcal{L}_0 t} \int_0^t dt_1 e^{-\mathcal{L}_0 t_1} K e^{\mathcal{L}_0 t_1} \mathcal{P}_0 = e^{\mathcal{L}_0 t} \int_0^t dt_1 e^{-\mathcal{L}_0 t_1} \mathbb{1} K e^{\mathcal{L}_0 t_1} \mathcal{P}_0 \quad (4.90)$$

$$= e^{\mathcal{L}_0 t} \int_0^t dt_1 e^{-\mathcal{L}_0 t_1} (\mathcal{P}_0 + \mathcal{Q}_0) K e^{\mathcal{L}_0 t_1} \mathcal{P}_0 \quad (4.91)$$

$$= t \mathcal{P}_0 K \mathcal{P}_0 + e^{\mathcal{L}_0 t} \int_0^t dt_1 e^{-\mathcal{L}_0 t_1} \mathcal{Q}_0 K \mathcal{P}_0. \quad (4.92)$$

Now, we modify the second term by splitting the integral using substitutions such that

$$e^{\mathcal{L}_0 t} \int_0^t dt_1 e^{-\mathcal{L}_0 t_1} \mathcal{Q}_0 K \mathcal{P}_0 = e^{\mathcal{L}_0 t} \left(\int_0^{-\infty} dt_1 \dots + \int_{-\infty}^t dt_1 \dots \right) \quad (4.93)$$

$$= e^{\mathcal{L}_0 t} \int_0^{-\infty} dt_1 e^{-\mathcal{L}_0 t_1} \mathcal{Q}_0 K \mathcal{P}_0 - \int_t^{-\infty} dt_1 e^{\mathcal{L}_0(t-t_1)} \mathcal{Q}_0 K \mathcal{P}_0. \quad (4.94)$$

Here, we first perform the following substitution

$$t_1 \rightarrow -\tilde{t}_1, \quad (4.95)$$

$$dt_1 \rightarrow -d\tilde{t}_1, \quad (4.96)$$

$$(4.97)$$

where the boundaries change as

$$0 \rightarrow 0, \quad (4.98)$$

$$-\infty \rightarrow \infty, \quad (4.99)$$

$$t \rightarrow -t. \quad (4.100)$$

Thus, we obtain

$$e^{\mathcal{L}_0 t} \int_0^t dt_1 e^{-\mathcal{L}_0 t_1} \mathcal{Q}_0 K \mathcal{P}_0 = -e^{\mathcal{L}_0 t} \int_0^{\infty} d\tilde{t}_1 e^{\mathcal{L}_0 \tilde{t}_1} \mathcal{Q}_0 K \mathcal{P}_0 + \int_{-t}^{\infty} d\tilde{t}_1 e^{\mathcal{L}_0(t+\tilde{t}_1)} \mathcal{Q}_0 K \mathcal{P}_0. \quad (4.101)$$

Next we substitute in the second integral

$$t + \tilde{t}_1 \rightarrow u, \quad (4.102)$$

$$d\tilde{t}_1 \rightarrow du, \quad (4.103)$$

$$(4.104)$$

where the boundaries change as

$$\infty \rightarrow \infty, \quad (4.105)$$

$$-t \rightarrow 0, \quad (4.106)$$

which leaves us with

$$e^{\mathcal{L}_0 t} \int_0^t dt_1 e^{-\mathcal{L}_0 t_1} \mathcal{Q}_0 K \mathcal{P}_0 = -e^{\mathcal{L}_0 t} \int_0^\infty d\tilde{t}_1 e^{\mathcal{L}_0 \tilde{t}_1} \mathcal{Q}_0 K \mathcal{P}_0 + \int_0^\infty du e^{\mathcal{L}_0 u} \mathcal{Q}_0 K \mathcal{P}_0. \quad (4.107)$$

Using a simple renaming of $\tilde{t}_1, u \rightarrow t$, we can now write

$$e^{\mathcal{L}_0 t} \int_0^t dt_1 e^{-\mathcal{L}_0 t_1} \mathcal{Q}_0 K \mathcal{P}_0 = (e^{\mathcal{L}_0 t} - \mathbb{1}) \underbrace{\left(- \int_0^\infty dt e^{\mathcal{L}_0 t} \mathcal{Q}_0 \right)}_{:=\mathcal{S}} K \mathcal{P}_0 \quad (4.108)$$

$$= (e^{\mathcal{L}_0 t} - \mathbb{1}) \mathcal{S} K \mathcal{P}_0, \quad (4.109)$$

where \mathcal{S} is the pseudo-inverse of the dissipator with the property

$$\mathcal{L}_0 \mathcal{S} = \mathcal{S} \mathcal{L}_0 = \mathcal{Q}_0. \quad (4.110)$$

This operator is bounded; recall that the eigenvalues \mathcal{L}_0 are real and negative.

Up to here we have:

$$\mathcal{E}(t) \mathcal{P}_0 = \mathcal{P}_0 + t \mathcal{P}_0 K \mathcal{P}_0 + (e^{\mathcal{L}_0 t} - \mathbb{1}) \mathcal{S} K \mathcal{P}_0 + e^{\mathcal{L}_0 t} \int_0^t dt_1 e^{-\mathcal{L}_0 t_1} K e^{\mathcal{L}_0 t_1} \int_0^{t_1} dt_2 e^{-\mathcal{L}_0 t_2} K e^{\mathcal{L}_0 t_2} \mathcal{P}_0, \quad (4.111)$$

where $t \mathcal{P}_0 K \mathcal{P}_0$ with $K = -\frac{i}{\Gamma} [H, \bullet]$ leads to a unitary evolution. The third term is more difficult to interpret. Looking at

$$\mathbb{1} (e^{\mathcal{L}_0 t} - \mathbb{1}) = (\mathcal{P}_0 + \mathcal{Q}_0) (e^{\mathcal{L}_0 t} - \mathbb{1}) = \mathcal{Q}_0 (e^{\mathcal{L}_0 t} - \mathbb{1}), \quad (4.112)$$

we see that this term accounts for processes driving the system out of the dissipation-projected subspace (note that \mathcal{Q}_0 projects onto the complementary space) and that these processes are instantaneously erased by dissipation (see first term \mathcal{P}_0). Let us look at the time-scales, at which these processes appear (remembering the rescaling $\Gamma t \rightarrow t$) by taking the norm:

$$\|\mathcal{P}_0\| \sim \|\mathcal{Q}_0\| \sim 0, \quad (4.113)$$

$$\|\mathcal{S}\| \sim 1, \quad (4.114)$$

$$K \sim \frac{1}{\Gamma}. \quad (4.115)$$

Then, the first three terms of the expansion of the time evolution operator stand for processes

which occur on the following time scales:

$$\mathcal{E}(t)\mathcal{P}_0 = \mathcal{P}_0 + \underbrace{t\mathcal{P}_0\mathcal{K}\mathcal{P}_0}_{\mathcal{O}(1)} + \underbrace{(e^{\mathcal{L}_0 t} - \mathbb{1})\mathcal{S}\mathcal{K}\mathcal{P}_0}_{\mathcal{O}(\frac{1}{\Gamma})} + \dots \quad (4.116)$$

Next, we want to learn what happens at the 2nd order. Instead of $\mathcal{E}(t)\mathcal{P}_0$, we look at $\mathcal{P}_0\mathcal{E}(t)\mathcal{P}_0$:

$$\mathcal{P}_0 e^{\mathcal{L}_0 t} \int_0^t dt_1 e^{-\mathcal{L}_0 t_1} \mathcal{K} e^{\mathcal{L}_0 t_1} \int_0^{t_1} dt_2 e^{-\mathcal{L}_0 t_2} \mathcal{K} e^{\mathcal{L}_0 t_2} \mathcal{P}_0 = \quad (4.117)$$

$$= \mathcal{P}_0 \int_0^t dt_1 \int_0^{t_1} dt_2 \mathcal{K} e^{\mathcal{L}_0 t_1 - \mathcal{L}_0 t_2} \mathcal{K} \mathcal{P}_0 \quad (4.118)$$

$$= \mathcal{P}_0 \int_0^t dt_1 \int_0^{t_1} dt_2 \mathcal{K} e^{\mathcal{L}_0 t_1 - \mathcal{L}_0 t_2} (\mathcal{P}_0 + \mathcal{Q}_0) \mathcal{K} \mathcal{P}_0 \quad (4.119)$$

$$= \frac{t^2}{2} (\mathcal{P}_0 \mathcal{K} \mathcal{P}_0)^2 + \mathcal{P}_0 \mathcal{K} \int_0^t dt_1 e^{\mathcal{L}_0 t_1} \int_0^{t_1} dt_2 e^{-\mathcal{L}_0 t_2} \mathcal{Q}_0 \mathcal{K} \mathcal{P}_0, \quad (4.120)$$

where we recognise the pseudo-inverse in the right term, (4.121)

$$= \frac{t^2}{2} (\mathcal{P}_0 \mathcal{K} \mathcal{P}_0)^2 + \mathcal{P}_0 \mathcal{K} \int_0^t dt_1 (e^{\mathcal{L}_0 t} - \mathbb{1}) \mathcal{S} \mathcal{K} \mathcal{P}_0,$$

the term with unity matrix can be integrated, (4.122)

$$= \frac{t^2}{2} (\mathcal{P}_0 \mathcal{K} \mathcal{P}_0)^2 - t \mathcal{P}_0 \mathcal{K} (\mathcal{P}_0 + \mathcal{Q}_0) \mathcal{S} \mathcal{K} \mathcal{P}_0 + \mathcal{P}_0 \mathcal{K} \int_0^t dt_1 e^{\mathcal{L}_0 t} \mathcal{S} \mathcal{K} \mathcal{P}_0$$

Let us concentrate on the last term of (4.123) and use the spectral decomposition

$$\mathcal{P}_0 \mathcal{K} \int_0^t dt_1 e^{\mathcal{L}_0 t} \mathcal{S} \mathcal{K} \mathcal{P}_0 = \mathcal{P}_0 \mathcal{K} \int_0^t dt_1 e^{\mathcal{L}_0 t} (\mathcal{P}_0 + \mathcal{Q}_0) \mathcal{S} \mathcal{K} \mathcal{P}_0 \quad (4.123)$$

$$= t \mathcal{P}_0 \mathcal{K} \mathcal{P}_0 \mathcal{S} \mathcal{K} \mathcal{P}_0 + \mathcal{P}_0 \mathcal{K} \int_0^t dt_1 e^{\mathcal{L}_0 t} \mathcal{Q}_0 \mathcal{S} \mathcal{K} \mathcal{P}_0. \quad (4.124)$$

Collecting all terms at order two gives:

$$\mathcal{P}_0 e^{\mathcal{L}_0 t} \int_0^t dt_1 e^{-\mathcal{L}_0 t_1} \mathcal{K} e^{\mathcal{L}_0 t_1} \int_0^{t_1} dt_2 e^{-\mathcal{L}_0 t_2} \mathcal{K} e^{\mathcal{L}_0 t_2} \mathcal{P}_0 = \quad (4.125)$$

$$= \underbrace{\frac{t^2}{2} (\mathcal{P}_0 \mathcal{K} \mathcal{P}_0)^2}_{\mathcal{O}(1)} - \underbrace{t \mathcal{P}_0 \mathcal{K} \mathcal{Q}_0 \mathcal{S} \mathcal{K} \mathcal{P}_0}_{\mathcal{O}(\frac{1}{\Gamma})} + \underbrace{\mathcal{P}_0 \mathcal{K} \int_0^t dt_1 e^{\mathcal{L}_0 t} \mathcal{Q}_0 \mathcal{S} \mathcal{K} \mathcal{P}_0}_{\mathcal{O}(\frac{1}{\Gamma^2})}.$$

$$(4.126)$$

To summarize, the evolution in the dissipation-free subspace (recognizing that the $\mathcal{P}_0 K \mathcal{P}_0$ terms can be exponentiated) reads

$$\mathcal{P}_0 \mathcal{E}(t) \mathcal{P}_0 = e^{t \mathcal{P}_0 K \mathcal{P}_0} - t \mathcal{P}_0 K \mathcal{Q}_0 S K \mathcal{P}_0 + \mathcal{O}\left(\frac{1}{\Gamma^2}\right). \quad (4.127)$$

We conclude that in total we observe three different processes, which take place at different times:

- at $t \sim \frac{1}{\Gamma}$, thus, almost instantaneously the system is projected by the strong dissipation into the decoherence-free subspace
- at $t \sim 1$, the evolution is governed by $\mathcal{P}_0 K \mathcal{P}_0 \sim -i[h_{00}, \bullet]$
- at $t \sim \Gamma$ the term $\propto \mathcal{P}_0 K \mathcal{Q}_0 S K \mathcal{P}_0 \sim K^2$ will set in

We know that the stochastic matrix equation is proportional to K^2 and we explicitly see elements of h_{0k} and h_{k0} , which, after first inspection, also arise in this newly derived term. Therefore, we assume the stochastic process will also emerge at this order in time-dependent perturbation theory.

By performing the Dyson expansion of the time evolution operator $\mathcal{E}(t)$, we identified three time scales, which in fact confirm the heuristic argument. In the long time limit, as expected, the behavior will be governed by the underlying stochastic process that we have identified in the stationary perturbation theory.

Results

In this chapter, we present the results of our investigations. We will start by giving an overview of the parameter space of the model and the physics of the non-equilibrium steady states in a case study, where we recover the predicted spin helix states and some of their properties. Particular focus will be cast on the points where a pure state is naively expected, but not encountered. A more detailed analysis is performed for those points, for which the fine-tuned system and dissipation parameters give rise to a state of rank 2. In the last section of this chapter, we perform another case study to confirm the predicted three different time scales in the dynamics and qualitatively see if the results of the strong coupling perturbation theory remain valid for smaller dissipation strengths.

5.1 Exploring the Parameter Space

For a fixed system size N , we can adjust seven free parameters: The action of the bath on the boundary spins with a dissipation strength Γ modifies their polarization on the left and on the right $\theta_L, \theta_R, \phi_L, \phi_R$. Besides that, the internal parameters of the Hamiltonian, coupling constant J and anisotropy Δ , govern the behavior of the chain. In the following, the coupling strength of neighboring spins will be fixed to $J = 1$ and we set $\hbar = 1$.

In the following case study, we restrict the targeted spin polarization to lie in XY-plane ($\theta_L = \theta_R = \frac{\pi}{2}$). The boundary spin polarization will be fixed due to strong coupling ($\Gamma = 1000$), while the anisotropy is changed in the range from -1.5 to 1.5 .

5.1.1 Case Study I: Fixed Boundaries, Changing Anisotropy

The specific case that we want to look at in this section should be representative of the generic situation that we encountered during the investigation of the whole parameter space. We perform an exemplary analysis for a chain of six spins ($N = 6$), whose first spin points along the X-axis $\phi_L = 0$ and whose last spin is chosen to lie in XY-plane with an angle $\phi_R = \frac{\pi}{3}$. The chain length of six spins is the maximal length that can still be comfortably computed using exact diagonalization (cf. Chapter 3). The expectation values for all spin operators σ^α with $\alpha = x, y, z$ for each spin are shown in Figure 5.1. The Z-component of each spin is zero for every anisotropy value. Due to the strong dissipation strength, the first and last spin are effectively pinned into the targeted directions

$$\begin{aligned}\langle \sigma_1^x \rangle &= 1 & \langle \sigma_1^y \rangle &= 0 \\ \langle \sigma_6^x \rangle &= \cos \phi_R, & \langle \sigma_6^y \rangle &= \sin \phi_R.\end{aligned}$$

However, in the numerics Γ is still finite and there are fluctuations in the order of $\sim 10^{-7}$ around these values.

Similar to the discussion in Section 2.2 for the Z-components, it is possible to understand the behavior of the spins in XY-plane qualitatively in the Luttinger liquid phase, where the transverse hopping terms dominate. For anisotropies close to $\Delta = -1$ and $\Delta = 1$, the spins tend to align and misalign, respectively. As expected, we observe a gradual change of X- and Y-components, when going from one to the next spin (Figure 5.1). These transitions occur close to $\Delta = -1$, however, sudden changes are observed in those components close to $\Delta = -1$.

The density profile will be useful to understand more complex quantities like the entropy, which is shown in Figure 5.3. The entropy as function of the anisotropy shows a qualitative behavior that reflects the general case. Coming from a plateau at $\Delta \rightarrow -\infty$, it drops to zero close to (or at) $\Delta = -1$, then rises to a maximum at $\Delta = 0$ and falls to zero again close to (or at) $\Delta = 1$, until it settles to a plateau at $\Delta \rightarrow \infty$. In between, for certain anisotropies, kinks appear in the entropy.

Let us now try to elucidate the features observed in Figure 5.3. At $\Delta = 0$, the XXZ model reduces to a XY model and one can show that the previously derived stochastic matrix F is symmetric and, thus, has equal left and right eigenvector. Furthermore, as we indicated in Section 4.1.3, the left eigenvector with eigenvalue zero is always the unit vector. Consequently, the right eigenvectors are equal to the unit vector and all the weights v_α are the same, as is the

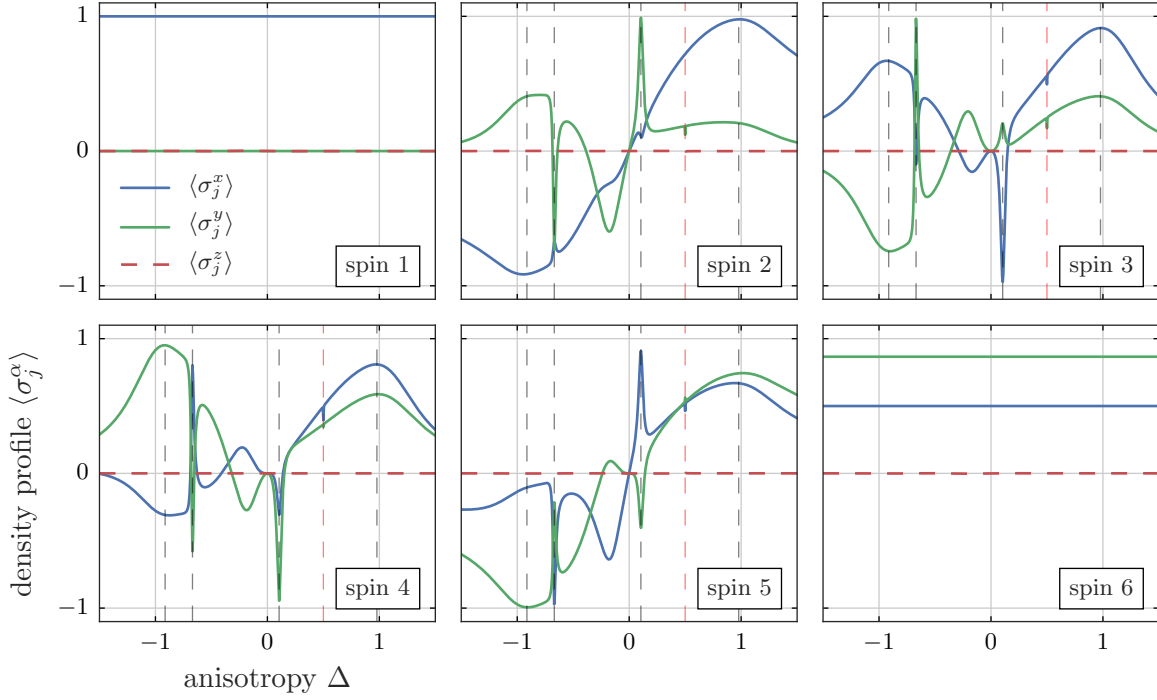


Figure 5.1: Density profiles of a spin chain of length $N = 6$ and Lindblad operators targeting $\theta_L = \theta_R = \frac{\pi}{2}$, $\phi_L = 0$, $\phi_R = \frac{\pi}{3}$ with a dissipation strength $\Gamma = 1000$ as function of the anisotropy Δ , which is varied from -1.5 to 1.5 , with a resolution of 600 points.

case for a totally mixed state.

The pure states ($S_{\text{VNE}} = 0$) occur, where density profiles have pure spin helix states. These were introduced above in Section 2.3.2. They occur at the predicted anisotropy values $\Delta = \cos \frac{\Phi + 2\pi m}{N-1}$ with $m = 0, 1, \dots, N-2$, which are marked by dashed lines in all figures of this case study. Using the notion of winding weights in Figure 5.3 the different helicities can be identified. Corresponding to these states, the steady state magnetization current j^z shown in Figure 5.3 is given by Equation (3.28).

In between two helical steady states, the spin chain undergoes transitions, during which the state of the system gets mixed (non-zero entropy) and different contributions of winding states occur. In Figure 5.3 the steady state transits from a helix state with winding $m = 2$ at $\Delta \approx -0.114$ to a helix state with winding $m = 3$ at $\Delta \approx -0.669$. In the intermediate range, a state with winding $m = 2$ remains dominant until suddenly at $\Delta \approx -0.7$ its contribution drops and eventually crosses the rising contribution of winding $m = 3$. This behavior is clearly visible in the current as well, where the $m = 3$ contribution leads to a sudden change of sign of the magnetization current (see [22]).

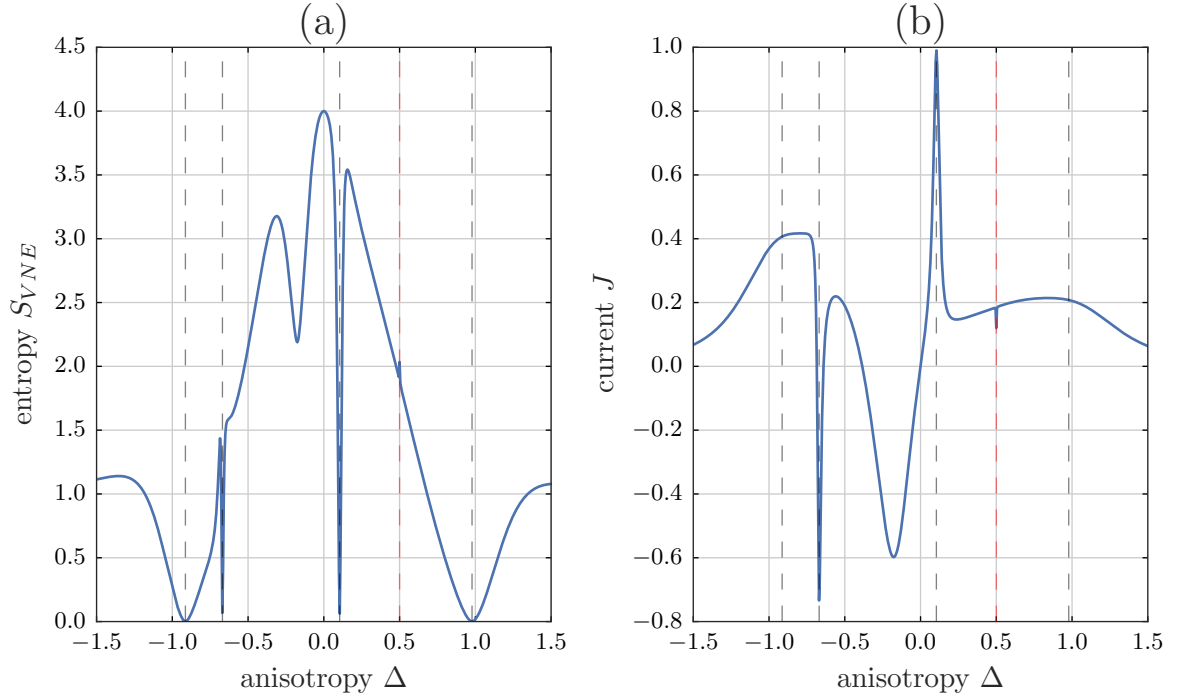


Figure 5.2: For a spin chain $N = 6$ and dissipatively targeted $\theta_L = \theta_R = \frac{\pi}{2}$, $\phi_L = 0$, $\phi_R = \frac{\pi}{3}$ and $\Gamma = 1000$ (a) shows the von Neumann entropy as function of the anisotropy and (b) shows the current as function of the anisotropy. The dashed lines indicate anisotropies for which pure helix states are predicted ($\Delta = \cos \frac{\Phi+2\pi m}{N-1}$) and the red one marks the anisotropy at which the spin helix state doesn't occur.

The behavior of these winding weights between the spin helix states of winding $m = 3$ at $\Delta \approx -0.669$ and the totally mixed state $\Delta = 0$ is more complex. The contribution of $m = 2$ and $m = 3$ remain dominant with a certain oscillating behavior until all windings have the same weight in the mixed state.

The fact that a transition from a pure winding state to another pure winding state always passes through an intermediate mixed phase, suggests to interpret these as topological sectors ¹.

It is striking that the predicted helix state with winding $m = 4$ at $\Delta = \cos \frac{15}{5} = \cos \frac{5}{3} = 0.5$ is suppressed. In Figure 5.4 the expected and the actually encountered spin configurations (polarization in XY-plane) are sketched. It is apparent that the first and the fourth spin would be

¹ The notion of a winding number immediately gives rise to associations with topology. Topology, as discussed in solid state systems, refers to topological invariants in the manifold in k -space that lead to the formation of edge states. The simplest model where topology can be described is the so-called *Su-Schrieffer-Heeger model* (or SSH model) [42]. In the spin chain context, the winding number describes an actual winding in spin space. Strictly speaking, the winding number is only well defined for parallel boundary spins. As far as this study is concerned, the incidence of winding numbers does not have any further consequences as robustness of the system against perturbations or the formation of edge states.

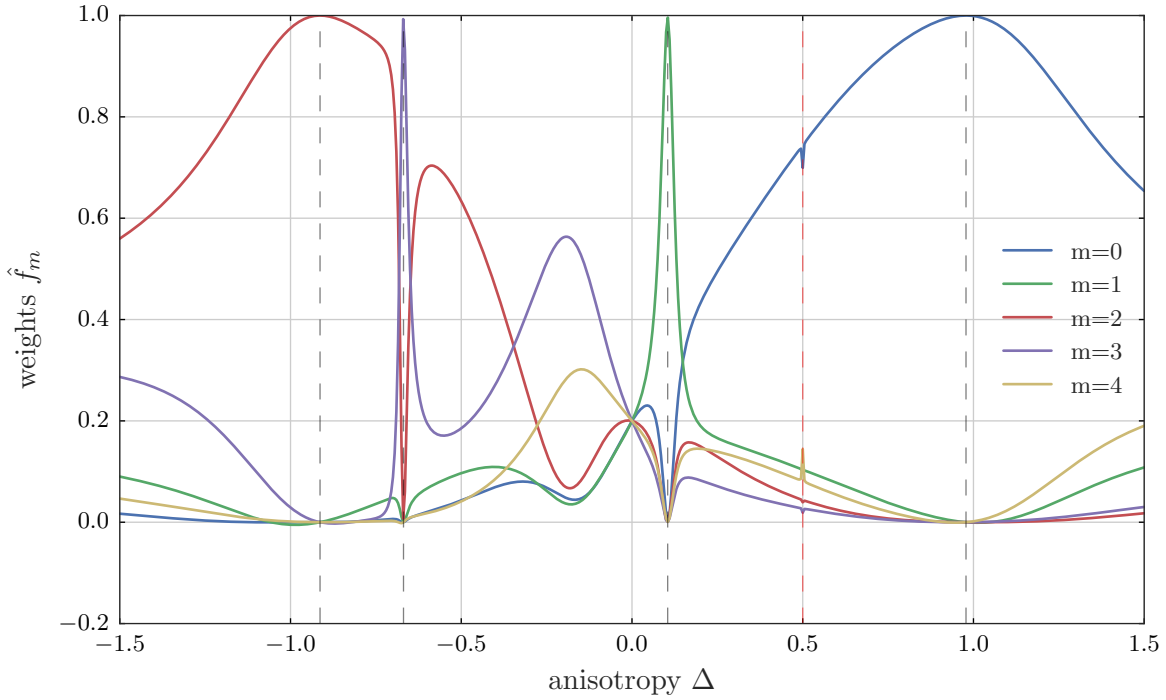


Figure 5.3: Weights for states with winding number m around Z-axis for a spin chain $N = 6$ and dissipatively targeted $\theta_L = \theta_R = \frac{\pi}{2}$, $\phi_L = 0$, $\phi_R = \frac{\pi}{3}$ and $\Gamma = 1000$. The dashed lines indicate anisotropies for which pure helix states are predicted ($\Delta = \cos \frac{\Phi + 2\pi m}{N-1}$) and the red one marks the anisotropy at which the spin helix state doesn't occur.

antiparallel in this situation.

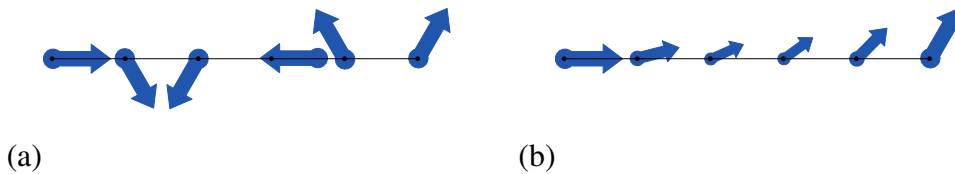


Figure 5.4: Sketches of (a) the expected steady state and (b) the actual steady state found by numerics of a chain with $N = 6$, $\theta = \frac{\pi}{2}$, $\phi_L = 0$, $\phi_R = \frac{\pi}{3}$ and anisotropy $\Delta = 0.5$. The size of the arrows is related to the pureness of the state and reconstructed from the expectation values for the X- and Y-components.

From this, the question arises whether we can find more points like this, for which the pure helix states are predicted but cannot form. In the next section, we will have a closer look at these points.

5.1.2 γ -Dependence

In this section, we identify these interesting points more systematically by fixing the left boundary spin to the x-axis and swiping through the incremental turning angle γ from 0 to π (still for $\theta = \frac{\pi}{2}$). The remaining parameters are chosen to fulfill conditions for the spin helix states to occur ($\phi_R = (N - 1)\gamma$ and $\Delta = \cos \gamma$). Naively, it is expected that the entropy for this scenario is zero except for $\gamma = \frac{1}{2}$ and, thus, $\Delta = 0$, as discussed in the previous section.

However, as can be seen at the exemplary plot for $N = 6$ in Figure 5.5 the entropy shows a couple of peaks, at fractions of π of the form $\frac{m\pi}{n}$ where $n, m \in \mathbb{N}$ and $m < N$. The low resolution of 120 points on this axis is not enough, to well resolve the singular points. A more formal treatment of this can be found in [25]. Physically, for these values of γ we encounter the same situation as in Figure 5.4: Whenever two or more spins in the chain should theoretically be collinear, a pure helix state fails to converge.

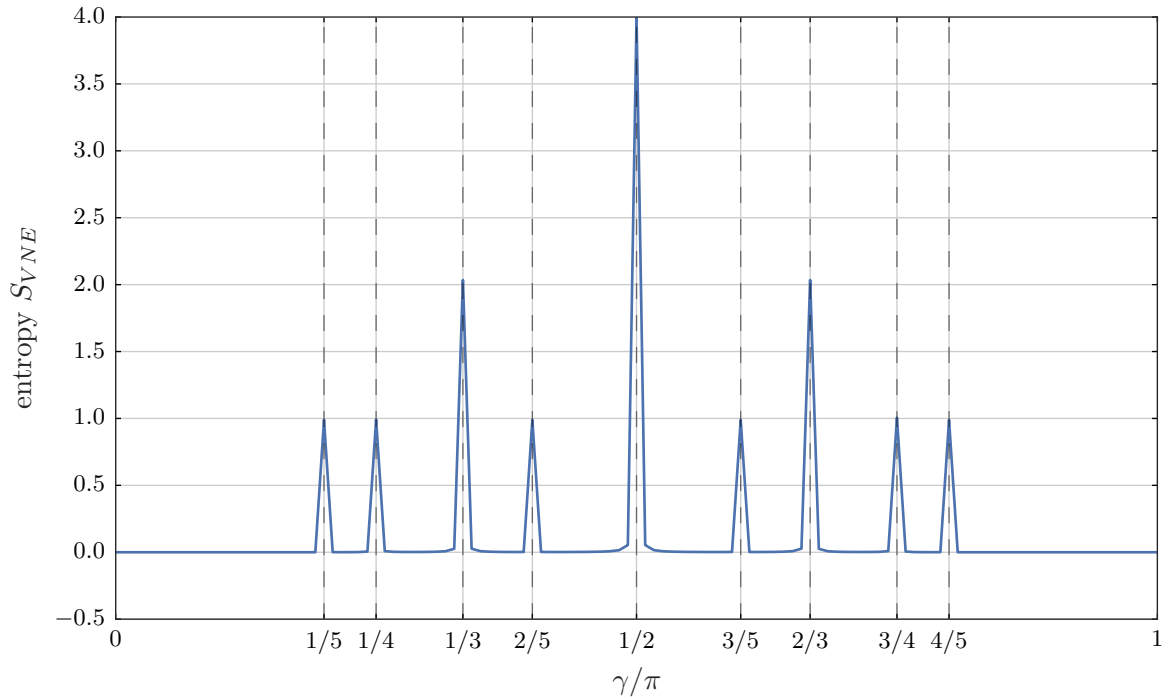


Figure 5.5: Entropy as function of the incremental turning angle γ for a spin chain of length $N = 6$, whose first spin is fixed via strong dissipation ($\Gamma = 1000$) to the X-axis and the last spin follows $\phi_R = (N - 1)\gamma$ and $\Delta = \cos \gamma$.

In Chapter 4.1.3, we mentioned that we can reliably determine the rank of the non-equilibrium steady state in Zeno limit by making use of the conditions on the states (Equation (4.46)) and the conditions on their weights (Equation (4.60)). We also argued that solving the system of

N	γ	rank	full rank
3	$\frac{\pi}{2}$	2	2
4	$\frac{\pi}{2}$	4	4
5	$\frac{\pi}{3}, \frac{2\pi}{3}$	2	8
	$\frac{\pi}{2}$	8	
	$\frac{\pi}{3}, \frac{2\pi}{3}$	5	
6	$\frac{\pi}{4}, \frac{3\pi}{4}$	2	16
	$\frac{\pi}{2}$	16	
	$\frac{\pi}{3}, \frac{2\pi}{3}$	11	
	$\frac{\pi}{4}, \frac{3\pi}{4}$	6	
7	$\frac{\pi}{5}, \dots, \frac{4\pi}{5}$	2	32
	$\frac{\pi}{2}$	32	
	$\frac{\pi}{3}, \frac{2\pi}{3}$	22	
	$\frac{\pi}{4}, \frac{3\pi}{4}$	16	
	$\frac{\pi}{5}, \dots, \frac{4\pi}{5}$	7	
8	$\frac{\pi}{6}, \frac{5\pi}{6}$	2	64
	$\frac{\pi}{2}$	64	
	$\frac{\pi}{3}, \frac{2\pi}{3}$	43	
	$\frac{\pi}{4}, \frac{3\pi}{4}$	36	
	$\frac{\pi}{5}, \dots, \frac{4\pi}{5}$	22	
	$\frac{\pi}{6}, \frac{5\pi}{6}$	8	
	$\frac{\pi}{7}, \dots, \frac{6\pi}{7}$	2	
9	$\frac{\pi}{2}$	128	128
	$\frac{\pi}{3}, \frac{2\pi}{3}$	85	
	$\frac{\pi}{4}, \frac{3\pi}{4}$	72	
	$\frac{\pi}{5}, \dots, \frac{4\pi}{5}$	57	
	$\frac{\pi}{6}, \frac{5\pi}{6}$	29	
	$\frac{\pi}{7}, \dots, \frac{6\pi}{7}$	9	
	$\frac{\pi}{8}, \frac{3\pi}{8}, \frac{5\pi}{8}, \frac{7\pi}{8}$	2	

Table 5.1: Summary of ranks for various spin chains of lengths $N \leq 9$ with anisotropy $\Delta = \cos \frac{m\pi}{n}$ and $m, n \in \mathbb{N}$. Solving the system of equation 4.60, we obtain a vector $|nu\rangle$. As we are dealing with numerical data, we used an absolute tolerance of $a_{tol} = 10^{-10}$ to determine which entries of the vector are zero. The γ values highlighted in red will be treated in Section 5.1.3.

equations defined by the stochastic matrix, makes larger system sizes amenable. In Table 5.1, we summarize the ranks of the non-equilibrium steady states, which occur for incremental turning angles γ of the form $\frac{m\pi}{n}$ up to $N = 9$. At this point, we are limited to systems $N \leq 9$, since we have to count the zero (or non-zero) eigenvalues for the determination of the rank. For larger systems, it gets more difficult to distinguish numerically between zero values from small, finite values. In Table 5.1, we assumed the eigenvalue to be zero up to a threshold $v_\alpha < 10^{-10}$.

We re-confirm that the non-equilibrium steady state has full rank for $\gamma = \frac{\pi}{2}$ ($\Delta = 0$). Having identified the ranks of these particular values of the incremental turning angle γ for system lengths $N \leq 9$ (cf. Table 5.1), certain patterns for the ranks could be identified:

$$r\left(\frac{\pi}{N-1}\right) = 2, \quad (5.1)$$

$$r\left(\frac{\pi}{N-2}\right) = N, \quad (5.2)$$

$$r\left(\frac{\pi}{N-3}\right) = 1 + \binom{N-1}{2}, \quad (5.3)$$

$$r\left(\frac{\pi}{N-4}\right) = 149 - 49\binom{N-1}{1} + 13\binom{N-1}{2} - \binom{N-1}{3}, \quad (5.4)$$

where the usual binomial coefficients are defined by $\binom{n}{k} = \frac{n!}{k!(n-k)!}$. This suggests a general formula for the rank of a spin chain with length N and an incremental turning angle $\gamma = \frac{\pi}{N-x}$ with $x \in \mathbb{N}$

$$r\left(\frac{\pi}{N-x}\right) = \alpha_1 \binom{N-1}{0} + \alpha_2 \binom{N-1}{1} + \cdots + \alpha_x \binom{N-1}{x-1}. \quad (5.5)$$

For the next rank $r\left(\frac{\pi}{N-5}\right)$, we require the corresponding five values to determine the five occurring integer coefficients α_i with $i = 1, \dots, 5$.

In the last section, we found that, whenever two spins in the chain are collinear, a pure helix state fails to converge. We analyzed similar situations for up to $N \leq 9$ and found a pattern in the ranks of the resulting steady state density matrices. In the following section, we confirm our physical intuition for simple cases and analytically determine the corresponding non-equilibrium steady state.

5.1.3 Analytical Results for Small Systems $N = 3, 4, 5$

We investigated three simple situations with few degrees of freedom (marked in red in Table 5.1). In that way, using the Software Wolfram Mathematica and employing the exact analytical expressions for the perturbation theory, we got analytical results for the density matrices with dependence on the following parameters:

Case 1: $N = 3, \gamma = \pi/2, \theta = \theta_L = \theta_R, \phi_L = 0, \phi_R = \pi$

Consider a system of three spins: In Zeno limit we target a pure state at the boundaries, where

the first spin points along positive X-direction and last spin point along negative X-direction ($\phi_L = 0, \phi_R = \pi$), but this time with a variable polar angle ($\theta_L = \theta_R = \theta$). The incremental twisting angle is $\gamma = \frac{\pi}{2}$ and the anisotropy is $\Delta = \cos \gamma = 0$. For $\theta = \frac{\pi}{2}$, we expect a totally mixed state, but the dependence on θ is non-trivial. The remaining spin in the middle is pure and we chose a general ansatz for its density matrix

$$\rho_{11}(\theta) = \frac{1 + A(\theta)}{2} \quad (5.6)$$

$$\rho_{22}(\theta) = \frac{1 - A(\theta)}{2}. \quad (5.7)$$

At first order of the stationary perturbation theory, we added a general traceless auxiliary matrix

$$m^{(1)} = \begin{pmatrix} a & b \\ c & -a \end{pmatrix}. \quad (5.8)$$

At the secular condition $\text{Tr}_{1,N}([H, \rho^{(0)}]) = 0$, the free parameter $A(\theta)$ was determined and fixed the density matrix to

$$\rho(\theta) = \begin{pmatrix} \frac{2 \cos(\theta)}{\cos(2\theta)+3} + \frac{1}{2} & 0 \\ 0 & \frac{4 \sin^4(\frac{\theta}{2})}{\cos(2\theta)+3} \end{pmatrix}. \quad (5.9)$$

Case 2: $N = 4, \gamma = \pi/3, \theta = \theta_L = \theta_R, \phi_L = 0, \phi_R = \pi$

Similarly, we looked at a system of four spins with anti-parallel boundary spins, with $\gamma = \frac{\pi}{3}$ and have $\Delta = \frac{1}{2}$. This time, we chose an ansatz for the bulk, where both spins are expressed in the most general density matrix with a total of 16 variables (remember Equation(2.8)). Again, at first order, a general, traceless auxiliary matrix $m^{(1)}$ was added (+ 15 variables). At the secular condition $\text{Tr}_{1,N}([H, \rho^{(0)}]) = 0$, the initial 16 variables were completely determined resulting in a density matrix

$$\rho(\theta) = \begin{pmatrix} \frac{16 \cos^4(\frac{\theta}{2})(3 \cos(2\theta)+13)}{60 \cos(2\theta)+9 \cos(4\theta)+187} & -\frac{2(3 \cos(2\theta)+13) \cot(\frac{\theta}{2}) \sin^2(\theta)}{60 \cos(2\theta)+9 \cos(4\theta)+187} & \frac{2(3 \cos(2\theta)+13) \cot(\frac{\theta}{2}) \sin^2(\theta)}{60 \cos(2\theta)+9 \cos(4\theta)+187} & -\frac{4(3 \cos(2\theta)+13) \sin^2(\theta)}{60 \cos(2\theta)+9 \cos(4\theta)+187} \\ -\frac{2(3 \cos(2\theta)+13) \cot(\frac{\theta}{2}) \sin^2(\theta)}{60 \cos(2\theta)+9 \cos(4\theta)+187} & \frac{\sin(\theta)(25 \sin(\theta)-3 \sin(3\theta))}{60 \cos(2\theta)+9 \cos(4\theta)+187} & -\frac{4(3 \cos(2\theta)+1) \sin^2(\theta)}{60 \cos(2\theta)+9 \cos(4\theta)+187} & \frac{2(3 \cos(2\theta)+13) \sin^2(\theta) \tan(\frac{\theta}{2})}{60 \cos(2\theta)+9 \cos(4\theta)+187} \\ \frac{2(3 \cos(2\theta)+13) \cot(\frac{\theta}{2}) \sin^2(\theta)}{60 \cos(2\theta)+9 \cos(4\theta)+187} & -\frac{4(3 \cos(2\theta)+1) \sin^2(\theta)}{60 \cos(2\theta)+9 \cos(4\theta)+187} & \frac{\sin(\theta)(25 \sin(\theta)-3 \sin(3\theta))}{60 \cos(2\theta)+9 \cos(4\theta)+187} & \frac{2(\cos(\theta)-1)(3 \cos(2\theta)+13) \sin(\theta)}{60 \cos(2\theta)+9 \cos(4\theta)+187} \\ -\frac{4(3 \cos(2\theta)+13) \sin^2(\theta)}{60 \cos(2\theta)+9 \cos(4\theta)+187} & \frac{2(3 \cos(2\theta)+13) \sin^2(\theta) \tan(\frac{\theta}{2})}{60 \cos(2\theta)+9 \cos(4\theta)+187} & \frac{2(\cos(\theta)-1)(3 \cos(2\theta)+13) \sin(\theta)}{60 \cos(2\theta)+9 \cos(4\theta)+187} & \frac{16(3 \cos(2\theta)+13) \sin^4(\frac{\theta}{2})}{60 \cos(2\theta)+9 \cos(4\theta)+187} \end{pmatrix} \quad (5.10)$$

The diagonalization of this matrix revealed that only two eigenvalues are non-zero for all polar

angles θ

$$\nu_1(\theta) = \frac{13 + 3 \cos 2\theta^2}{187 + 60 \cos 2\theta + 9 \cos 4\theta} \quad (5.11)$$

$$\nu_2(\theta) = \frac{36 \sin \theta^4}{187 + 60 \cos 2\theta + 9 \cos 4\theta} \quad (5.12)$$

$$\nu_3(\theta) = \nu_4(\theta) = 0, \quad (5.13)$$

which was tested against the exact diagonalization results in Figure 5.6 and which is consistent with the prediction in Table 5.1 for $\theta = \frac{\pi}{2}$. Furthermore, a look at the winding weights revealed that the windings $m = 1$ and $m = 2$ have the same weight for all θ , see Figure 5.6.

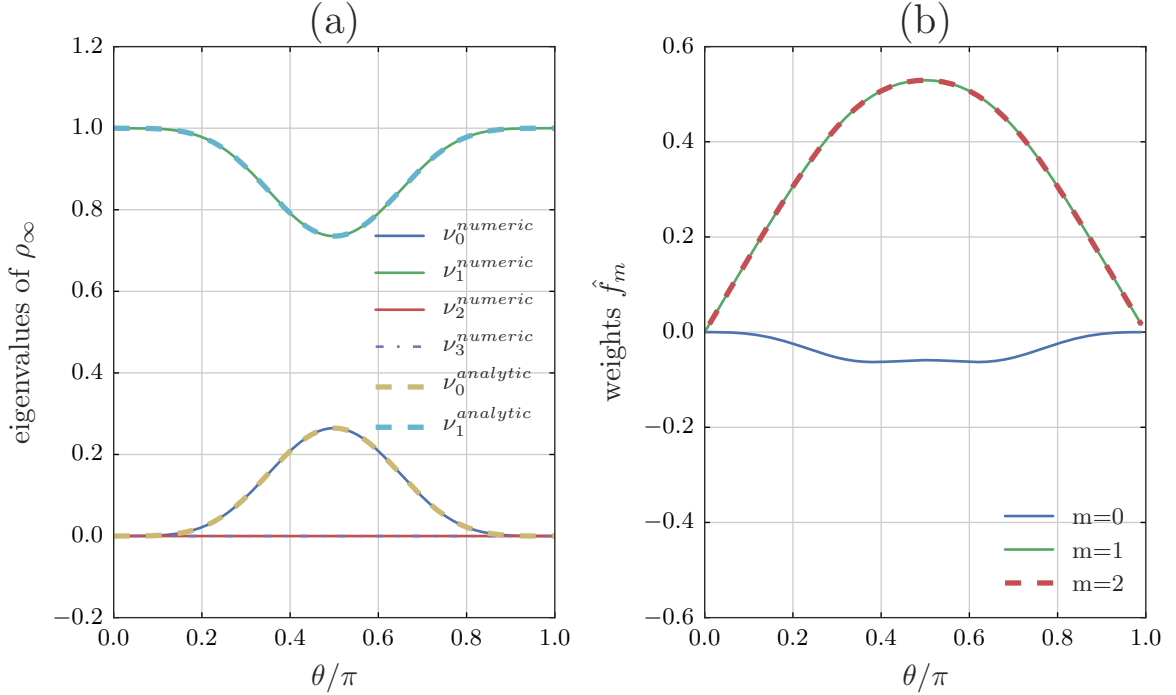


Figure 5.6: (a) Eigenvalues of the density matrix and (b) winding weights as function of polar angle θ for a spin chain $N = 4$, $\gamma = \pi/3$, $\theta = \theta_L = \theta_R$, $\phi_L = 0$, $\phi_R = \pi$. We were able to analytically solve the Lindblad master equation via perturbation theory and obtained analytical expressions (5.11) - (5.13) for the eigenvalues of the density matrix depending on θ . This result was confirmed by exact diagonalization.

Case 3: $N = 5, \gamma = \pi/3, \theta = \theta_L = \theta_R = \pi/2, \phi_L = 0, \phi_R = 4\pi/3$

In the same way, we investigated the situation for five spins with $\gamma = \pi/3$ and a boundary gradient $\Phi = 4\pi/3$. Due to exponentially growing complexity, we restricted this example to $\theta = \pi/2$. The density matrix could be determined and is given in the Appendix C. The diagonalization returned exactly five non-zero eigenvalues out of eight (see Table 5.3).

We diagonalized the dissipation-projected Hamiltonian for this situation and found that the eigenvalue equal to zero is two times degenerate. The corresponding eigenvectors can be found in Appendix C. Furthermore, we identified the eigenvectors of the steady state ρ_∞ with the eigenvectors of h_{00} by calculating the elements $\langle \alpha | \rho_\infty | \beta \rangle$, where $\alpha, \beta = 0, \dots, 7$. In Table 5.3, we listed the results for the identification. Note that the degeneracy subspace is spanned by the eigenvectors $|6\rangle, |7\rangle$ and any orthogonal combination can be chosen to be the proper basis. Analytically, we know that the spin helix state corresponding to the boundary gradient $\Phi = \frac{4\pi}{3}$ is an eigenvector of h_{00} and we found it to be this subspace. We also set the spin helix state as first basis vector of the degenerate subspace and obtained the second via Gram-Schmidt orthogonalization.

We checked explicitly that ρ_∞ obeys the reversal symmetry in Equation (2.35) and confirmed that the five projectors, which it is composed of, do as well.

spin	$\langle \sigma_x \rangle$	$\langle \sigma_y \rangle$	$\langle \sigma_z \rangle$
1	1	0	0
2	0.678414	-0.244166	0
3	0.193833	-0.335728	0
4	-0.127753	-0.709607	0
5	-0.5	-0.866	0

Table 5.2: Density profile of the non-equilibrium steady state for $N = 5, \gamma = \pi/3, \theta = \theta_L = \theta_R = \pi/2, \phi_L = 0, \phi_R = 4\pi/3$.

The analytic treatment again confirmed the calculation of ranks via the stochastic matrix F . Furthermore, we have seen that the appearance of rank 2 states is linked to symmetrical setups in which exactly two winding states play equally dominant roles. In the next section, we produce a situation for which a pure helix state description breaks down and a rank 2 state is generated.

	analytic ν_α	numeric ν_α	eigenvectors of h_{00}	using $ \Psi_{\text{helix}}^\perp\rangle$
ν_1	$\frac{9}{908} (33 + 7\sqrt{17})$	0.6132	$ 5\rangle$	
ν_2	$\frac{1}{227} (37 + 8\sqrt{10})$	0.2744	$A 7\rangle + B 8\rangle$	$\frac{3i\sqrt{5}(3i+\sqrt{5})}{-10+8\sqrt{10}} \Psi_{\text{helix}}\rangle + \Psi_{\text{helix}}^\perp\rangle$
ν_3	$\frac{1}{227} (37 - 8\sqrt{10})$	0.0515	$C 7\rangle + D 8\rangle$	$\frac{3\sqrt{5}(3-i\sqrt{5})}{10+8\sqrt{10}} \Psi_{\text{helix}}\rangle + \Psi_{\text{helix}}^\perp\rangle$
ν_4	$\frac{9}{908} (33 - 7\sqrt{17})$	0.0410	$ 4\rangle$	
ν_5	$\frac{9}{454}$	0.0198	$ 2\rangle$	
ν_6	0	0	$ 1\rangle$	
ν_7	0	0	$ 3\rangle$	
ν_8	0	0	$ 6\rangle$	

Table 5.3: The eigenvectors of the non-equilibrium steady state for $N = 5, \gamma = \pi/3, \theta = \theta_L = \theta_R = \pi/2, \phi_L = 0, \phi_R = 4\pi/3$ are given in its analytic representation and its numerical values. We identified the corresponding eigenvectors with eigenvectors of the dissipation-projected Hamiltonian h_{00} . In the last column we used the fact, that one spin helix state is an eigenvector of h_{00} in the degenerate subspace, built a basis in that subspace via Gram-Schmidt orthogonalization and expressed the eigenvectors of ρ in terms of this new basis.

5.1.4 Breakdown of Pure Description

The system we treat here consists of $N = 4$ spins with a boundary gradient $\Phi = \frac{\pi}{3}$ and spins lying in XY-plane $\theta = \pi/2$. The dissipation strength was chosen to be $\Gamma = 1000$ for the numerics. In Figure 5.7, we look at the entropy and the winding weights for variable anisotropy in -1.5 to 1.5 and observe what happens if the boundary gradient is slightly tilted towards the X-axis and finally is $\Phi = 0$.

We directed our focus on the two pure helix states with winding $m = 1$ and $m = 2$ which arise at $\Delta_{m=1} = -0.766$ and $\Delta_{m=2} = -0.174$ for $\Phi = \frac{\pi}{3}$. First, we note that for four sites, there is a total of $N - 1 = 3$ different windings. Two clockwise windings $m = 2$ correspond to one anticlockwise winding $m = -1$.

When decreasing the boundary gradient Φ , the two anisotropies at which pure helix states occur approach each other. For $\Phi = \frac{\pi}{100}$, we observe two closely singular kinks in the entropy related to the pure states and a sudden change from unit contribution of $m = 1$ to $m = -1$. In the case of parallel boundaries, however, these two windings have the same contribution. The third weight for $m = 0$ is small but finite because the helix states are not mutually orthogonal. The entropy at $\Delta = -0.5$ is $S_{\text{VNE}} \approx 1$, which can be understood when diagonalizing the

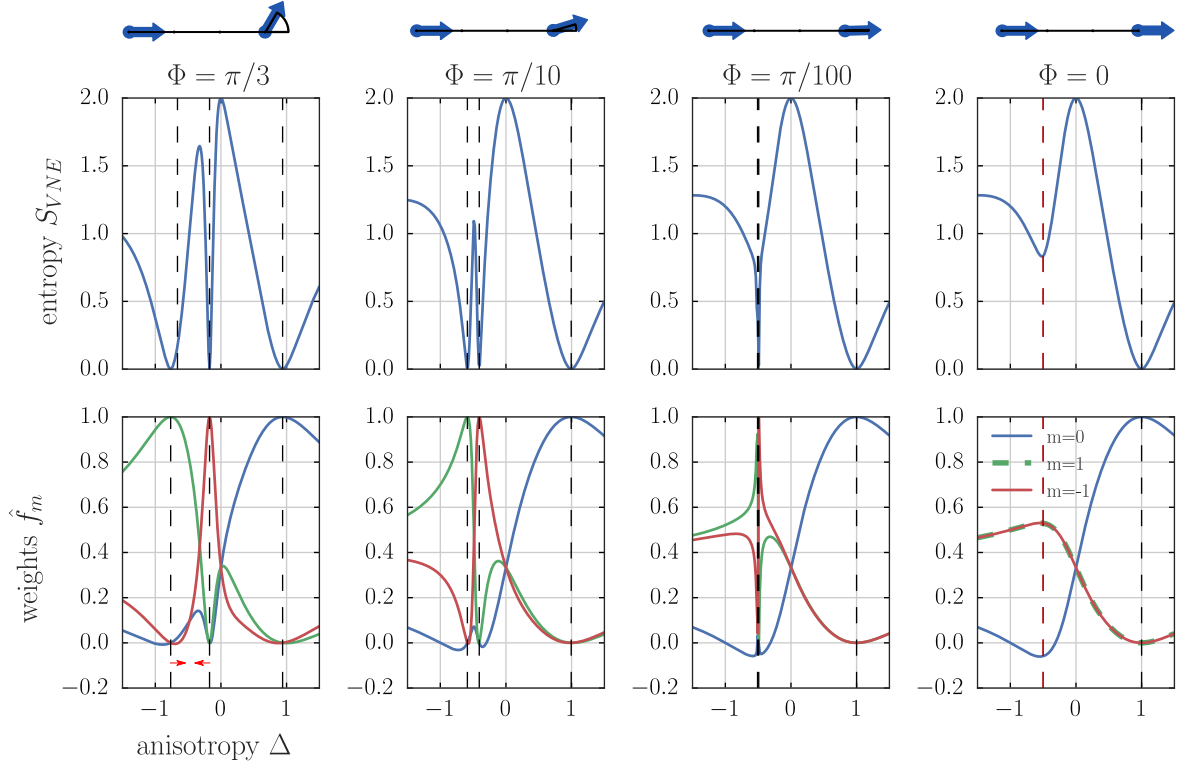


Figure 5.7: Entropy and winding weights for the breakdown of the pure helix state description for a spin chain $N = 4$ with changing boundary gradient Φ . The boundary setting is illustrate above each column. From left to right the boundary gradient is decreased. The dashed lines indicate anisotropies for which pure helix states are predicted ($\Delta = \cos \frac{\Phi+2\pi m}{N-1}$). The anisotropies at which the helix states with $m = 1$ and $m = -1$ occur, approach each other (red arrows) until they coincide (red dashed line)

corresponding density matrix. It has two eigenvalues

$$\nu_0 = 0,265 \quad (5.14)$$

$$\nu_1 = 0,735 \quad (5.15)$$

$$\rightarrow S_{\text{VNE}} = 0.834. \quad (5.16)$$

The above generation of a rank 2 state suggests that for the symmetrical setup of parallel boundary spins, two helix states with opposite winding number are superposed. In the following, we made an ansatz to describe the reduced density matrix of the non-equilibrium steady state. The bulk density matrix is hermitian and has only two eigenvalues and, thus, can be build by

two eigenvectors which need to be orthogonal. We expect it to be of the following form

$$|u\rangle = |\Psi_{\text{helix}}(+)\rangle \quad (5.17)$$

$$|v\rangle = |\Psi_{\text{helix}}(-)\rangle \quad (5.18)$$

$$\rho = \lambda_1 |u\rangle\langle u| + \lambda_2 |v\rangle\langle v|, \quad (5.19)$$

with $\lambda_{1/2}$ being related to the winding weights. Unfortunately, for even system sizes the spin helix states are not orthogonal to each other and the overlap is finite and real

$$\langle u|v\rangle = \eta \neq 0 \quad (5.20)$$

$$\eta = \eta^*. \quad (5.21)$$

We took this into account and used the following ansatz

$$\rho(B) = |u\rangle\langle u| + |v\rangle\langle v| + B(|u-v\rangle\langle u-v|) \quad (5.22)$$

$$\Leftrightarrow \rho(B)|u\rangle = |u\rangle + \langle v|u\rangle|v\rangle + B|u-v\rangle(\langle u|u\rangle - \langle v|u\rangle), \quad (5.23)$$

using $\langle u|v\rangle = \eta$ and $\langle u|u\rangle = 1$ (same for v) to get the system of equations

$$\rho(B)|u\rangle = |u\rangle + \eta|v\rangle + B|u-v\rangle(1-\eta) \quad (5.24)$$

$$\rho(B)|v\rangle = |v\rangle + \eta|u\rangle + B|u-v\rangle(\eta-1) \quad (5.25)$$

where we can set $b = B(1-\eta)$ and obtain

$$\rho \begin{pmatrix} |u\rangle \\ |v\rangle \end{pmatrix} = \begin{pmatrix} 1+b & \eta-b \\ \eta-b & 1+b \end{pmatrix} \begin{pmatrix} |u\rangle \\ |v\rangle \end{pmatrix}. \quad (5.26)$$

Solving for eigenvalues of the matrix, we find that

$$\lambda_1 = 1 + \eta \quad (5.27)$$

$$\lambda_2 = 1 - \eta + 2b, \quad (5.28)$$

with the corresponding eigenvectors

$$e_{\lambda_1} = \begin{pmatrix} 1 \\ 1 \end{pmatrix} \quad \& \quad e_{\lambda_2} = \begin{pmatrix} -1 \\ 1 \end{pmatrix}. \quad (5.29)$$

On the one hand, we know the ratio of the eigenvalues we obtain

$$\frac{\lambda_1(B)}{\lambda_2(B)} = \frac{1 + \eta}{1 - \eta} \frac{1}{1 + 2B}, \quad (5.30)$$

and on the other hand, in the case of N being even and $\theta = \frac{\pi}{2}$, we have been able to obtain such ratios of the eigenvalues numerically

$$N = 4 : \frac{3^2}{5^2} \quad (5.31)$$

$$N = 6 : \frac{17^2}{15^2}. \quad (5.32)$$

Furthermore, as for N even and $\theta = \frac{\pi}{2}$ the overlap of two spin helix states with opposite windings can be shown to be $\eta = \langle u|v \rangle = \left(\frac{i}{2}\right)^{N-2}$, we deduce

$$\frac{\lambda_1(B)}{\lambda_2(B)} = \left(\frac{\lambda_1(0)}{\lambda_2(0)}\right)^2 = \left(\frac{1 + \eta}{1 - \eta}\right)^2 \quad (5.33)$$

$$\rightarrow B = -\frac{\eta}{1 + \eta} = \frac{4}{-4 + \left(\frac{i}{2}\right)^{-N}}. \quad (5.34)$$

Here, we used mainly heuristic arguments. It is instructive to see that in the limit of $N \rightarrow \infty$, the spin helix states will be orthogonal and, thus, B must be 0. In the following, we assume that the pattern for the ratio remains of the type $\eta = \frac{((N-2)^2 \mp 1)^2}{((N-2)^2 \pm 1)^2}$. Inserting B into the ansatz, one can show with some algebra that

$$\rho(\eta) = |u\rangle \langle u| + |v\rangle \langle v| - \frac{1}{1 + 2^{N-2}} |u - v\rangle \langle u - v|. \quad (5.35)$$

From the eigenvectors in Equation (5.29), we deduced that the eigenvectors of the density matrix are of the form $|u \pm v\rangle$. Exploiting this, we can express our vectors in the following form:

$$|u\rangle = \frac{1}{2} |u + v + (u - v)\rangle \quad (5.36)$$

$$|v\rangle = \frac{1}{2} |u + v - (u - v)\rangle. \quad (5.37)$$

Plugging this into the earlier result (5.35) and normalizing to $Tr(\rho) = 1$, we get

$$\rho = \frac{(1 + \eta) |u + v\rangle \langle u + v| + (1 - \eta) |u - v\rangle \langle u - v|}{2((1 + \eta)^2 + (1 - \eta)^2)}. \quad (5.38)$$

For N being odd, one can perform the same calculation noting that the overlap for general θ is given by

$$\langle u | v \rangle = i \cos(\theta). \quad (5.39)$$

In order to avoid the overlap being imaginary (and, thus, being able to reuse the above procedure), we can multiply by a phase

$$|u\rangle = e^{-i\frac{\pi}{4}} |\tilde{v}\rangle \quad (5.40)$$

$$|v\rangle = e^{i\frac{\pi}{4}} |\tilde{v}\rangle \quad (5.41)$$

$$\langle \tilde{u} | \tilde{v} \rangle = \cos(\theta) = \eta_{\text{odd}}. \quad (5.42)$$

By performing the exact same steps as before, we end up with

$$\rho = \frac{(1 + \eta_{\text{odd}}) |\tilde{u} + \tilde{v}\rangle \langle \tilde{u} + \tilde{v}| + (1 - \eta_{\text{odd}}) |\tilde{u} - \tilde{v}\rangle \langle \tilde{u} - \tilde{v}|}{2((1 + \eta_{\text{odd}})^2 + (1 - \eta_{\text{odd}})^2)}. \quad (5.43)$$

Let us summarize. In the preceding Section 5.1.1, we presented an exemplary analysis of the non-equilibrium steady states of a setting, in which the boundary spin polarizations are fixed via dissipation to certain azimuthal angles, while the anisotropy was variable. Over the course of the study, many situations like this have been investigated and the systematics behind the appearance of particular (singular) points of Γ has become clearer. We found a pattern that we explained in Section 5.1.2. Using the example of small systems and treating them analytically in Section 5.1.3, we furthermore, showed that the eigenvectors contributing to these states of reduced rank have a simple structure. The precise structure for situations, in which a rank 2 state appears, was understood and could be generated as demonstrated in 5.1.4. The aim of the following section is to formalize our findings of the appearance of rank 2 states by stating a hypothesis. Subsequently, this hypothesis will be supported by numerical and analytical evidence.

5.2 Rank 2 Hypothesis

Hypothesis 1 Consider a boundary-driven XXZ model in 1D as introduced in 2.3 with parameters $\Gamma \rightarrow \infty$ (in Zeno limit), targeted states at the boundary defined by polar angles $\theta_L = \theta_R = \theta$ and boundary gradients $\Phi = \varphi_R - \varphi_L = 0, \pm\pi$. The anisotropy is $\Delta = \cos \gamma$ with $\gamma = (\Phi + 2\pi m)/(N - 1)$ and $m = 0, 1, \dots, N - 2$, but excluding explicitly all γ of the form $\frac{x\pi}{y}$ with $x, y \in \mathbb{N}^+$ for which the fraction $\frac{x}{y}$ can be reduced and for which $x = 0$. For these settings, the dissipation-projected Hamiltonian $h_{00} = \langle e^0 | H | e^0 \rangle$ has two degenerate eigenvectors with eigenvalue zero of spin helix structure (2.31) with opposite winding

$$|\Psi_{helix}(+)\rangle = \begin{cases} |\Psi_{helix}(\theta, \varphi)\rangle, & \text{when } N \text{ is even,} \\ e^{i\frac{\pi}{4}} |\Psi_{helix}(\theta, \varphi)\rangle, & \text{when } N \text{ is odd,} \end{cases} \quad (5.44)$$

$$|\Psi_{helix}(-)\rangle = \begin{cases} |\Psi_{helix}(\theta, -\varphi)\rangle, & \text{when } N \text{ is even,} \\ e^{-i\frac{\pi}{4}} |\Psi_{helix}(\theta, -\varphi)\rangle, & \text{when } N \text{ is odd,} \end{cases} \quad (5.45)$$

and an overlap $\langle \Psi_{helix}(+) | \Psi_{helix}(-) \rangle = \eta$, $\eta^* = \eta$. Building an orthonormal basis out of these eigenvectors

$$|0\rangle = \frac{1}{\sqrt{2}} \frac{1}{\sqrt{1+\eta}} (|\Psi_{helix}(+)\rangle + |\Psi_{helix}(-)\rangle), \quad (5.46)$$

$$|1\rangle = \frac{1}{\sqrt{2}} \frac{1}{\sqrt{1-\eta}} (|\Psi_{helix}(+)\rangle - |\Psi_{helix}(-)\rangle), \quad (5.47)$$

one can obtain, making use of $h_{j0} |\Psi_{helix}\rangle = \kappa(\theta, \varphi) \delta_{j,1} |\Psi_{helix}\rangle$ where $\kappa(\varphi, \theta) = -i\sqrt{2} \sin \theta \sin \varphi$, that

$$h_{j0} |0\rangle = a_0, \delta_{j,1} |1\rangle \quad \text{with } a_0 = \sqrt{\frac{1-\eta}{1+\eta}} \kappa(\varphi, \theta), \quad (5.48)$$

$$h_{j0} |1\rangle = a_1, \delta_{j,1} |0\rangle \quad \text{with } a_1 = \sqrt{\frac{1+\eta}{1-\eta}} \kappa(\varphi, \theta), \quad (5.49)$$

and, consequently, the following elements of the stochastic matrix F (see Equation (4.63))

$$F_{1,0} \equiv \omega_{0 \rightarrow 1} = |a_0|^2, \quad (5.50)$$

$$F_{0,1} \equiv \omega_{1 \rightarrow 0} = |a_1|^2 \quad (5.51)$$

$$F_{\alpha,0} = F_{\alpha,1} = 0, \quad \alpha > 1. \quad (5.52)$$

Following the line of argumentation in Section 4.1.3, such a setup leads to the generation of a non-equilibrium steady state of rank 2 with eigenvalues determined by (4.60) and (5.52)

$$\lim_{\Gamma \rightarrow \infty} \rho_{NESS}(\Gamma) = |e^0\rangle \langle e^0| \otimes (v_1 |1\rangle \langle 1| + v_2 |2\rangle \langle 2|) \quad (5.53)$$

$$v_1 = \frac{(1 + \eta)^2}{2 + 2\eta^2}$$

$$v_2 = 1 - v_1 = \frac{(1 - \eta)^2}{2 + 2\eta^2}.$$

The above hypothesis asserts in simpler terms that the non-equilibrium steady state for a boundary-driven XXZ chain, where first and last spin are dissipatively set parallel or antiparallel, avoiding situations of (anti)parallel spins in the bulk and excluding $\Delta = -1, 0, 1$, can be described by two spin helix states of opposite winding. Intuitively, a superposition of states with positive and negative windings makes sense, since due to symmetry no direction is preferred. Note that our conclusion (5.53) assumes generic non-zero elements of the stochastic matrix $F_{\alpha,\beta} \neq 0$ for $\beta > 1$. Heuristically, from Mathematica, analyzing systems of finite size $N \leq 10$ in these setups, we can confirm this.

A general form of the overlap η can be obtained heuristically

$$\eta(N, \theta) = \begin{cases} \sum_{n=0}^{(N-2)/2} A_n \cos((2n)\theta), & \text{when } N \text{ is even,} \\ \sum_{n=0}^{(N-2-1)/2} B_n \cos((2n+1)\theta), & \text{when } N \text{ is odd,} \end{cases} \quad (5.54)$$

$$(5.55)$$

and coefficients for small systems $N \leq 8$ are listed in the Tables 5.4. Note that for the particular

polar angle $\theta = \frac{\pi}{2}$, the expression for the overlap simplifies to

$$\eta(N, \frac{\pi}{2}) = \begin{cases} \left(\frac{i}{2}\right)^{N-2}, & \text{when } N \text{ is even,} \\ 0, & \text{when } N \text{ is odd,} \end{cases} \quad (5.56)$$

$$(5.57)$$

where for odd systems, the corresponding spin helix states of opposite winding are orthogonal and the overlap vanishes.

N	A_0	A_1	A_2	A_3	N	B_0	B_1	B_2
4	$-\frac{5}{8}$	$-\frac{3}{8}$	0	0	3	1	0	0
6	$\frac{63}{128}$	$\frac{60}{128}$	$\frac{5}{128}$	0	5	$-\frac{7}{8}$	$-\frac{1}{8}$	0
8	$-\frac{858}{2048}$	$-\frac{1001}{2048}$	$-\frac{182}{2048}$	$-\frac{7}{2048}$	7	$\frac{198}{256}$	$\frac{55}{256}$	$\frac{3}{256}$
(a)					(b)			

Table 5.4: Coefficients for the overlap η for (a) even and (b) odd system size and a boundary gradient $\Phi = \pi$.

The hypothesis forms a basis for discussion and can be tested. In the following, we will provide supporting evidence for it and even proof its validity for small system sizes up to $N = 13$. We start by presenting results from exact diagonalization.

5.2.1 Numerical Evidence

For system sizes which are solvable via exact diagonalization we checked the predicted state (5.53) against the numerical non-equilibrium steady state and obtained correspondence up to errors of the order $\frac{1}{\Gamma}$. However, we focused the numerical investigation on the parallel boundary spins $\Phi = 0$, where the anisotropy is simplified to $\cos((2\pi m)/(N-1))$ and N is even to ensure $N-1$ being prime. By setting $N-1$, we naturally exclude all reducible fractions of γ . In the Δ -dependence plot for the entropy and the Fourier coefficients in Figure 5.8, one clearly sees that two windings dominate with the same weights denoted with dashed lines. We explicitly checked the numerically obtained non-equilibrium steady states to the predicted ones and found agreement up to corrections $1/\Gamma$, due to the numerically finite dissipation strength.

As a side remark, we notice that the rank 2 state has no net magnetization current. This is particularly interesting, because the two spin helix states that it consists of carry a current.

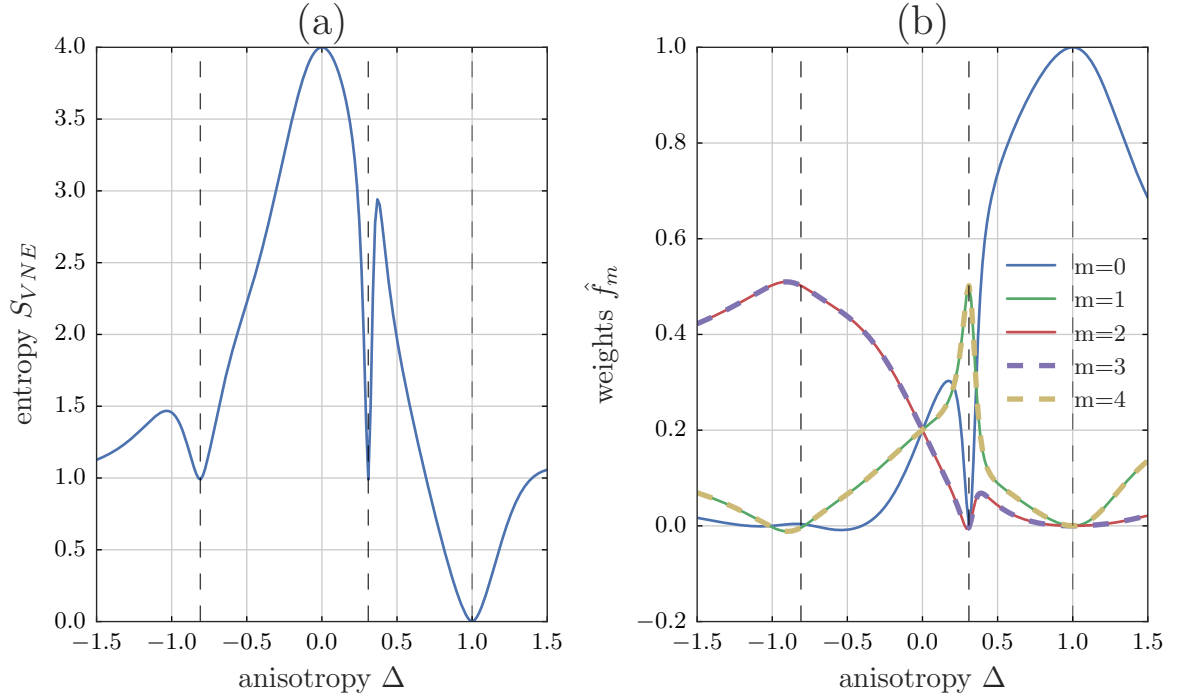


Figure 5.8: (a) Entropy and (b) winding weights as function of the anisotropy for a spin chain $N = 6$ with dissipatively oriented ($\Gamma = 1000$) parallel boundary spins. The entropy is maximal at $\Delta = 0$. Dashed lines indicate anisotropies for which pure helix states are predicted ($\Delta = \cos \frac{\Phi + 2\pi m}{N-1}$), in this case there are double dashed lines at $\Delta = -0.809$ and $\Delta = 0.309$

However, these currents are of equal strength and opposite sign, so they cancel out.

5.2.2 Analytical Evidence

Eigenvectors of h_{00}

In the hypothesis, we claim that the dissipation-projected Hamiltonian has two eigenvectors corresponding to two eigenvalues zero. These can be given by (5.45). At this point, we quickly refer to Table 5.5, where we checked the two-fold degeneracy of the zero eigenvalue explicitly for all γ satisfying our requirements and $\theta = \frac{\pi}{2}$. Furthermore, we analytically confirmed in a lengthy, but straightforward, calculation that (5.45) are eigenvectors h_{00} with eigenvalue zero (the definition can be found in Appendix B) in the specific case of boundary gradient $\Phi = 0$ (thus $\phi_L = \phi_R = 0$). At this point, we want to refer to the article [25], where the calculation is sketched for the case of a single spin helix state, instead of boring the reader with another tedious calculation.

Theorem and Proof for Rank 2 State

We mentioned in Section 4.1.3 that the rank of the non-equilibrium steady state can only be predicted reliably via the stochastic matrix F , if the generic elements are non-zero. We have tested this for attainable system sizes. The stochastic matrix F in these rank 2 situations has the general form

$$F = \left(\begin{array}{cc|ccc} F_{00} & F_{01} & F_{02} & \cdots & F_{0N} \\ F_{10} & F_{11} & F_{12} & \cdots & F_{1N} \\ \hline 0 & 0 & F_{22} & \cdots & F_{2N} \\ \vdots & \vdots & \vdots & \ddots & \vdots \\ 0 & 0 & F_{N2} & \cdots & F_{NN} \end{array} \right). \quad (5.58)$$

We define the submatrix on the lower right

$$K = \begin{pmatrix} F_{22} & \cdots & F_{2N} \\ \vdots & \ddots & \vdots \\ F_{N2} & \cdots & F_{NN} \end{pmatrix}. \quad (5.59)$$

The calculations of the 2nd order perturbation theory and the corresponding secular condition suggest that this submatrix is crucial for the determination of the elements of the auxiliary matrix $m^{(1)}$ and, thus, indirectly for the validity of our hypothesis.

Let me sum up the idea of the following theorem. The rank of the non-equilibrium steady state is determined by the equation

$$\sum_{\gamma} F_{\gamma\gamma'} v_{\gamma'} = 0. \quad (5.60)$$

For the hypothesis to be true, F should have a unique eigenvector with only $v_0, v_1 \neq 0$ and the existence of a unique eigenvector is coupled to the form of its submatrix K . It determines the values $v_{\alpha} = 0$ for $\alpha > 1$ through

$$\sum_{\alpha>1} K_{\alpha\gamma'} v_{\gamma'} = 0. \quad (5.61)$$

If $\text{Det}(K) = 0$, in principle, there exists an eigenvector $v_{\alpha} \neq 0$. However, if we demand $\text{Det}(K) \neq 0$, there can only be a unique set $v_{\alpha} = 0$ for $\alpha > 1$. Following this line of argumentation, we came up with a theorem, which we will proof by showing the necessary and sufficient condition.

Theorem 2 For the system of equations

$$\sum_{\gamma} F_{\gamma\gamma'} v_{\gamma'} = 0, \quad (5.62)$$

there exists a unique solution with $v_0, v_1 \neq 0$ and $v_{\alpha} = 0$ where $\alpha > 1$ if and only if

$$F_{\alpha 0} = F_{\alpha 1} = 0 \quad \forall \alpha > 1 \quad (5.63)$$

$$\det K \neq 0 \quad (5.64)$$

$$F_{01}, F_{10} \neq 0. \quad (5.65)$$

Let us start to prove this theorem by checking if the conditions for the theorem are sufficient. To do so, we assume the theorem to be true and see if everything is consistent.

Proof 2

Sufficiency

We can rewrite

$$\sum_{\gamma} F_{\gamma\gamma'} v_{\gamma'} = 0 \quad (5.66)$$

into equations for each row of F

$$\sum_{\gamma} F_{0\gamma} v_{\gamma} = 0 \quad (5.67)$$

$$\sum_{\gamma} F_{1\gamma} v_{\gamma} = 0 \quad (5.68)$$

$$\sum_{\beta} K_{\alpha\beta} v_{\beta} = 0 \quad \text{with} \quad \alpha, \beta > 1 \quad (5.69)$$

where K is a submatrix of F as showed above. With the condition $\text{Det}(K) \neq 0$, equation (5.69) can only be fulfilled if

$$v_{\beta} = 0 \quad \forall \beta > 1. \quad (5.70)$$

Thus, the initial equation (5.74) reduces to a system of two equations

$$\begin{pmatrix} F_{00} & F_{01} \\ F_{10} & F_{11} \end{pmatrix} \begin{pmatrix} v_0 \\ v_1 \end{pmatrix} = \begin{pmatrix} -F_{10} & F_{01} \\ F_{10} & -F_{01} \end{pmatrix} \begin{pmatrix} v_0 \\ v_1 \end{pmatrix} = 0, \quad (5.71)$$

where we have used (5.97) and the property of the stochastic matrix that the sum of each

column has to be 0. Another property of the stochastic matrix is that it has zero determinant $\text{Det}(F) = 0$ and, thus, its column vectors are linearly dependent. The two equations that we get are equivalent, so we end up with

$$-F_{10}v_0 + F_{01}v_1 = 0 \quad (5.72)$$

which together with the normalization condition $\sum_k v_k = v_0 + v_1 = 1$ gives us

$$v_0 = \frac{F_{01}}{F_{10} + F_{01}}. \quad (5.73)$$

At this point, we see that in order for $v_0, v_1 \neq 0$, indeed, $F_{01}, F_{10} \neq 0$ has to be true. Up to here, there are no inconsistencies, the condition is sufficient.

Necessity

Now, we also want to show that the conditions in the theorem are necessary. In order to do so, we need to show that we can derive the conditions only given the statement: "For the system of equations

$$\sum_{\gamma} F_{\gamma\gamma'} v_{\gamma'} = 0, \quad (5.74)$$

there exists a unique solution with $v_0, v_1 \neq 0$ and $v_{\alpha} = 0$ where $\alpha > 1$."

We use knowledge about the vector v_{γ} to write

$$\begin{pmatrix} F_{00} & F_{01} \\ F_{10} & F_{11} \end{pmatrix} \begin{pmatrix} v_0 \\ v_1 \end{pmatrix} = 0, \quad (5.75)$$

$$F_{\alpha 0}v_0 + F_{\alpha 1}v_1 = 0, \quad (5.76)$$

and, thus, conversely:

$$F_{\alpha\gamma'} v_{\gamma'} = 0, \quad \text{with } \alpha > 1. \quad (5.77)$$

From the stochastic property (columns add up to zero) of the matrix F , we know

$$F_{00} = -F_{10} - \sum_{\alpha>1} F_{\alpha 0} = -F_{10} - a, \quad (5.78)$$

$$F_{11} = -F_{01} - \sum_{\beta>1} F_{\beta 1} = -F_{01} - b, \quad (5.79)$$

or in matrix form

$$F' \begin{pmatrix} v_0 \\ v_1 \end{pmatrix} = \begin{pmatrix} -F_{10} - a & F_{01} \\ F_{10} & -F_{01} - b \end{pmatrix} \begin{pmatrix} v_0 \\ v_1 \end{pmatrix} = 0. \quad (5.80)$$

For this to exist with non-zero v_0, v_1 , the determinant of this matrix has to be zero:

$$\det F' = (-F_{01} - a)(-F_{10} - b) - F_{10}F_{01} \quad (5.81)$$

$$= F_{01}b + aF_{10} + ab \stackrel{!}{=} 0. \quad (5.82)$$

Because all terms are positive, they have to vanish one by one. At this step, there are several possibilities, which we need to check for consistency:

1. **suppose: $F_{01}, F_{10} = 0$ and $ab = 0$**

- to ensure $ab = 0$, we start by setting $a = 0, b \neq 0$

The matrix F' then becomes:

$$F' \begin{pmatrix} v_0 \\ v_1 \end{pmatrix} = \begin{pmatrix} -a & 0 \\ 0 & -b \end{pmatrix} \begin{pmatrix} v_0 \\ v_1 \end{pmatrix} = 0 \quad (5.83)$$

$$\rightarrow bv_1 = 0. \quad (5.84)$$

But here we have a contradiction, as $b \neq 0$ and $v_1 \neq 0$.

- the same would happen if a instead of b is not zero

→ At least one of the elements F_{01}, F_{10} has to be non-zero.

2. **suppose: $F_{01} = 0, F_{10} \neq 0$** The matrix F' then becomes:

$$F' \begin{pmatrix} v_0 \\ v_1 \end{pmatrix} = \begin{pmatrix} -F_{10} - a & 0 \\ F_{10} & -b \end{pmatrix} \begin{pmatrix} v_0 \\ v_1 \end{pmatrix} = 0 \quad (5.85)$$

$$\rightarrow (F_{10} + a)v_0 = 0 \quad (5.86)$$

$$\rightarrow F_{10}v_0 + bv_1 = 0. \quad (5.87)$$

As F_{10} and a are both positive, the first equation would only vanish if $F_{10} = a = 0$, which again contradicts our supposition.

3. **suppose: $F_{01} \neq 0, F_{10} = 0$** The matrix F' then becomes

$$F' \begin{pmatrix} v_0 \\ v_1 \end{pmatrix} = \begin{pmatrix} -a & F_{01} \\ 0 & -F_{01} - b \end{pmatrix} \begin{pmatrix} v_0 \\ v_1 \end{pmatrix} = 0, \quad (5.88)$$

$$\rightarrow -av_0 + F_{01}v_1 = 0, \quad (5.89)$$

$$\rightarrow (F_{01} + b)v_1 = 0. \quad (5.90)$$

Again, the second equation would only vanish, if $F_{01} = b = 0$, which contradicts our supposition.

4. **suppose: $F_{01} \neq 0$ and $F_{10} \neq 0$**

- consequently, to ensure $\text{Det}(F' = 0)$ also $a = b = 0$

Shortly, remember that $a = b = 0$ means

$$\sum_{\alpha > 1} F_{\alpha 0} = 0 \quad (5.91)$$

$$\sum_{\beta > 1} F_{\beta 1} = 0 \quad (5.92)$$

and, as all elements in these sum are positive, $F_{\alpha 0}, F_{\alpha 1} = 0 \quad \forall \alpha$. Let us look at the matrix F' :

$$F' \begin{pmatrix} v_0 \\ v_1 \end{pmatrix} = \begin{pmatrix} -F_{10} & F_{01} \\ F_{10} & -F_{01} \end{pmatrix} \begin{pmatrix} v_0 \\ v_1 \end{pmatrix} = 0, \quad (5.93)$$

$$\rightarrow -F_{10}v_0 + F_{01}v_1 = 0 \quad (5.94)$$

$$\rightarrow F_{10}v_0 - F_{01}v_1 = 0, \quad (5.95)$$

which has a solution for:

$$\frac{v_0}{v_1} = \frac{F_{01}}{F_{10}}. \quad (5.96)$$

This is consistent with (5.75) and (5.76). This does not yet fix v_0, v_1 which can be done using normalization such that $v_0 + v_1 = 1$.

Out of (5.97) to (5.99), it remains to be shown that $K \neq 0$. Suppose for a moment $\text{Det}(K) = 0$: The consequence of this would be that for $K_{\alpha\beta} \tilde{v}_\beta = 0$, there exists a non-zero solution for the set $\tilde{v} = \{v_2, v_3, \dots, v_N\}$ and, thus, a non-zero set $v = \{v_0, v_1, v_2, v_3, \dots, v_N\}$ which again contradicts our starting requirements.

Thus, $\text{Det}(K) \neq 0$. And with this we have shown that the conditions in the theorem are also necessary, thus, the theorem is proven.

To verify that for a given system the rank 2 state is the unique non-equilibrium steady state, we just need to satisfy

$$F_{\alpha 0} = F_{\alpha 1} = 0 \quad \forall \alpha > 1 \quad (5.97)$$

$$\det K \neq 0 \quad (5.98)$$

$$F_{01}, F_{10} \neq 0. \quad (5.99)$$

This can be done by diagonalizing the dissipation-projected Hamiltonian h_{00} and constructing the matrix F . This was done for up to $N = 13$ and the results are summarized in Table 5.5. Furthermore, we illustrate for values of γ , which do not fit into the hypothesis in Table 5.6, that the above is not trivially given.

N	r_{full}	Φ	γ	Deg(λ_0) in h_{00}	$F_{01} \neq 0, F_{10} \neq 0$	$F_{0\alpha} = F_{1\alpha} = 0$	Det($K \neq 0$)
4	4	0	$\frac{2\pi}{3}, \frac{4\pi}{3}$	2	✓	✓	✓
		π	$\frac{\pi}{3}, \frac{5\pi}{3}$	2	✓	✓	✓
5	8	0	-	2	✓	✓	✓
		π	$\frac{\pi}{4}, \frac{3\pi}{4}, \frac{5\pi}{4}, \frac{7\pi}{4}$	2	✓	✓	✓
6	16	0	$\frac{2\pi}{5}, \frac{4\pi}{5}, \frac{6\pi}{5}, \frac{8\pi}{5}$	2	✓	✓	✓
		π	$\frac{\pi}{5}, \frac{3\pi}{5}, \frac{7\pi}{5}, \frac{9\pi}{5}$	2	✓	✓	✓
7	32	0	-	2	✓	✓	✓
		π	$\frac{\pi}{6}, \frac{5\pi}{6}, \frac{7\pi}{6}, \frac{11\pi}{6}$	2	✓	✓	✓
8	64	0	$\frac{2\pi}{7}, \frac{4\pi}{7}, \dots, \frac{12\pi}{7}$	2	✓	✓	✓
		π	$\frac{\pi}{7}, \frac{3\pi}{7}, \frac{5\pi}{7}, \frac{9\pi}{7}, \frac{11\pi}{7}, \frac{13\pi}{7}$	2	✓	✓	✓
9	128	0	-	2	✓	✓	✓
		π	$\frac{\pi}{8}, \dots, \frac{15\pi}{8}$	2	✓	✓	✓
10	256	0	$\frac{2\pi}{9}, \frac{4\pi}{9}, \frac{8\pi}{9}, \frac{10\pi}{9}, \frac{14\pi}{9}, \frac{16\pi}{9}$	2	✓	✓	✓
		π	$\frac{\pi}{9}, \frac{5\pi}{9}, \frac{7\pi}{9}, \frac{11\pi}{9}, \frac{13\pi}{9}, \frac{17\pi}{9}$	2	✓	✓	✓
11	512	0	-	2	✓	✓	✓
		π	$\frac{\pi}{10}, \frac{3\pi}{10}, \frac{7\pi}{10}, \dots, \frac{13\pi}{10}, \frac{17\pi}{10}$	2	✓	✓	✓
12	1024	0	$\frac{2\pi}{11}, \dots, \frac{20\pi}{11}$	2	✓	✓	✓
		π	$\frac{\pi}{11}, \dots, \frac{9\pi}{11}, \frac{13\pi}{11}, \dots, \frac{21\pi}{11}$	2	✓	✓	✓

N	r_{full}	Φ	γ	Deg(λ_0) in h_{00}	$F_{01} \neq 0, F_{10} \neq 0$	$F_{0\alpha} = F_{1\alpha} = 0$	Det($K \neq 0$)
13	2048	0	-	2	✓	✓	✓
		π	$\frac{\pi}{12}, \frac{5\pi}{12}, \frac{7\pi}{12}, \frac{11\pi}{12}, \frac{12\pi}{12}, \frac{17\pi}{12}, \frac{19\pi}{12}, \frac{23\pi}{12}$	2	✓	✓	✓

Table 5.5: Table confirming the conditions (5.97) to (5.99) for all the incremental turning angles γ corresponding to the hypothesis and sorted by corresponding boundary gradient Φ for system sizes up to $N = 13$. Furthermore, the degeneracy of the eigenvalues $\lambda_0 = 0$ of the dissipation-projected Hamiltonian obtained by diagonalization is validated to be two.

N	r_{full}	Φ	γ	Δ	Deg(λ_0) in h_{00}
4	4	π	$\frac{\pi}{3}, \frac{3\pi}{3}$	-1	1
6	16	π	$\frac{5\pi}{5}$	-1	1
7	32	π	$\frac{3\pi}{6}, \frac{9\pi}{6}$	0	8
8	64	π	$\frac{7\pi}{7}$	-1	1
10	256	0	$\frac{6\pi}{9}, \frac{12\pi}{9}$	$-\frac{1}{2}$	8
		π	$\frac{3\pi}{9}, \frac{15\pi}{9}, (\frac{9\pi}{9})$	$\frac{1}{2}, (-1)$	8 (1)
11	512	π	$\frac{5\pi}{10}, \frac{15\pi}{10}$	0	32
12	1024	π	$\frac{11\pi}{11}$	-1	1
13	2048	π	$\frac{3\pi}{12}, \frac{9\pi}{12}, \frac{15\pi}{12}, \frac{21\pi}{12}$	$\pm \frac{1}{\sqrt{2}}$	8

Table 5.6: Table illustrating that the degeneracy of the eigenvalue $\lambda_0 = 0$ of the dissipation-projected Hamiltonian can not be trivially predicted and confirming that for the explicitly excluded values for γ in the hypothesis a rank 2 state indeed fails.

By combining the proof with numerical testing, we have proven the existence of a rank 2 state for all suggested situations for system sizes up to $N = 13$. With a fine-tuned Hamiltonian and specific dissipation in Zeno limit at the boundary, we can reliably generate an entangled state in the XXZ chain. In the next paragraph, we want to see, whether we can determine the error for finite dissipation strength Γ .

Perturbative Corrections onto Rank 2 State for Finite Γ

For a finite dissipation strength Γ , higher order corrections of the perturbation expansion enter the non-equilibrium steady state. In order to examine how big these corrections are and how they are calculated, let us first recapitulate the corrections for a pure spin helix state

$$\rho(\Gamma) = |\psi\rangle\langle\psi| + \frac{\rho^{(1)}}{\Gamma} + \frac{\rho^{(2)}}{\Gamma^2} + \dots \quad (5.100)$$

Let us have a look at the quantity $1 - \text{Tr}(\rho^2)$, which determines the purity for such a state and finite Γ

$$1 - \text{Tr}(\rho(\Gamma)^2) = 1 - \text{Tr}\left(\left(|\psi\rangle\langle\psi| + \frac{\rho^{(1)}}{\Gamma} + \frac{\rho^{(2)}}{\Gamma^2} + \dots\right)\left(|\psi\rangle\langle\psi| + \frac{\rho^{(1)}}{\Gamma} + \frac{\rho^{(2)}}{\Gamma^2} + \dots\right)\right) \quad (5.101)$$

$$= 1 - 1 - \frac{2}{\Gamma}\text{Tr}\left(|\psi\rangle\langle\psi|\rho^{(1)}\right) + \mathcal{O}\left(\frac{1}{\Gamma^2}\right). \quad (5.102)$$

We are specifically interested in the term $\sim \frac{1}{\Gamma}$. We know that

$$\rho^{(1)} = i\mathcal{D}^{-1}\left[[H, \rho^{(0)}]\right] + M^{(1)} \quad (5.103)$$

$$= -2i[H, \rho^{(0)}] + M^{(1)} \quad (5.104)$$

$$= -2i[H, \rho^{(0)}] + |e^0\rangle\langle e^0| \otimes m^{(1)}. \quad (5.105)$$

With this, we can calculate

$$\text{Tr}(\rho^{(0)}\rho^{(1)}) = -2i\text{Tr}\left(\rho^{(0)}[H, \rho^{(0)}]\right) - 2i\text{Tr}\left(\rho^{(0)}(|e^0\rangle\langle e^0| \otimes m^{(1)})\right) \quad (5.106)$$

$$= -2i\langle 0|m^{(1)}|0\rangle. \quad (5.107)$$

It was shown analytically [25] that this element vanishes and thus

$$1 - \text{Tr}(\rho^2) = \mathcal{O}\left(\frac{1}{\Gamma^2}\right). \quad (5.108)$$

In a similar fashion, we can calculate the quantity $\text{Tr}((\rho^{(0)})^2) - \text{Tr}(\rho(\Gamma)^2)$ for the rank 2 situation

as

$$\rho(\Gamma) = \rho^{(0)} + \frac{\rho^{(1)}}{\Gamma} + \frac{\rho^{(2)}}{\Gamma^2} + \dots \quad (5.109)$$

$$\rho^{(0)} = |e^0\rangle\langle e^0| \otimes \underbrace{(v_0 |0\rangle\langle 0| + v_1 |1\rangle\langle 1|)}_{R^{(0)}}. \quad (5.110)$$

We know immediately that $\text{Tr}(\rho^{(0)}) = v_1^2 + v_2^2 < 1$. Similarly to before:

$$\text{Tr}(\rho^{(0)}\rho^{(1)}) \propto v_0 \langle 0|m^{(1)}|0\rangle + v_1 \langle 1|m^{(1)}|1\rangle. \quad (5.111)$$

For $\text{Tr}((\rho^{(0)})^2) - \text{Tr}(\rho(\Gamma)^2) = \mathcal{O}(\frac{1}{\Gamma^2})$, these two elements have to vanish.

Using the explicit $\rho^{(0)}$ for $N = 4, \Phi = 0, \Delta = \frac{2\pi}{3}$ and the explicit inverse dissipator, we can solve for higher order density matrices and corresponding secular conditions. At each order, a general bulk matrix $M^{(n)}$ is added. The matrix $m^{(1)}$ represented in the eigenbasis of h_{00} can be completely determined via secular conditions at first and second order:

$$m^{(1)} = \begin{pmatrix} 0 & 0 & \frac{3i}{34} & 0 \\ 0 & 0 & 0 & 0 \\ -\frac{3i}{34} & 0 & 0 & 0 \\ 0 & 0 & 0 & 0 \end{pmatrix} \quad (5.112)$$

Note that, here, this representation is written in the basis of eigenvectors of h_{00} . The order of the eigenvectors is such that the third and fourth column/row lie in the degenerate subspace of eigenvalue 0.

The off-diagonal elements $m_{\alpha\beta}^{(1)}$ of this result can be verified by the analytical expression (4.58). Furthermore, equations for $m_{0\alpha}^{(1)}$ and $m_{1\alpha}^{(1)}$ with $\alpha > 1$ can be obtained using the explicit form of the states $|0\rangle, |1\rangle$

$$m_{0\alpha}^{(1)} = \frac{v_0}{2} \frac{-i}{\lambda_0 - \lambda_\alpha} \langle 0|h_{10}|\alpha\rangle \quad (5.113)$$

$$m_{1\alpha}^{(1)} = \frac{-v_0}{2} \frac{-i}{\lambda_1 - \lambda_\alpha} \langle 1|h_{10}|\alpha\rangle. \quad (5.114)$$

Using the secular conditions at second and third order, we can obtain the matrix $m^{(2)}$ in the

same manner:

$$m^{(2)} = \begin{pmatrix} \frac{36}{85} & 0 & -\frac{99}{170} & 0 \\ 0 & \frac{18}{17} & 0 & 0 \\ -\frac{99}{170} & 0 & -\frac{1782}{1445} & 0 \\ 0 & 0 & 0 & -\frac{72}{289} \end{pmatrix} \quad (5.115)$$

Following the same procedure, the auxiliary matrices for $N = 5$, $\Phi = 0$, $\Delta = \frac{\pi}{4}$ can be obtained and are given in Appendix C.2. Unfortunately, the elements $m_{01}^{(2)}$ and $m_{10}^{(2)}$ could not be determined in this case. Based on the two analytically obtained matrices $m^{(1)}$ for $N = 4, 5$, where the elements of (5.111) vanish, we claim that the corrections for finite Γ scale like $\sim \frac{1}{\Gamma^2}$. Further evidence has to be collected to support this claim.

5.3 Time evolution: Relaxation Towards Spin Helix State

In the previous sections, we focused on the non-equilibrium steady states and used the results of stationary perturbation theory to further understand the numerics. This section focuses on the time evolution and compares it to the prediction gained from time dependent perturbation theory.

We show data on the numerical time evolution for a system of $N = 4$ spins. The dissipation with strength Γ targets boundary spins $\theta_L = \theta_R = \frac{\pi}{2}$, $\phi_L = 0$, $\phi_R = \frac{\pi}{3}$. Furthermore, the anisotropy is set to $\Delta = \cos \frac{\pi}{9}$ such that the non-equilibrium steady state of this situation is a spin helix state with winding $m = 0$. Initially, we prepare the chain in a pure state

$$\rho(0) = \frac{1}{2} |\uparrow\downarrow\downarrow\uparrow + \uparrow\uparrow\uparrow\uparrow\rangle \langle \uparrow\downarrow\downarrow\uparrow + \uparrow\uparrow\uparrow\uparrow|. \quad (5.116)$$

5.3.1 Identification of Time Scales

In order to compare the time evolution to the predicted behavior in Section 4.1.4, we projected the reduced density matrix at each time step onto the eigenbasis of the dissipation-projected Hamiltonian h_{00} . As defined in (4.76), the diagonal elements of the reduced density matrix in that basis are equal to the weights ν_α which are governed via the stochastic matrix F (see Equation (4.78)). We solved the four differential equations for this particular case with `Mathematica`. Here, all numbers are rounded to three decimal places and a scaling factor ξ for

the time is introduced

$$\nu_0(\xi t) \rightarrow -0.462e^{-5.440\xi t} + 0.298e^{-4.540\xi t} + 0.221e^{-3.310\xi t} \quad (5.117)$$

$$\nu_1(\xi t) \rightarrow 0.183e^{-5.440\xi t} + 0.087e^{-4.540\xi t} + 0.049e^{-3.310\xi t} \quad (5.118)$$

$$\nu_2(\xi t) \rightarrow 0.123e^{-5.440\xi t} - 0.802e^{-4.540\xi t} + 0.929e^{-3.310\xi t} \quad (5.119)$$

$$\nu_3(\xi t) \rightarrow 1.000 + 0.157e^{-5.440\xi t} + 0.417e^{-4.540\xi t} - 1.200e^{-3.310\xi t}. \quad (5.120)$$

We fitted the obtained formula for the occupations to the data (see Figure 5.9) and determined the scaling factor $\xi = \frac{1}{1000} = \frac{1}{\Gamma}$ with a maximal standard deviation of $\approx 10^{-8}$. In Section 4.1.4, we, thus, called $t_{\text{slow}} = \frac{t}{\Gamma}$.

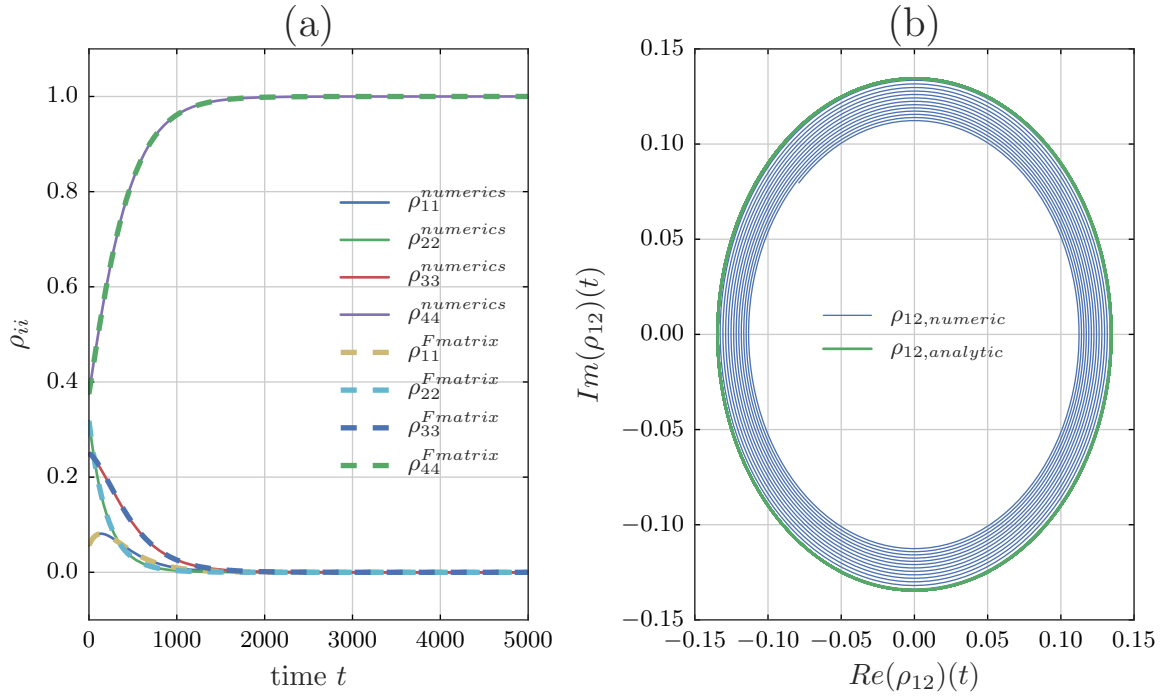


Figure 5.9: Comparison of analytics and numerics for the time evolution of (a) diagonal elements and (b) the off-diagonal element ρ_{12} of the density matrix of an initial state (5.116) for dissipation characterized by $\Gamma = 1000$, $\theta_L = \theta_R = \frac{\pi}{2}$, $\phi_L = 0$, $\phi_R = \frac{\pi}{3}$ and anisotropy $\Delta = \cos \frac{\pi}{9}$. The non-equilibrium steady state is expected to be a pure spin helix state with winding $m = 0$. For the off-diagonal element, time was mapped onto a phase angle and the plot shows relatively small times up to $t = 100$.

In Figure 5.9, we look at the off-diagonal element $\langle 1|\rho(t)|2\rangle$ of the reduced density matrix projected onto the eigenbasis of h_{00} in a representation for which time is mapped onto a phase. In Equation (4.75), we did not account for any decay, hence, the predicted element oscillates

with a constant frequency, while the numerically obtained element clearly decays. Note that the time in this figure only goes up to $t = 100$. Already for times $t = 1000$, we observe that the real and imaginary parts of $\langle 1|\rho(t)|2\rangle$ have decayed to values $\approx 10^{-4}$.

Up to here we have recovered the time scale, at which the stochastic process dominates, and the time scale, at which unitary dynamics is observed. We want to go further and see if for small times $t \sim \frac{1}{\Gamma}$, the system relaxes to the dissipation-free subspace. Let us have a look on entropy and the winding weights.

In Figure 5.10, we see, indeed, that the initial entropy is zero, as well as the entropy in the long time limit. Furthermore, we observe that the entropy rises once at a time $t \approx 7 \cdot 10^{-4}$ before it relaxes to almost zero. The entropy reaches a maximum of $S_{VNE} \approx 1,29$ at $t \approx 52$ and decreases in the long time limit to zero as we approach the pure helix state.

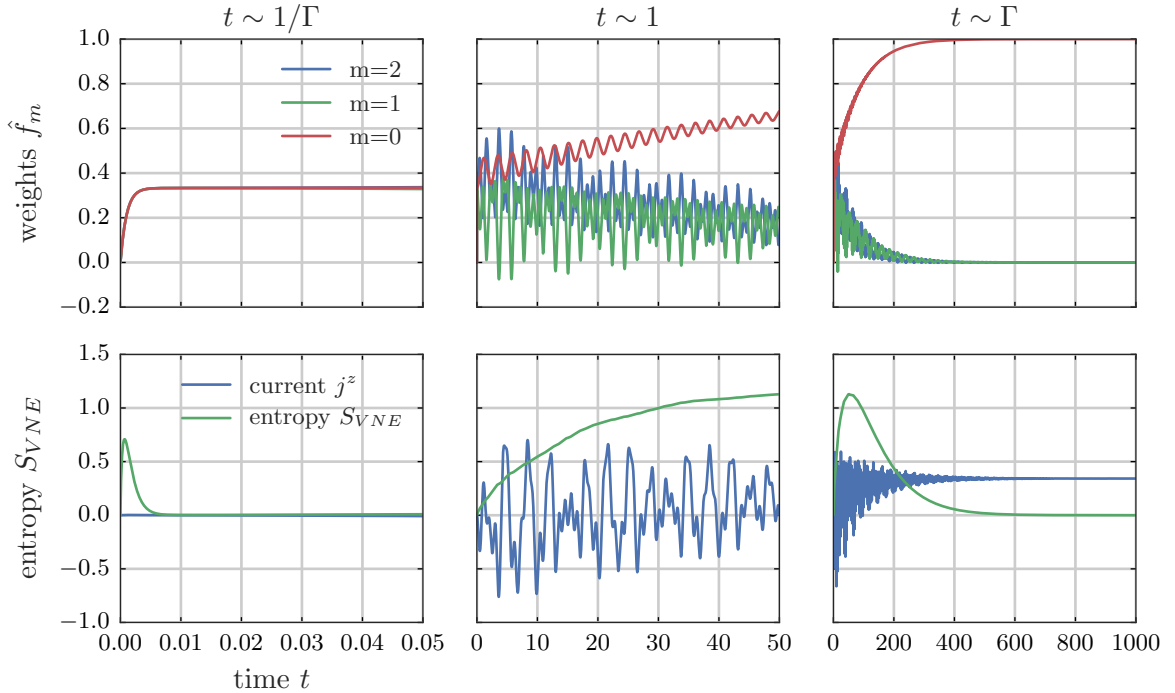


Figure 5.10: Winding weights and entropy for the time evolution of an initial state (5.116) for dissipation characterized by $\Gamma = 1000$, $\theta_L = \theta_R = \frac{\pi}{2}$, $\phi_L = 0$, $\phi_R = \frac{\pi}{3}$ and anisotropy $\Delta = \cos \frac{\pi}{9}$. The non-equilibrium steady state is expected to be a spin helix state with winding $m = 0$.

Interesting behavior can be seen in the current: At initial times, it stays constant until it starts to oscillate between $j_{min}^z \approx -0.75$ and $j_{max}^z \approx 0.75$, then, the amplitude of these oscillations decays and eventually the current settles to the predicted (cp. 3.2) $j_{SHS}^z = \sin \frac{\pi}{9} \approx 0.342$.

Figure 5.10 shows the winding weights over the course of time evolution. It seems strange

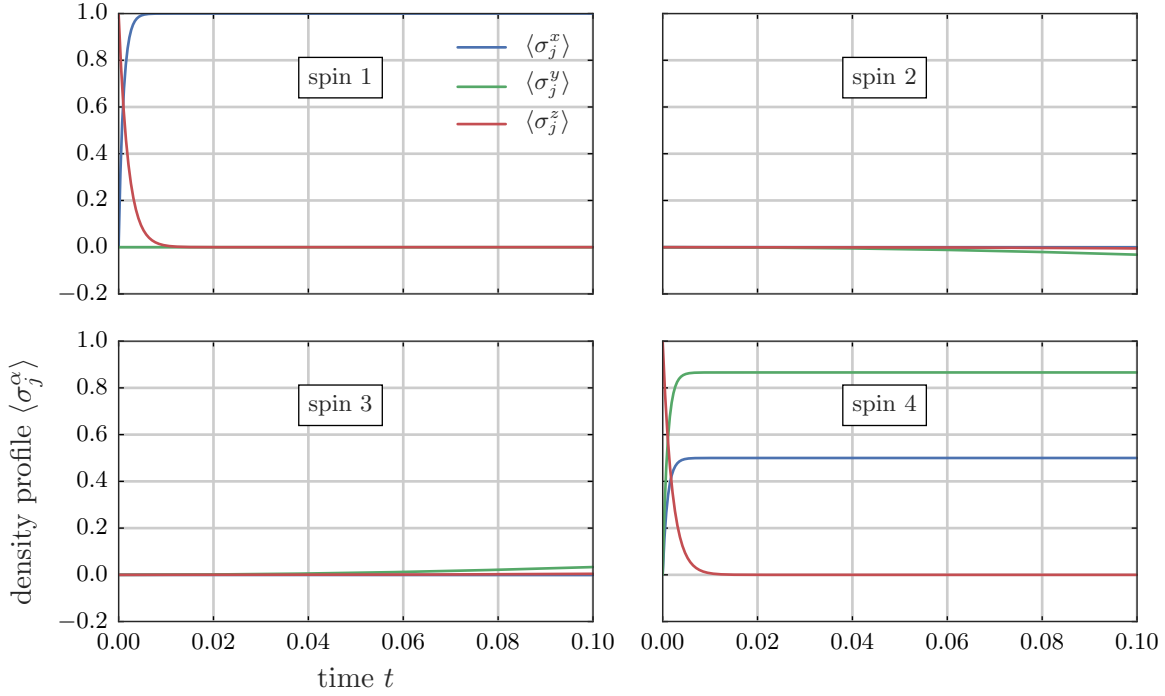


Figure 5.11: Density profiles for the short time scale of the time evolution of an initial state (5.116) for dissipation characterized by $\Gamma = 1000$, $\theta_L = \theta_R = \frac{\pi}{2}$, $\phi_L = 0$, $\phi_R = \frac{\pi}{3}$ and anisotropy $\Delta = \cos \frac{\pi}{9}$. The non-equilibrium steady state is expected to be a spin helix state with winding $m = 0$

that all the weights start at zero for the initial state. However, looking at the initial state (5.116) and the definition of the weights in Equation (3.26), we realize that, initially, the boundary spins point up, thus, have zero components in xy -plane and, similarly, the bulk spins are in a superposition of up and down with zero components in xy -plane. We conclude that $\langle \sigma^+ \rangle$ is zero for all spins and so are the weights. This changes within $t \approx 10^{-4}$, where all the weights start having equal value. On the intermediate time scale, decaying oscillations are visible and the expected relaxation towards the spin helix states with winding $m = 0$ can be observed for long times.

The kinks at very short times of the order $t \sim \frac{1}{\Gamma}$ strongly indicate the instantaneous relaxation towards the decoherence-free subspace. We can confirm this with Figures 5.11 and 5.12, where we plotted the density profile of all four spins for small times $t \in [0, 0.01]$ and for long times $t \in [0, 10000]$. Indeed, the first and last spin get changed from the initial polarization in Z -direction towards the targeted directions. The bulk spins rarely move during these initial times. On the long run, the boundary spins are basically frozen into the dissipatively targeted direction and the bulk spins show oscillatory behavior in an intermediate time range, which decays until

all spins reach the spin helix state configuration.

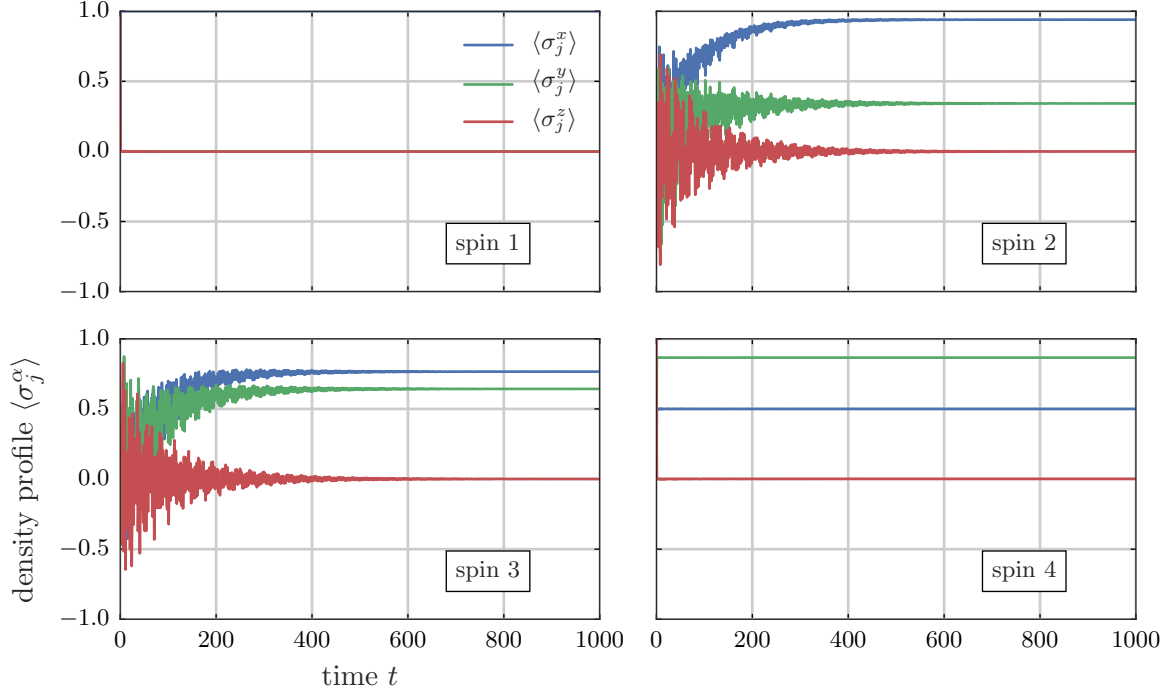


Figure 5.12: Density profiles for the long time scale of the time evolution of an initial state (5.116) for dissipation characterized by $\Gamma = 1000$, $\theta_L = \theta_R = \frac{\pi}{2}$, $\phi_L = 0$, $\phi_R = \frac{\pi}{3}$ and anisotropy $\Delta = \cos \frac{\pi}{9}$. The non-equilibrium steady state is expected to be a spin helix state with winding $m = 0$

5.3.2 Validity of Stochastic Prediction for Finite Γ

The perturbation theory was performed for the strong coupling limit, so are the derived formula for the weights ν_α . In the following, we want to discuss qualitatively for which sizes of Γ the results remain valid. For that we ran the same time evolution as described above, but for $\Gamma = 1, 10, 50$. In Figure 5.13 the three situations are plotted and compared to the solutions (5.117) to (5.120) with $\xi = \frac{1}{\Gamma}$.

For $\Gamma = 50$ the prediction of the strong coupling perturbation theory coincides well with the numerics. The smaller Γ gets, the more fluctuations can be observed in the time evolution. Physically, the boundary spins are not fixed in the targeted direction, but rather fluctuate around it. The analytic solution does not describe this behavior, however, the prediction for the long time limit seems to hold.

In this section, we compared the predictions for the dynamics made in the strong coupling

perturbation theory with a numerical case study for $N = 4$. We could demonstrate that all the three described processes occur. The stochastic time evolution discovered for strong dissipation, on long time scales, agrees well with the numerics for finite $\Gamma = 50$, however, doesn't describe the details for smaller Γ .

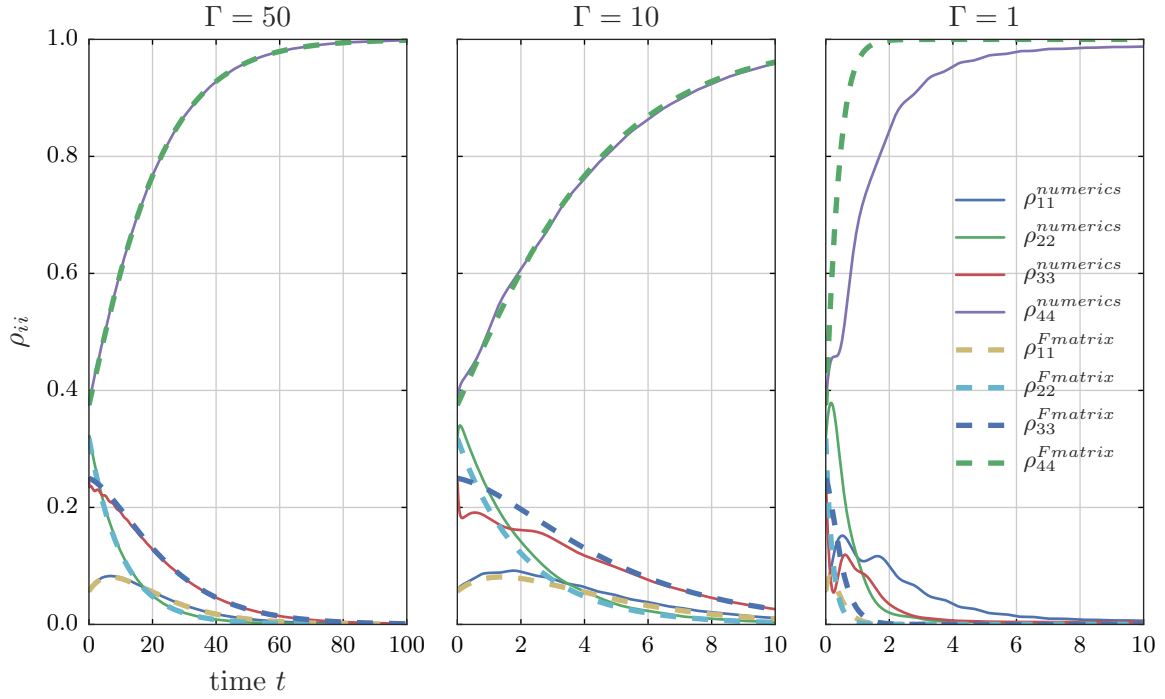


Figure 5.13: Comparison of analytic stochastic time evolution of the occupation ρ_{ii} to the numerics for finite dissipation strengths $\Gamma = 50, 10, 1$ for $N = 4$ spins.

Conclusion

The XXZ model is one of the few physical models, that due to its reduced complexity, has attracted immense theoretical interest over the past. Furthermore, it is experimentally realizable and thus testable. In this thesis, we studied a boundary-driven version of the XXZ model, pursuing two aims: First, to investigate the surprising failure of the generation of pure states with helical structure, which were theoretically expected from the for certain strong dissipation and a fine-tuned Hamiltonian. Second, to better understand the fundamental physics inherent to dissipative systems and described by the Lindblad formalism.

With the aim of answering these two research questions, we made substantial progress in the development of a thorough description of the strong coupling limit via stationary and time-dependent perturbation theory. We found that for times of the order of the dissipation strength, one can effectively describe the dynamics by a classical Markov process (Chapter 4). Making use of this stochastic process and its formalism, we were able to understand and proof the generation of an entangled non-equilibrium steady state consisting of two projectors. These occur, precisely when Lindblad operators polarize the boundary spins of the chain into a parallel configuration in Zeno limit, while the XXZ Hamiltonian takes specified values for the anisotropy (Chapter 5).

In a first step, we laid the foundations for the description of open quantum systems by the Lindblad master equation, for the XXZ model and the corresponding boundary-driven XXZ chain in Chapter 2. We mainly used the exact diagonalization (Chapter 3) to obtain the non-equilibrium steady state or the dynamics of small systems of length $N \leq 7$. It is important to highlight that for our particular model a unique steady state exists (Section 2.3.3) and that the

spectrum of the Liouvillian in the strong coupling limit is structured in bands, whose lowest lying band can be associated with the dissipation-projected Hamiltonian (Section 3.1.4).

Chapter 4 introduced the theoretical framework that we used to treat the model with a particular focus on the stationary problem. To solve the perturbative recurrence equation for the strong coupling limit, we have to ensure invertibility of the dissipator at each order, which, for our particular model, can be derived exactly and leads to a condition that we called secular condition (Section 4.1.1). In this thesis, we used a general ansatz, which assumes a pure state at the boundaries targeted by the strong dissipation and an arbitrary mixture of states in the bulk of the XXZ chain. Employing the recurrence relation and imposing the secular condition, we derived at 0th order, that these bulk states have to be eigenstates of the dissipation-projected Hamiltonian. Furthermore, at 1st order, we found that the weights of these states are determined by a stochastic matrix and the resulting rate equations (Sections 4.1.2 and 4.1.3). Based on these findings, we made a guess for the dynamics and confirmed via more formal Dyson expansion in a time-dependent perturbation theory that for strong dissipation the system enters the decoherence-free subspace very fast ($t \sim \frac{1}{\Gamma}$), followed by an intermediate unitary evolution ($t \sim 1$), which eventually decays and gets dominated by a stochastic process ($t \sim \Gamma$) (Sections 4.2 and 4.1.4).

The derivation of these technical results was closely intertwined with the mostly numerical results presented in Chapter 5. In an extensive study of the large parameter space of this model, we could first recover the well-understood appearance of pure non-equilibrium steady states with helix structure, discuss its topological nature and, most importantly, interpret the particular behavior appearing for certain parameters (Section 5.1.2). The Sections 5.1.1 illustrates the type of analysis that was performed. Restricting ourselves to the Zeno limit, we found that, for anisotropy $\Delta = 0$ always a totally mixed steady state is generated. In contrast, the steady state for $\Delta = -1, 1$ converges to a helical pure state with antiferromagnetic or ferromagnetic alignment of the spins. Whenever the boundary polarization and the anisotropy are chosen such that one or more spins are aligned to the same axis no such helical states are generated and the non-equilibrium steady state is of finite rank.

The main result of this thesis (Section 5.2) is the confirmation of the hypothesis that targeting (anti)parallel boundary spins via dissipation in Zeno limit and setting specific anisotropies leads to the generation of non-equilibrium steady states of rank 2 for chains of lengths up to $N = 13$. Using perturbation theory, we derived a set of conditions, which are formally proven in a theorem, and validated numerically for these small systems. Furthermore, as showed in the last Section 5.3 of the results, we could confirm the results of the time-dependent perturbation theory via numerical results of time evolutions. In this thesis, we made use of the rather fundamental

exact diagonalization which set natural restrictions on the system sizes one can study. This was helpful in the sense, that we could focus on the microscopic details and test the behavior of sensible observables. This knowledge could be significantly expanded by more elaborate techniques. In the realm of exact diagonalization one could go further by exploiting symmetries. To confirm the predicted rank 2 state for larger systems, matrix product state algorithms seem to be favorable. Furthermore, given the underlying stochastic process in our problem, it would be exciting to investigate how purely stochastic Monte-Carlo methods can be used to predict steady states.

We have seen indications for particular properties of the XXZ model or more specific the dissipation-projected Hamiltonian at anisotropies related to roots of unity. The XXZ chain with boundary fields has been solved via Bethe Ansatz [31], even at these root of unity values solutions were obtained [43]. It would be interesting to study the integrability of our model in more detail and discuss the influence of integrability on the systems properties (e.g. transport properties [44]).

The broader field of open quantum systems is evolving at a fast pace and a thorough literature study would be necessary to see whether our results can be generalized onto other models. For example there is a notion of a *pointer basis*, whose off-diagonal elements decay in the long-time limit. The diagonal elements are determined by rate equations, similar to our findings. Yet, how to obtain this pointer basis for different models is not clear and remains to be studied. Another approach for the description of the relaxation dynamics is the adiabatic elimination. The dissipation drives the system into the decoherence-free subspace on a fast time scale, which can be adiabatically eliminated [45–47]. The system then evolves via an effective Lindblad equation, which takes into account second order processes. These are not included in our stochastic equations. It would be necessary to compare these results in detail in order to see if the more formal and technical discussion of the perturbation (Chapter 4) could be generalizable to other models in the strong coupling limit and help to advance the understanding of dissipative generation of non-equilibrium steady states.

One example of a well-controlled dissipative generation of an entangled non-equilibrium steady state was presented in this thesis. Once this model can be realized in experiments [11, 12], a strongly dissipative system could be paradoxically used to generate entangled states in robust fashion [18], which, in turn, could be of use for quantum information purposes.

Bibliography

- [1] K. B. Davis et al., *Bose-Einstein condensation in a gas of sodium atoms*, *Physical Review Letters* **75** (1995), pp. 3969–3973, ISSN: 00319007, arXiv: [9604005 \[quant-ph\]](#) (cit. on p. 1).
- [2] C. C. Bradley et al., *Evidence of Bose-Einstein condensation in an atomic gas with attractive interactions*, *Physical Review Letters* **75** (1995), pp. 1687–1690, ISSN: 00319007, arXiv: [0507204 \[quant-ph\]](#) (cit. on p. 1).
- [3] M. H. Anderson et al., *Observation of bose-einstein condensation in a dilute atomic vapor*, *Science (New York, N.Y.)* **269** (1995), pp. 198–201, ISSN: 0036-8075 (cit. on p. 1).
- [4] D. Jaksch et al., *Cold bosonic atoms in optical lattices*, *Physical Review Letters* **81** (1998), pp. 3108–3111, ISSN: 10797114, arXiv: [9805329 \[cond-mat\]](#) (cit. on p. 1).
- [5] M. Greiner et al., *Quantum phase transition from a superfluid to a Mott insulator in a gas of ultracold atoms*, *Nature* **415** (2002), p. 39 (cit. on p. 1).
- [6] M. Köhl et al., *Fermionic atoms in a three dimensional optical lattice: Observing Fermi surfaces, dynamics, and interactions*, *Physical Review Letters* **94** (2005), pp. 1–4, ISSN: 00319007, arXiv: [0410389v3 \[arXiv:cond-mat\]](#) (cit. on p. 1).
- [7] L. M. Duan, E. Demler and M. D. Lukin, *Controlling Spin Exchange Interactions of Ultracold Atoms in Optical Lattices*, *Physical Review Letters* **91** (2003), pp. 1–4, ISSN: 10797114 (cit. on p. 1).
- [8] M. Lewenstein, A. Sanpera and V. Ahufinger, *Advances in Physics Ultracold atomic gases in optical lattices : mimicking condensed matter physics and beyond*, (2007), pp. 37–41 (cit. on p. 1).

- [9] I. Bloch, J. Dalibard and W. Zwerger, *Many-body physics with ultracold gases*, *Reviews of Modern Physics* **80** (2008), pp. 885–964, ISSN: 00346861, arXiv: [0704.3011](#) (cit. on p. 1).
- [10] A. G. Volosniev et al., *Engineering the Dynamics of Effective Spin-Chain Models for Strongly Interacting Atomic Gases*, (2014), pp. 1–10, arXiv: [1408.3414](#) (cit. on p. 1).
- [11] P. Massignan, J. Levinsen and M. M. Parish, *Magnetism in Strongly Interacting One-Dimensional Quantum Mixtures*, *Physical Review Letters* **115** (2015), pp. 1–6, ISSN: 10797114, arXiv: [arXiv:1507.02814v1](#) (cit. on pp. 1, 85).
- [12] L. Yang and X. Cui, *Effective spin-chain model for strongly interacting one-dimensional atomic gases with an arbitrary spin*, *Physical Review A* **93** (2016), pp. 1–11, ISSN: 24699934, arXiv: [1510.06087](#) (cit. on pp. 1, 85).
- [13] G. Lindblad, *On the generators of quantum dynamical semigroups*, *Communications in Mathematical Physics* **48** (1976), pp. 119–130, ISSN: 00103616, arXiv: [arXiv:1402.7287v1](#) (cit. on pp. 1, 8).
- [14] V. Gorini, *Completely positive dynamical semigroups of N-level systems*, *Journal of Mathematical Physics* **17** (1976), p. 821, ISSN: 00222488 (cit. on pp. 1, 8).
- [15] A. J. Daley, *Quantum trajectories and open many-body quantum systems*, 2014, arXiv: [1405.6694](#) (cit. on pp. 1, 8).
- [16] P. Zanardi and L. Campos Venuti, *Coherent quantum dynamics in steady-state manifolds of strongly dissipative systems*, *Physical Review Letters* **113** (2014), pp. 1–5, ISSN: 10797114, arXiv: [1404.4673](#) (cit. on pp. 2, 41).
- [17] P. Zanardi and L. Campos Venuti, *Geometry, robustness, and emerging unitarity in dissipation-projected dynamics*, *Physical Review A - Atomic, Molecular, and Optical Physics* **91** (2015), pp. 1–8, ISSN: 10941622, arXiv: [1412.6198](#) (cit. on pp. 2, 41).
- [18] G. Morigi et al., *Dissipative Quantum Control of a Spin Chain*, *Physical Review Letters* **115** (2015), pp. 1–5, ISSN: 10797114, arXiv: [1507.02997](#) (cit. on pp. 2, 85).

-
- [19] T. Prosen, *Exact nonequilibrium steady state of a strongly driven open XXZ chain*, *Physical Review Letters* **107** (2011), pp. 1–5, ISSN: 00319007, arXiv: [1106.2978](#) (cit. on p. 2).
- [20] T. Prosen, *Open XXZ spin chain: Nonequilibrium steady state and a strict bound on ballistic transport*, *Physical Review Letters* **106** (2011), pp. 2–5, ISSN: 00319007, arXiv: [1103.1350](#) (cit. on p. 2).
- [21] T. Prosen, *Comments on a boundary-driven open XXZ chain: asymmetric driving and uniqueness of steady states*, *Physica Scripta* **86** (2012), p. 058511, ISSN: 0031-8949, arXiv: [arXiv:1205.3126v1](#) (cit. on pp. 2, 14).
- [22] V. Popkov, *Alternation of sign of magnetization current in driven XXZ chains with twisted XY boundary gradients*, *Journal of Statistical Mechanics: Theory and Experiment* **2012** (2012), P12015, ISSN: 1742-5468, arXiv: [arXiv:1210.4555v2](#) (cit. on pp. 2, 49).
- [23] D. Karevski, V. Popkov and G. M. Schütz, *Exact matrix product solution for the boundary-driven Lindblad XXZ chain*, *Physical Review Letters* **110** (2013), pp. 1–4, ISSN: 00319007, arXiv: [1211.7010](#) (cit. on p. 2).
- [24] V. Popkov and C. Presilla, *Obtaining pure steady states in nonequilibrium quantum systems with strong dissipative couplings*, *Physical Review A - Atomic, Molecular, and Optical Physics* **93** (2016), ISSN: 10941622, arXiv: [1509.04946](#) (cit. on pp. 2, 13, 22, 27, 28).
- [25] V. Popkov, J. Schmidt and C. Presilla, *Spin-helix states in the XXZ spin chain with strong dissipation*, *Journal of Physics A: Mathematical and Theoretical* **50** (2017), pp. 1–20, arXiv: [1703.08233](#) (cit. on pp. 2, 13, 25, 27, 33, 52, 66, 74, 109).
- [26] V. Popkov and G. M. Schütz, *Solution of the Lindblad equation for spin helix states*, *Physical Review E* **95** (2017), pp. 1–23, ISSN: 24700053, arXiv: [arXiv:1702.04586v1](#) (cit. on pp. 2, 13, 27).
- [27] V. Popkov, C. Presilla and J. Schmidt, *Targeting pure quantum states by strong noncommutative dissipation*, **052131** (2017), pp. 1–11, ISSN: 2469-9926, arXiv: [1702.00287](#) (cit. on pp. 2, 13, 27).

- [28] J.-L. Basdevant and J. Dalibard, *Quantum Mechanics*, Springer-Verlag, 2002, p. 511, ISBN: 3-540-42739-2 (cit. on p. 7).
- [29] H.-P. Breuer and F. Petruccione, *The Theory of Open Quantum Systems*, Oxford University Press, 2007, pp. 1–656, ISBN: 9780199213900 (cit. on p. 8).
- [30] H.-J. Mikeska and A. K. Kolezhuk, “One-dimensional magnetism”, 2004, pp. 1–83, ISBN: 978-3-540-21847-0, arXiv: [0501603 \[cond-mat\]](#) (cit. on p. 9).
- [31] F. Franchini,
An introduction to integrable techniques for one-dimensional quantum systems, (2016), arXiv: [1609.02100](#) (cit. on pp. 10, 85).
- [32] B. Misra and E. C. G. Sudarshan, *The Zeno’s paradox in quantum theory*, *Journal of Mathematical Physics* **18** (1977), pp. 756–763, ISSN: 0022-2488, arXiv: [arXiv:1011.1669v3](#) (cit. on p. 12).
- [33] F. Schäfer et al., *Experimental realization of quantum zeno dynamics*, *Nature Communications* **5** (2014), pp. 1–6, ISSN: 20411723, arXiv: [1309.1552](#) (cit. on p. 12).
- [34] D. E. Evans, *Irreducible quantum dynamical semigroups*, *Communications in Mathematical Physics* **54** (1977), pp. 293–297, ISSN: 00103616 (cit. on p. 14).
- [35] J. Thijssen, *Computational Physics*, 2007, p. 638, ISBN: 0521575885 (cit. on p. 18).
- [36] C. Navarrete-Benlloch,
Open systems dynamics: Simulating master equations in the computer, (2015), pp. 1–18, arXiv: [1504.05266](#) (cit. on p. 19).
- [37] M. Am-Shallem et al.,
Three approaches for representing Lindblad dynamics by a matrix-vector notation, arXiv (2015), pp. 1–17, arXiv: [1510.08634](#) (cit. on pp. 19, 20).
- [38] D. Glasser, F. J. M. Horn and R. Meidan, *Properties of certain zero column-sum matrices with applications to the optimization of chemical reactors*, *Journal of Mathematical Analysis and Applications* **73** (1980), pp. 315–337, ISSN: 10960813 (cit. on p. 36).
- [39] J. G. Kemeny, J. L. Snell and A. W. Knapp, *Denumerable Markov Chains*, vol. 40, Graduate Texts in Mathematics, Springer New York, 1976, ISBN: 978-1-4684-9457-0 (cit. on p. 37).

-
- [40] G. R. Grimmett and D. R. Stirzaker, *Probability and Random Processes*, vol. 80, 2001, p. 608, ISBN: 0198572220 (cit. on p. 37).
- [41] V. Popkov, *private communication*, 2018 (cit. on p. 37).
- [42] J. K. Asbóth, L. Oroszlány and A. Pályi, *A Short Course on Topological Insulators*, *Lecture Notes in Physics* **919** (2015), ISSN: 0075-8450, arXiv: 1509.02295 (cit. on p. 50).
- [43] R. Murgan, R. I. Nepomechie and C. Shi, *Exact solution of the open XXZ chain with general integrable boundary terms at roots of unity*, *Journal of Statistical Mechanics: Theory and Experiment* (2006), ISSN: 17425468, arXiv: 0605223 [hep-th] (cit. on p. 85).
- [44] A. De Luca, M. Collura and J. De Nardis, *Nonequilibrium spin transport in integrable spin chains: Persistent currents and emergence of magnetic domains*, *Physical Review B* **96** (2017), pp. 1–5, ISSN: 24699969, arXiv: 1612.07265 (cit. on p. 85).
- [45] A. C. Li, F. Petruccione and J. Koch, *Perturbative approach to Markovian open quantum systems*, *Scientific Reports* **4** (2014), ISSN: 20452322, arXiv: 1311.3227 (cit. on p. 85).
- [46] B. Scioffa, D. Poletti and C. Kollath, *Two-Time Correlations Probing the Dynamics of Dissipative Many-Body Quantum Systems: Aging and Fast Relaxation*, *Physical Review Letters* **114** (2015), ISSN: 10797114, arXiv: 1407.4939 (cit. on p. 85).
- [47] R. Azouit, A. Sarlette and P. Rouchon, *Adiabatic elimination for open quantum systems with effective Lindblad master equations*, *2016 IEEE 55th Conference on Decision and Control, CDC 2016* (2016), pp. 4559–4565, arXiv: 1603.04630 (cit. on p. 85).

APPENDIX A

Code

```
# This code was developed using the following versions:

#>>> import sys
#>>> print(sys.version)
#3.6.1 |Anaconda 4.4.0 (64-bit)| (default, May 11 2017, 13:09:58)
#[GCC 4.4.7 20120313 (Red Hat 4.4.7-1)]

#>>> import numpy
#>>> numpy.version.version
#'1.12.1'

#>>> import scipy
#>>> scipy.__version__
#'0.19.0'

# It was tested to be compatible with earlier versions, as on the used
Cluster in the AG Kollath at HISKP.

import numpy as np
import scipy.linalg
import scipy.optimize

# In this class, we define the operators using the usual Z-eigenbasis. It
takes the spin chain length N as input.
class HeisenbergBasis(object):
```

```
def __init__(self, number_of_spins):
    self.N = number_of_spins

def int2bin(self, integer):
    bin_list = []
    for x in range(self.N):
        temp = integer % 2
        integer = integer // 2
        bin_list.append(temp)
    return bin_list[::-1]

def bin2int(self, bin_list):
    integer = 0
    temp = bin_list[::-1]
    for x in range(self.N):
        if temp[x] == 1:
            integer += 2 ** x
    return integer

# Spin operators
def s_plus(self, spin):
    s_plus = np.zeros([2 ** self.N, 2 ** self.N]) + 1j * np.zeros([2
        ** self.N, 2 ** self.N])
    for i in range(2 ** self.N):
        for j in range(2 ** self.N):
            i_bin = self.int2bin(i)
            j_bin = self.int2bin(j)
            if i_bin[spin] == 1 and j_bin[spin] == 0:
                same_state = True
                for k in range(self.N):
                    if k != spin and i_bin[k] != j_bin[k]:
                        same_state = False
                if same_state:
                    s_plus[i, j] += 1
    return s_plus

def s_minus(self, spin):
    s_minus = np.zeros([2 ** self.N, 2 ** self.N]) + 1j * np.zeros([2
        ** self.N, 2 ** self.N])
    for i in range(2 ** self.N):
        for j in range(2 ** self.N):
            i_bin = self.int2bin(i)
            j_bin = self.int2bin(j)
```

```

        if i_bin[spin] == 0 and j_bin[spin] == 1:
            same_state = True
            for k in range(self.N):
                if k != spin and i_bin[k] != j_bin[k]:
                    same_state = False
            if same_state:
                s_minus[i, j] += 1
    return s_minus
# Pauli matrices
def s_x(self, spin):
    s_x = 0.5 * (self.s_plus(spin) + self.s_minus(spin))
    return s_x

def s_y(self, spin):
    s_y = -1j * 0.5 * (self.s_plus(spin) - self.s_minus(spin))
    return s_y

def s_z(self, spin):
    s_z = np.zeros([2 ** self.N, 2 ** self.N]) + 1j * np.zeros([2 **
        self.N, 2 ** self.N])
    for i in range(2 ** self.N):
        i_bin = self.int2bin(i)
        if i_bin[spin] == 1:
            s_z[i, i] += 0.5
        elif i_bin[spin] == 0:
            s_z[i, i] -= 0.5
    return s_z

def sigma_x(self, spin):
    return self.s_x(spin) * 2

def sigma_y(self, spin):
    return self.s_y(spin) * 2

def sigma_z(self, spin):
    return self.s_z(spin) * 2

def hamiltonian_spinop(self, jx, jz): # in terms spin operators
    hamilton_matrix = np.zeros([2 ** self.N, 2 ** self.N]) + 1j * np.
        zeros([2 ** self.N, 2 ** self.N])
    for i in range(self.N - 1):
        hamilton_matrix += 1.0 / 2.0 * jx * \

```

```

        (np.dot(self.s_plus(i), self.s_minus(i +
            1)) + \
         np.dot(self.s_minus(i), self.s_plus(i + 1)
            )) + \
         jz * np.dot(self.s_z(i), self.s_z(i + 1))
    return hamilton_matrix

def hamiltonian_pauliop(self, jx, jz): # in terms of Pauli matrices
    hamilton_matrix = np.zeros([2 ** self.N, 2 ** self.N]) + 1j * np.
        zeros([2 ** self.N, 2 ** self.N])
    for i in range(self.N - 1):
        hamilton_matrix += 2 * jx * (
            np.dot(self.s_plus(i), self.s_minus(i + 1)) + \
            np.dot(self.s_minus(i), self.s_plus(i + 1))) + jz * \
            np.dot(self.sigma_z(i), self.sigma_z(i + 1))
    return hamilton_matrix

def initial_state(self, bin_list):
    initial_state = np.zeros([2 ** self.N, 1]) + 1j * np.zeros([2 **
        self.N, 1])
    temp = self.bin2int(bin_list)
    initial_state[temp] = 1
    return initial_state

# Lindblad operator as defined by Slava
def lindblad_op(self, spin, lamda, theta, phi):
    operator = -np.sin(theta) * self.sigma_z(spin) + \
        (1 + np.cos(theta)) * np.exp(-1j * phi) * self.s_plus(
            spin) - \
        (1 - np.cos(theta)) * np.exp(1j * phi) * self.s_minus(
            spin)
    operator_lamda = lamda * np.identity(2 ** self.N) + 1/2.0 *
        operator
    return operator_lamda

def fourier_k(self, spin, dens_mat): # spin = spin site number
    return measurement(2 * self.s_plus(spin), dens_mat)

def fourier_n(self, m, phi, dens_mat):
    temp = 0
    for i in range(self.N - 1): # effectively to N-2 = M-1

```

```

        temp += self.fourier_k(i, dens_mat) * np.exp(
            -1j * ((phi + 2 * np.pi * m) / (self.N - 1)) * i)
    return 1.0 / (self.N - 1) * temp

def spin_current_operator(self, const, site1, site2):
    spin_current = 2 * 1j * const * (
        np.dot(self.s_plus(site1), self.s_minus(site2)) - np.dot(self
            .s_minus(site1), self.s_plus(site2)))
    return spin_current

# Diagonalization
def eigensystem(matrix):
    eig_val, eig_vec = np.linalg.eig(matrix)
    idx = eig_val.argsort()[::-1]
    eigen_values = eig_val[idx]
    eigen_vectors = eig_vec[:, idx]
    return eigen_values, eigen_vectors

# Diagonalization for hermitian matrices
def eigensystem_herm(matrix):
    eig_val, eig_vec = scipy.linalg.eigh(matrix)
    idx = eig_val.argsort()[::-1]
    eigen_values = eig_val[idx]
    eigen_vectors = eig_vec[:, idx]
    return eigen_values, eigen_vectors

def time_evolve(initial_state, eigen_values, eigen_vectors, time):
    if initial_state.shape[0] == initial_state.shape[1]: # case for a
        density matrix
        eig_diag = np.diag(np.exp(time * eigen_values))
        state_t = np.dot(np.dot(eigen_vectors, \
            np.dot(eig_diag, np.linalg.inv(
                eigen_vectors))), vectorize(
                initial_state))
    else: # case for a ket
        eig_diag = np.diag(np.exp(- 1j * time * eigen_values))
        state_t = np.dot(np.dot(eigen_vectors, \
            np.dot(eig_diag, np.transpose(np.conjugate
                (eigen_vectors)))), initial_state)

    return state_t

```

```
def density_matrix(state):
    dens_mat = np.dot(state, np.transpose(np.conjugate(state)))
    return dens_mat

def normalize_densmat(dens_mat):
    return dens_mat / np.trace(dens_mat)

def pureness(dens_mat):
    return 1 - np.trace(np.dot(dens_mat, dens_mat))

def neumann_entropy(dens_mat):
    eigen_values, eigen_vectors = np.linalg.eig(dens_mat)
    temp = 0
    for i in range(eigen_values.shape[0]):
        temp += -np.dot(eigen_values[i], np.log2(eigen_values[i]))
    return temp

def measurement(operator, state): # state can be ket or density matrix
    if state.shape[0] == state.shape[1]: # case for a density matrix
        exp_val = np.trace(np.dot(operator, state))
    else: # case for a ket
        exp_val = np.asscalar(np.dot(np.transpose(np.conjugate(state)),
            np.dot(operator, state)))
    return exp_val

def vectorize(matrix):
    vector = np.reshape(matrix, (matrix.shape[1] ** 2, 1), order='F')
    return vector

def reverse_vectorize(vector):
    matrix = np.reshape(vector, (int(np.sqrt(vector.shape[0])), int(np.
        sqrt(vector.shape[0]))), order='F')
    return matrix
```

```

def partial_trace_1(matrix, dim): # tracing out the first subsystem (
    square matrices of dimension dim)
    new_dim = int(matrix.shape[0] / dim)
    temp = np.zeros([new_dim, new_dim]) + 1j * np.zeros([new_dim, new_dim]
    ])
    for i in range(dim):
        temp += matrix[i * new_dim:(i + 1) * new_dim, i * new_dim:(i + 1)
            * new_dim]
    return temp

def partial_trace_N(matrix, dim): # tracing out the last subsystem (
    square matrices of dimension dim)
    new_dim = int(matrix.shape[0] / dim)
    temp = np.zeros([new_dim, new_dim]) + 1j * np.zeros([new_dim, new_dim]
    ])
    for i in range(new_dim):
        for j in range(new_dim):
            for k in range(dim):
                temp[i][j] += matrix[i * dim + k][j * dim + k]
    return temp

def unitary_lindblad(hamiltonian): # vectorized unitary part
    unit_lind = -1j * (np.mat(np.kron(np.identity(hamiltonian.shape[1]),
        hamiltonian)) - np.mat(
            np.kron(np.transpose(hamiltonian), np.identity(hamiltonian.shape
                [1]))))
    return unit_lind

# In the following we vectorize the dissipator
def both_multi(operator):
    operator_conj_trans = np.transpose(np.transpose(np.conjugate(operator
        ))) # create the conjugate transpose
    result = np.kron(operator_conj_trans, operator) # do the tensor
        product LtxL
    return result

def left_multi(operator):
    operator1 = np.dot(np.transpose(np.conjugate(operator)), operator) #
        dot Lt and L together

```

```

    result = np.kron(np.identity(operator.shape[1]), operator1) # do the
        tensor product 1xLtL
    return result

def right_multi(operator):
    operator1 = np.dot(np.transpose(np.conjugate(operator)), operator) #
        dot Lt and L together
    result = np.kron(np.transpose(operator1), np.identity(operator.shape
        [1])) # do the tensor product LtLx1
    return result

# Generates the dissipator. Takes the nested list lindblad_list as
    argument:
# arguments = [[lamda_1, theta_L, phi_L], [lamda_2, theta_R, phi_R]]
# gammas = [Gamma, Gamma]
# lindblad_list = [sites, operators, arguments, gammas]

def dissipative_lindblad(lindblad_list):
    diss_lind = 0
    for i in range(len(lindblad_list[0])):
        temp1 = both_multi(lindblad_list[1][i](lindblad_list[0][i],
            lindblad_list[2][i][0], lindblad_list[2][i][1],
                lindblad_list[2][i][2]))
        temp2 = left_multi(lindblad_list[1][i](lindblad_list[0][i],
            lindblad_list[2][i][0], lindblad_list[2][i][1],
                lindblad_list[2][i][2]))
        temp3 = right_multi(lindblad_list[1][i](lindblad_list[0][i],
            lindblad_list[2][i][0], lindblad_list[2][i][1],
                lindblad_list[2][i][2]))
        diss_lind += lindblad_list[3][i] * temp1 - lindblad_list[3][i] *
            0.5 * (temp2 + temp3)
    return diss_lind

def correlator(site1, site2, operator_a, operator_b, dens_mat):
    corr = measurement(np.dot(operator_a(site1), operator_b(site2)),
        dens_mat) - measurement(
        operator_a(site1), dens_mat) * measurement(operator_b(site2),
        dens_mat)
    return corr

```

```

# Code for the F matrix construction. We just use analytical expressions.

analyticBasis = HeisenbergBasis(1)
X = np.flipud(np.fliplr(analyticBasis.sigma_x(0)))
Y = np.flipud(np.fliplr(analyticBasis.sigma_y(0)))
Z = np.flipud(np.fliplr(analyticBasis.sigma_z(0)))
U = np.identity(2)
SP = np.flipud(np.fliplr(analyticBasis.s_plus(0)))
SM = np.flipud(np.fliplr(analyticBasis.s_minus(0)))

def MiddleSite(mat1, site, numsites0):
    return np.kron(np.identity(2 ** (site - 1)), np.kron(mat1, np.
        identity(2 ** (numsites0 - site))))

def XXZ(N, Delta):
    hXXZ = (np.kron(X, X) + np.kron(Y, Y)) + Delta * (np.kron(Z, Z) - np.
        kron(U, U));
    temp = np.zeros([2 ** N, 2 ** N]) + 1j * np.zeros([2 ** N, 2 ** N]);
    for site in range(1, N):
        temp += MiddleSite(hXXZ, site, N - 1)
    return temp

def vec0(theta, phi):
    vec0 = np.zeros([2, 1]) + 1j * np.zeros([2, 1])
    vec0[0] = np.cos(theta / 2.0) * np.exp(-1j * phi / 2.0)
    vec0[1] = np.sin(theta / 2.0) * np.exp(1j * phi / 2.0)
    return vec0

def vec0perp(theta, phi):
    vec0perp = np.zeros([2, 1]) + 1j * np.zeros([2, 1])
    vec0perp[0] = np.sin(theta / 2.0) * np.exp(-1j * phi / 2.0) # np.
        random.rand()
    vec0perp[1] = -np.cos(theta / 2.0) * np.exp(1j * phi / 2.0) # np.
        random.rand()
    return vec0perp

def projector(N, vec_L, vec_R):

```

```

dens_L = density_matrix(vec_L)
dens_R = density_matrix(vec_R)
projector = np.kron(dens_L, np.kron(np.identity(2 ** (N - 2)), dens_R
    ))
return projector

def h00direct(N, Delta, theta_L, phi_L, theta_R, phi_R):
    h00 = partial_trace_1(
        partial_trace_N(np.dot(XXZ(N, Delta), projector(N, vec0(theta_L,
            phi_L), vec0(theta_R, phi_R))), 2), 2)
    return h00

def C00(theta, phi, Delta):
    return np.sin(theta) * (np.exp(-1j * phi) * SP + np.exp(1j * phi) *
        SM) + Delta * (np.cos(theta) * Z - U)

def h00analytical(N, Delta, theta_L, phi_L, theta_R, phi_R):
    res = XXZ(N - 2, Delta) + np.kron(C00(theta_L, phi_L, Delta), np.
        identity(2 ** (N - 3))) + np.kron(
        np.identity(2 ** (N - 3)), C00(theta_R, phi_R, Delta))
    return res

# Perturbation to lift degeneracies of h00

def h00perp(N, Delta, theta_L, phi_L, theta_R, phi_R, epsilon1, epsilon2)
:
    temp1 = np.kron((1 / 2.0) * (U + (1 / np.sqrt(2)) * (Y + Z)),
        np.kron(np.identity(2 ** (N - 2)), (1 / 2.0) * (U + X
            )))
    h00perp = partial_trace_1(partial_trace_N(np.dot(XXZ(N, Delta), temp1
        ), 2), 2)
    return h00perp

# def h00perp(N, Delta, theta_L, phi_L, theta_R, phi_R, epsilon1,
    epsilon2):
#     temp1 = partial_trace_1(partial_trace_N(np.dot(XXZ(N, Delta),
        projector(N, vec0perp(theta_L, phi_L), vec0(theta_R, phi_R))), 2), 2)
#     temp2 = partial_trace_1(partial_trace_N(np.dot(XXZ(N, Delta),

```

```

    projector(N, vec0(theta_L, phi_L), vec0perp(theta_R, phi_R)), 2), 2)
#     h00perp = epsilon1*temp1 + epsilon2*temp2
#     return h00perp

def uniq(lst):
    last = object()
    for item in lst:
        if item == last:
            continue
        yield item
        last = item

def sort_and_deduplicate(lst):
    return list(uniq(sorted(lst, reverse=False)))

def GetDegenerateSubspaces(eiv, precision_in_digits):
    roundedEiv = [round(element, precision_in_digits) for element in eiv]

    spaces = []
    for i in range(len(roundedEiv)):
        spaces.append([j for j, x in enumerate(roundedEiv) if x ==
            roundedEiv[i]]) # => [1, 3]

    relevant_spaces = []
    for i in range(len(spaces)):
        if len(spaces[i]) > 1:
            relevant_spaces.append(spaces[i])

    degenerate_spaces = sort_and_deduplicate(relevant_spaces)

    return degenerate_spaces, len(degenerate_spaces)

def GetNewCombination(N, ListOfIndices, vec, h00perp, newVec):
    dim = len(ListOfIndices)

    MatCoeff = np.zeros([dim, dim]) + 1j * np.zeros([dim, dim])

    count_i = -1
    count_j = -1

```

```
for i in ListOfIndices:
    count_i += 1
    for j in ListOfIndices:
        if count_j < dim - 1:
            count_j += 1
        else:
            count_j += 1 - dim

    MatCoeff[count_i, count_j] = np.asscalar(
        np.dot(np.transpose(np.conjugate(vec[:, i])), np.dot(
            h00perp, vec[:, j])))

# the following lines are needed, if the Matrix is numerically non-
# zero, it's eigenvectors are "arbitrary" and thus
# the new combinations, builded later are non-orthogonal

if np.allclose(MatCoeff, 0, atol=10e-12) == True:
    MatCoeff = np.zeros([dim, dim]) + 1j * np.zeros([dim, dim])

newEiv, coeffVec = eigensystem(MatCoeff)

for j in range(dim):
    for k in range(dim):
        newVec[:, ListOfIndices[j]] += coeffVec[:, j][k] * vec[:,
            ListOfIndices[k]] d

return newVec

def flatten_list(ls, flattened_list=[]):
    for elem in ls:
        if not isinstance(elem, list):
            flattened_list.append(elem)
        else:
            flatten_list(elem, flattened_list)
    return flattened_list

def C01(theta, phi, Delta):
    return (1 - np.cos(theta)) * np.exp(-1j * phi) * SP - (1 + np.cos(
        theta)) * np.exp(1j * phi) * SM + Delta * np.sin(
```

```

        theta) * Z

def C01_hc(theta, phi, Delta):
    return (1 - np.cos(theta)) * np.exp(1j * phi) * SM - (1 + np.cos(
        theta)) * np.exp(-1j * phi) * SP + Delta * np.sin(
        theta) * Z

# Here h[k0] is defined in arbitrary basis parametrized by the angle eta

def Makeh01(N, Delta, theta_L, phi_L, theta_R, phi_R, eta):
    return np.cos(eta) * np.kron(C01(theta_L, phi_L, Delta), np.identity
        (2 ** (N - 3))) - np.sin(eta) * np.kron(
        np.identity(2 ** (N - 3)), C01(theta_R, phi_R, Delta))

def Makeh10(N, Delta, theta_L, phi_L, theta_R, phi_R, eta):
    return np.transpose(np.conjugate(Makeh01(N, Delta, bound_grad, eta)))

def Makeh02(N, Delta, theta_L, phi_L, theta_R, phi_R, eta):
    return np.sin(eta) * np.kron(C01(theta_L, phi_L, Delta), np.identity
        (2 ** (N - 3))) + np.cos(eta) * np.kron(
        np.identity(2 ** (N - 3)), C01(theta_R, phi_R, Delta))

def Makeh20(N, Delta, theta_L, phi_L, theta_R, phi_R, eta):
    return np.transpose(np.conjugate(Makeh02(N, Delta, bound_grad, eta)))

def ProceedSimon(N, Delta, theta_L, phi_L, theta_R, phi_R, epsilon1,
    epsilon2):
    Ham = XXZ(N, Delta)
    h00 = h00analytical(N, Delta, theta_L, phi_L, theta_R, phi_R)
    hperp = h00perp(N, Delta, theta_L, phi_L, theta_R, phi_R, epsilon1,
        epsilon2)

    eiv, vec = eigensystem_herm(h00)
    dim = eiv.shape[0]

```

```

DegSpaces, NumSpaces = GetDegenerateSubspaces(eiv, 12)

newVec = np.zeros([2 ** (N - 2), 2 ** (N - 2)]) + 1j * np.zeros([2 **
    (N - 2), 2 ** (N - 2)])

for i in range(NumSpaces):
    newVec = GetNewCombination(N, DegSpaces[i], vec, hperp, newVec)

correctVec = np.copy(vec)

NumFalseVec = len(flatten_list(DegSpaces, []))

for i in range(NumFalseVec):
    correctVec[:, flatten_list(DegSpaces, [])[i]] = newVec[:,
        flatten_list(DegSpaces, [])[i]]

dim = len(eiv)

for i in range(dim):
    correctVec[:, i] = correctVec[:, i] / (np.linalg.norm(correctVec
       [:, i]))

# check orthogonality
ortho = np.zeros([dim, dim]) + 1j * np.zeros([dim, dim])
for i in range(dim):
    for j in range(dim):
        ortho[i, j] = np.dot(np.conjugate(np.transpose(correctVec[:,
            i])), correctVec[:, j])
        if i != j and np.allclose(ortho[i, j], 0) == False:
            print('Warning! Eigenvectors %i and %i are not orthogonal
                ' % (i, j))
            print('Delta', Delta)

eta = np.pi / 5.0
h = [Makeh01(N, Delta, theta_L, phi_L, theta_R, phi_R, eta), Makeh02(
    N, Delta, theta_L, phi_L, theta_R, phi_R, eta)]

def Q(k0):
    Q = np.zeros([dim, dim]) + 1j * np.zeros([dim, dim])
    for j in range(dim):
        for k in range(dim):
            Q[k, j] = np.abs(np.asscalar(

```

```

        np.dot(np.transpose(np.conjugate(correctVec[:, j])),
              np.dot(h[k0], correctVec[:, k]))) ** 2
    return Q

Q0 = Q(0) + Q(1)

F = Q0
temp = 0
for i in range(dim):
    F[i, i] = 0
    for j in range(dim):
        temp += F[j, i]
    F[i, i] = -temp
    temp = 0

# Numerically solve the system of equations F nu = 0

def equations(y):
    null_vec = np.zeros(dim)
    for i in range(F.shape[0]):
        for j in range(F.shape[1]):
            null_vec[i] += np.real(F[i, j]) * y[j]
    return null_vec

# y = scipy.optimize.fsolve(equations, (np.random.rand(dim)))
y = scipy.optimize.newton_krylov(equations, (np.random.rand(dim)))
# y = scipy.optimize.broyden2(equations, (np.random.rand(dim)))

eigvals = y / np.sum(y)
idx = eigvals.argsort()[::-1]
eigen_values = eigvals[idx]

NESS = 0
for i in range(dim):
    NESS += eigvals[i] * (np.asmatrix(correctVec[:, i]).T * np.
                        conjugate(np.asmatrix(correctVec[:, i])))

return NESS

```


Details on Perturbative Calculation

B.1 Definitions of Subhamiltonians

Using the basis defined in Equations (4.28) to (4.31) it is straightforward to derive the following expressions, see [25] for details:

$$h^{00} \equiv h^{00}(\theta_L, \varphi_L, \theta_R, \varphi_R) = H' + C_{++}(2, \theta_L, \varphi_L) + C_{++}(N-1, \theta_R, \varphi_R), \quad (\text{B.1})$$

$$H' = \sum_{j=2}^{N-2} h_{j,j+1}^{XXZ}(\Delta), \quad (\text{B.2})$$

$$\begin{aligned} C_{++}(m, \theta, \varphi) &= \text{tr}_{m-1} \left((|\psi(\varphi)\rangle \langle \psi(\varphi)|)_{m-1} h_{m-1,m}^{XXZ} \right) \\ &= J(\sin \theta (e^{i\varphi} \sigma_m^- + e^{-i\varphi} \sigma_m^+) + \Delta \sigma_m^z \cos \theta - \Delta I_{2,3,\dots,N-1}), \end{aligned} \quad (\text{B.3})$$

where $h_{j,j+1}^{XXZ}$ are the local energy densities of the XXZ Hamiltonian and $\sigma_m^\alpha = I_{2,3,\dots,m-1} \otimes \sigma^\alpha \otimes I_{m+1,\dots,N-1}$, with $1 \leq m \leq N$ and $\alpha = \pm, z$.

The other sub-hamiltonians h^{k0} are given by

$$h^{10}(w) = \cos w (C_{+-}(2, \theta_L, \varphi_L) - C_{+-}(N-1, \theta_R, \varphi_R)), \quad (\text{B.4})$$

$$h^{20}(w) = \sin w (C_{+-}(2, \theta_L, \varphi_L) + C_{+-}(N-1, \theta_R, \varphi_R)), \quad (\text{B.5})$$

$$h^{30}(w) = 0, \quad \text{for } N > 2. \quad (\text{B.6})$$

where

$$\begin{aligned}
 C_{+-}(m, \theta, \varphi) &= \text{tr}_{m-1} \left((|\psi(\varphi)\rangle\langle\psi^\perp(\varphi)|)_{m-1} h_{m-1,m}^{\text{XXZ}} \right) \\
 &= J \left(2 \sin^2 \frac{\theta}{2} (e^{i\varphi} \sigma_m^-) - 2 \cos^2 \frac{\theta}{2} (e^{-i\varphi} \sigma_m^+) + \Delta \sigma_m^z \sin \theta \right). \tag{B.7}
 \end{aligned}$$

B.2 Calculation of the Commutator and the Secular Condition at First Order

We split $[H, \rho^{(1)}]$ into $H\rho^{(1)}$ and $\rho^{(1)}H$ to make it easier to handle and mulitply out all the terms which don't vanish on first sight

$$H\rho^{(1)} = \left(H_{00} + \sum_{n \neq 0} (H_{n0} + H_{0n}) + \sum_{n \neq 0} \sum_{m \neq 0} H_{nm} \right) \times \tag{B.8}$$

$$\left(-\frac{i}{2} \sum_{j \neq 0} (|e^j\rangle\langle e^0| \otimes h_{j0} R^{(0)} - |e^0\rangle\langle e^j| \otimes R^{(0)} h_{0j}) + |e^1\rangle\langle e^0| \otimes m^{(1)} \right) \tag{B.9}$$

$$\begin{aligned}
 &= -\frac{i}{2} \sum_{m \neq 0} \sum_{j \neq 0} |e^0\rangle\langle e^m| \underbrace{|e^j\rangle\langle e^0|}_{\delta_{mj}} \otimes h_{0m} h_{j0} R^{(0)} - \frac{i}{2} \sum_{n \neq 0} \sum_{m \neq 0} \sum_{j \neq 0} |e^n\rangle\langle e^m| \underbrace{|e^j\rangle\langle e^0|}_{\delta_{mj}} \otimes h_{nm} h_{j0} R^{(0)} \\
 &\tag{B.10}
 \end{aligned}$$

$$+ \frac{i}{2} \sum_{j \neq 0} |e^0\rangle\langle e^0| \underbrace{|e^0\rangle\langle e^0|}_{=1} \langle e^j| \otimes h_{00} R^{(0)} h_{0j} + \frac{i}{2} \sum_{n \neq 0} \sum_{j \neq 0} |e^n\rangle\langle e^0| \underbrace{|e^0\rangle\langle e^0|}_{=1} \langle e^j| \otimes h_{n0} R^{(0)} h_{0j} \tag{B.11}$$

$$+ |e^0\rangle\langle e^0| \otimes h_{00} m^{(1)} + \sum_{n \neq 0} |e^n\rangle\langle e^0| \otimes h_{n0} m^{(1)} \tag{B.12}$$

and

$$-\rho^{(1)}H = -\left(-\frac{i}{2}\sum_{j\neq 0}(|e^j\rangle\langle e^0|\otimes h_{j0}R^{(0)} - |e^0\rangle\langle e^j|\otimes R^{(0)}h_{0j}) + |e^1\rangle\langle e^0|\otimes m^{(1)}\right)\times \quad (\text{B.13})$$

$$\left(H_{00} + \sum_{n\neq 0}(H_{n0} + H_{0n}) + \sum_{n\neq 0}\sum_{m\neq 0}H_{nm}\right) \quad (\text{B.14})$$

$$= +\frac{i}{2}\sum_{j\neq 0}|e^j\rangle\langle e^0|\otimes h_{j0}R^{(0)}h_{00} + \frac{i}{2}\sum_{m\neq 0}\sum_{j\neq 0}|e^j\rangle\langle e^0|e^0\rangle\langle e^m|\otimes h_{j0}R^{(0)}h_{0m} \quad (\text{B.15})$$

$$- \frac{i}{2}\sum_{n\neq 0}\sum_{j\neq 0}|e^0\rangle\langle e^j|e^n\rangle\langle e^0|\otimes R^{(0)}h_{0j}h_{n0} - \frac{i}{2}\sum_{n\neq 0}\sum_{m\neq 0}\sum_{j\neq 0}|e^0\rangle\langle e^j|e^n\rangle\langle e^j|\otimes R^{(0)}h_{0j}h_{nm} \quad (\text{B.16})$$

$$- |e^0\rangle\langle e^0|\otimes m^{(1)}h_{00} - \sum_{m\neq 0}|e^0\rangle\langle e^m|\otimes m^{(1)}h_{0m} \quad (\text{B.17})$$

Now we put it together and resolve the Kronecker deltas

$$[H, \rho^{(1)}] = -\frac{i}{2}\sum_{j\neq 0}|e^0\rangle\langle e^0|\otimes h_{0j}h_{j0}R^{(0)} - \frac{i}{2}\sum_{n\neq 0}\sum_{j\neq 0}|e^n\rangle\langle e^0|\otimes h_{nj}h_{j0}R^{(0)} \quad (\text{B.18})$$

$$+ \frac{i}{2}\sum_{j\neq 0}|e^0\rangle\langle e^j|\otimes h_{00}R^{(0)}h_{0j} + \frac{i}{2}\sum_{n\neq 0}\sum_{j\neq 0}|e^n\rangle\langle e^j|\otimes h_{n0}R^{(0)}h_{0j} \quad (\text{B.19})$$

$$+ \frac{i}{2}\sum_{j\neq 0}|e^j\rangle\langle e^0|\otimes h_{j0}R^{(0)}h_{00} + \frac{i}{2}\sum_{m\neq 0}\sum_{j\neq 0}|e^j\rangle\langle e^m|\otimes h_{j0}R^{(0)}h_{0m} \quad (\text{B.20})$$

$$- \frac{i}{2}\sum_{j\neq 0}|e^0\rangle\langle e^0|\otimes R^{(0)}h_{0j}h_{j0} - \frac{i}{2}\sum_{m\neq 0}\sum_{j\neq 0}|e^0\rangle\langle e^j|\otimes R^{(0)}h_{0j}h_{jm} \quad (\text{B.21})$$

$$+ |e^0\rangle\langle e^0|\otimes [h_{00}, m^{(1)}] + \sum_{n\neq 0}|e^n\rangle\langle e^0|\otimes h_{n0}m^{(1)} - \sum_{m\neq 0}|e^0\rangle\langle e^m|\otimes m^{(1)}h_{0m}. \quad (\text{B.22})$$

and finally take the trace

$$\text{Tr}_{1,N}([H, \rho^{(0)}]) = [h_{00}, m^{(1)}] - \frac{i}{2}\sum_{j\neq 0}(-2h_{j0}R^{(0)}h_{0j} + R^{(0)}h_{0j}h_{j0} + h_{0j}h_{j0}R^{(0)}) \quad (\text{B.23})$$

$$= [h_{00}, m^{(1)}] - \frac{i}{2}\sum_{j\neq 0}(-2h_{j0}R^{(0)}h_{j0}^\dagger + R^{(0)}h_{j0}^\dagger h_{j0} + h_{j0}^\dagger h_{j0}R^{(0)}) \quad (\text{B.24})$$

$$= [h_{00}, m^{(1)}] + 4i\sum_{j\neq 0}\mathcal{D}_{h_{j0}}[R^{(0)}] \stackrel{!}{=} 0. \quad (\text{B.25})$$

where

$$\mathcal{D}_{h_{j_0}} [R^{(0)}] = h_{j_0} R^{(0)} h_{j_0}^\dagger - \frac{1}{2} \{h_{j_0}^\dagger h_{j_0}, R^{(0)}\} \quad (\text{B.26})$$

B.3 Diagonal Elements of $\text{Tr}_{1,N}([H, \rho^{(1)}]) = 0$

$$\langle \gamma | \text{Tr}_{1,N}([H, \rho^{(0)}]) | \gamma \rangle = \langle \gamma | [h_{00}, m^{(1)}] | \gamma \rangle + 4i \sum_{j \neq 0} \langle \gamma | \mathcal{D}_{h_{j_0}} [R^{(0)}] | \gamma \rangle \quad (\text{B.27})$$

where we can use (4.46) namely $h_{00} | \gamma \rangle = \lambda_\gamma | \gamma \rangle$ and hermiticity of h_{00} to show that the first term is equal to zero

$$\langle \gamma | [h_{00}, m^{(1)}] | \gamma \rangle = \langle \gamma | h_{00} m^{(1)} | \gamma \rangle \cdot \langle \gamma | m^{(1)} h_{00} | \gamma \rangle \quad (\text{B.28})$$

$$= (\lambda_\gamma - \lambda_\gamma) \langle \gamma | m^{(1)} | \gamma \rangle \quad (\text{B.29})$$

$$= 0 \quad (\text{B.30})$$

We can further calculate the remaining term by inserting $R^{(0)} = \sum_\alpha v_\alpha | \alpha \rangle \langle \alpha |$ which leads to

$$4i \sum_{j \neq 0} \langle \gamma | \mathcal{D}_{h_{j_0}} [R^{(0)}] | \gamma \rangle = 4i \sum_{j \neq 0} \sum_{\alpha=0}^{d_1-1} v_\alpha \langle \gamma | \mathcal{D}_{h_{j_0}} [| \alpha \rangle \langle \alpha |] | \gamma \rangle \quad (\text{B.31})$$

$$= 4i \sum_{j \neq 0} \sum_{\alpha=0}^{d_1-1} v_\alpha \left(\langle \gamma | h_{j_0} | \alpha \rangle \langle \alpha | h_{j_0}^\dagger | \gamma \rangle - \frac{1}{2} \langle \gamma | h_{j_0}^\dagger h_{j_0} | \alpha \rangle \underbrace{\langle \alpha | \gamma \rangle}_{\delta_{\alpha\gamma}} - \frac{1}{2} \underbrace{\langle \gamma | \alpha \rangle}_{\delta_{\gamma\alpha}} \langle \alpha | h_{j_0}^\dagger h_{j_0} | \gamma \rangle \right) \quad (\text{B.32})$$

$$= 4i \sum_{j \neq 0} \left(\sum_{\alpha=0}^{d_1-1} v_\alpha \left(|\langle \gamma | h_{j_0} | \alpha \rangle|^2 \right) - v_\gamma \langle \gamma | h_{j_0}^\dagger h_{j_0} | \gamma \rangle \right) \quad (\text{B.33})$$

and we can insert a resolution of unity inside the second term $\mathbb{1} = \sum_{\beta=0}^{d_1-1} |\beta\rangle\langle\beta|$

$$4i \sum_{j \neq 0} \langle \gamma | \mathcal{D}_{h_{j0}} [R^{(0)}] | \gamma \rangle = 4i \sum_{j \neq 0} \left(\sum_{\alpha=0}^{d_1-1} v_{\alpha} \left(|\langle \gamma | h_{j0} | \alpha \rangle|^2 \right) - v_{\gamma} \sum_{\beta=0}^{d_1-1} \langle \gamma | h_{j0}^{\dagger} | \beta \rangle \langle \beta | h_{j0} | \gamma \rangle \right) \quad (\text{B.34})$$

$$= 4i \sum_{j \neq 0} \left(\sum_{\alpha=0}^{d_1-1} v_{\alpha} \left(|\langle \gamma | h_{j0} | \alpha \rangle|^2 \right) - v_{\gamma} \sum_{\beta=0}^{d_1-1} \left(|\langle \beta | h_{j0} | \gamma \rangle|^2 \right) \right) \quad (\text{B.35})$$

$$= 4i \sum_{j \neq 0} \left(\sum_{\alpha \neq \gamma}^{d_1-1} v_{\alpha} \left(|\langle \gamma | h_{j0} | \alpha \rangle|^2 \right) - v_{\gamma} \sum_{\beta \neq \gamma}^{d_1-1} \left(|\langle \beta | h_{j0} | \gamma \rangle|^2 \right) \right) \quad (\text{B.36})$$

where we noticed in the last step, that the term $\alpha, \beta = \gamma$ cancel each other.

APPENDIX C

Analytical Results for $N = 5$

C.1 Steady State Density Matrix for $N = 5$ and Unnormalized Eigenvectors of h_{00}

The precise situation we look at is defined by the parameters: $N = 5, \gamma = \pi/3, \theta = \theta_L = \theta_R = \pi/2, \phi_L = 0, \phi_R = 4\pi/3$.

$$\rho = \begin{pmatrix} \frac{28}{227} & \frac{1}{8} \left(-\frac{44}{227} + \frac{84i\sqrt{3}}{227} \right) & \frac{1}{8} \left(\frac{38}{227} + \frac{38i\sqrt{3}}{227} \right) & \frac{1}{8} \left(\frac{4}{227} + \frac{52i\sqrt{3}}{227} \right) & \frac{1}{8} \left(\frac{148}{227} + \frac{20i\sqrt{3}}{227} \right) & \frac{1}{8} \left(-\frac{70}{227} + \frac{70i\sqrt{3}}{227} \right) & \frac{1}{8} \left(-\frac{80}{227} + \frac{24i\sqrt{3}}{227} \right) & \frac{10}{227} \\ \frac{1}{8} \left(-\frac{44}{227} - \frac{84i\sqrt{3}}{227} \right) & \frac{28}{227} & \frac{1}{8} \left(\frac{160}{227} - \frac{32i\sqrt{3}}{227} \right) & \frac{1}{8} \left(\frac{50}{227} + \frac{50i\sqrt{3}}{227} \right) & \frac{1}{8} \left(\frac{50}{227} - \frac{62i\sqrt{3}}{227} \right) & \frac{1}{8} \left(\frac{160}{227} + \frac{44i\sqrt{3}}{227} \right) & \frac{1}{8} \left(\frac{152}{227} + \frac{24i\sqrt{3}}{227} \right) & \frac{1}{8} \left(-\frac{80}{227} + \frac{24i\sqrt{3}}{227} \right) \\ \frac{1}{8} \left(\frac{38}{227} - \frac{38i\sqrt{3}}{227} \right) & \frac{1}{8} \left(\frac{160}{227} + \frac{32i\sqrt{3}}{227} \right) & \frac{59}{454} & \frac{1}{8} \left(-\frac{14}{227} + \frac{102i\sqrt{3}}{227} \right) & \frac{1}{8} \left(\frac{160}{227} - \frac{32i\sqrt{3}}{227} \right) & \frac{1}{8} \left(\frac{80}{227} + \frac{80i\sqrt{3}}{227} \right) & \frac{1}{8} \left(\frac{160}{227} + \frac{44i\sqrt{3}}{227} \right) & \frac{1}{8} \left(-\frac{70}{227} + \frac{70i\sqrt{3}}{227} \right) \\ \frac{1}{8} \left(\frac{4}{227} - \frac{52i\sqrt{3}}{227} \right) & \frac{1}{8} \left(\frac{50}{227} - \frac{50i\sqrt{3}}{227} \right) & \frac{1}{8} \left(-\frac{14}{227} - \frac{102i\sqrt{3}}{227} \right) & \frac{28}{227} & \frac{1}{8} \left(-\frac{40}{227} - \frac{88i\sqrt{3}}{227} \right) & \frac{1}{8} \left(\frac{160}{227} - \frac{32i\sqrt{3}}{227} \right) & \frac{1}{8} \left(\frac{50}{227} - \frac{62i\sqrt{3}}{227} \right) & \frac{1}{8} \left(\frac{148}{227} + \frac{20i\sqrt{3}}{227} \right) \\ \frac{1}{8} \left(\frac{148}{227} - \frac{20i\sqrt{3}}{227} \right) & \frac{1}{8} \left(\frac{50}{227} + \frac{62i\sqrt{3}}{227} \right) & \frac{1}{8} \left(\frac{160}{227} + \frac{32i\sqrt{3}}{227} \right) & \frac{1}{8} \left(-\frac{40}{227} + \frac{88i\sqrt{3}}{227} \right) & \frac{28}{227} & \frac{1}{8} \left(-\frac{14}{227} + \frac{102i\sqrt{3}}{227} \right) & \frac{1}{8} \left(\frac{50}{227} + \frac{50i\sqrt{3}}{227} \right) & \frac{1}{8} \left(\frac{4}{227} + \frac{52i\sqrt{3}}{227} \right) \\ \frac{1}{8} \left(-\frac{70}{227} - \frac{70i\sqrt{3}}{227} \right) & \frac{1}{8} \left(\frac{160}{227} - \frac{44i\sqrt{3}}{227} \right) & \frac{1}{8} \left(\frac{80}{227} - \frac{80i\sqrt{3}}{227} \right) & \frac{1}{8} \left(\frac{160}{227} + \frac{32i\sqrt{3}}{227} \right) & \frac{1}{8} \left(-\frac{14}{227} - \frac{102i\sqrt{3}}{227} \right) & \frac{59}{454} & \frac{1}{8} \left(\frac{160}{227} - \frac{32i\sqrt{3}}{227} \right) & \frac{1}{8} \left(\frac{38}{227} + \frac{38i\sqrt{3}}{227} \right) \\ \frac{1}{8} \left(-\frac{80}{227} - \frac{24i\sqrt{3}}{227} \right) & \frac{1}{8} \left(\frac{152}{227} - \frac{24i\sqrt{3}}{227} \right) & \frac{1}{8} \left(\frac{160}{227} - \frac{44i\sqrt{3}}{227} \right) & \frac{1}{8} \left(\frac{50}{227} + \frac{62i\sqrt{3}}{227} \right) & \frac{1}{8} \left(\frac{50}{227} - \frac{50i\sqrt{3}}{227} \right) & \frac{1}{8} \left(\frac{160}{227} + \frac{32i\sqrt{3}}{227} \right) & \frac{28}{227} & \frac{1}{8} \left(-\frac{44}{227} + \frac{84i\sqrt{3}}{227} \right) \\ \frac{10}{227} & \frac{1}{8} \left(-\frac{80}{227} - \frac{24i\sqrt{3}}{227} \right) & \frac{1}{8} \left(-\frac{70}{227} - \frac{70i\sqrt{3}}{227} \right) & \frac{1}{8} \left(\frac{148}{227} - \frac{20i\sqrt{3}}{227} \right) & \frac{1}{8} \left(\frac{4}{227} - \frac{52i\sqrt{3}}{227} \right) & \frac{1}{8} \left(\frac{38}{227} - \frac{38i\sqrt{3}}{227} \right) & \frac{1}{8} \left(-\frac{44}{227} - \frac{84i\sqrt{3}}{227} \right) & \frac{28}{227} \end{pmatrix}. \quad (\text{C.1})$$

$$\begin{aligned}
 |0\rangle &= \begin{pmatrix} -1 \\ \frac{6(41-9i\sqrt{3}-5i\sqrt{11}+7\sqrt{33})}{(\sqrt{3}-3i)^2(7+\sqrt{33})} \\ \frac{2(51i+17\sqrt{3}+9\sqrt{11}+9i\sqrt{33})}{(\sqrt{3}-3i)(7+\sqrt{33})} \\ \frac{17+8i\sqrt{3}+4i\sqrt{11}+3\sqrt{33}}{7+\sqrt{33}} \\ -\frac{6(41+9i\sqrt{3}+5i\sqrt{11}+7\sqrt{33})}{(\sqrt{3}-3i)^2(7+\sqrt{33})} \\ \frac{4(17\sqrt{3}+9\sqrt{11})}{(\sqrt{3}-3i)(7+\sqrt{33})} \\ -\frac{7+25i\sqrt{3}+13i\sqrt{11}+\sqrt{33}}{2(7+\sqrt{33})} \\ 1 \end{pmatrix} & \quad |1\rangle = \begin{pmatrix} 0 \\ \frac{2\sqrt{3}}{\sqrt{3}+3i} \\ -3 + \frac{12i}{\sqrt{3}+3i} \\ \frac{1}{2}(1+i\sqrt{3}) \\ \frac{\sqrt{3}-3i}{\sqrt{3}+3i} \\ -\frac{6i}{\sqrt{3}+3i} \\ 1 \\ 0 \end{pmatrix} & \quad |2\rangle = \begin{pmatrix} 1 \\ \frac{1}{2}(1+i\sqrt{3}) \\ 0 \\ -1 \\ -1 \\ 0 \\ \frac{1}{2}(1-i\sqrt{3}) \\ 1 \end{pmatrix} \quad (C.2)
 \end{aligned}$$

$$\begin{aligned}
 |3\rangle &= \begin{pmatrix} -1 \\ \frac{-13i-3\sqrt{3}+3i\sqrt{17}+\sqrt{51}}{(\sqrt{3}-i)(\sqrt{17}-5)} \\ \frac{2(\sqrt{3}+3i)(\sqrt{17}-4)}{(\sqrt{3}-3i)(\sqrt{17}-5)} \\ \frac{11+5i\sqrt{3}-3\sqrt{17}-i\sqrt{51}}{10-2\sqrt{17}} \\ \frac{-13i+3\sqrt{3}+3i\sqrt{17}-\sqrt{51}}{(\sqrt{3}-i)(\sqrt{17}-5)} \\ \frac{4\sqrt{3}(\sqrt{17}-4)}{(\sqrt{3}-3i)(\sqrt{17}-5)} \\ \frac{i(i-4\sqrt{3}+\sqrt{51})}{\sqrt{17}-5} \\ 1 \end{pmatrix} & \quad |4\rangle = \begin{pmatrix} -1 \\ \frac{13i+3\sqrt{3}+3i\sqrt{17}+\sqrt{51}}{(\sqrt{3}-i)(5+\sqrt{17})} \\ \frac{2(\sqrt{3}+3i)(4+\sqrt{17})}{(\sqrt{3}-3i)(5+\sqrt{17})} \\ \frac{11+5i\sqrt{3}+3\sqrt{17}+i\sqrt{51}}{10+2\sqrt{17}} \\ \frac{6(13+3i\sqrt{3}+3\sqrt{17}+i\sqrt{51})}{(\sqrt{3}-3i)^2(5+\sqrt{17})} \\ \frac{4\sqrt{3}(4+\sqrt{17})}{(\sqrt{3}-3i)(5+\sqrt{17})} \\ \frac{1+4i\sqrt{3}+i\sqrt{51}}{5+\sqrt{17}} \\ 1 \end{pmatrix} & \quad |5\rangle = \begin{pmatrix} -1 \\ \frac{41i+9\sqrt{3}-5\sqrt{11}-7i\sqrt{33}}{(\sqrt{3}-i)(\sqrt{33}-7)} \\ \frac{2(-51i-17\sqrt{3}+9\sqrt{11}+9i\sqrt{33})}{(\sqrt{3}-3i)(\sqrt{33}-7)} \\ \frac{17+8i\sqrt{3}-4i\sqrt{11}-3\sqrt{33}}{\sqrt{33}-7} \\ \frac{41i-9\sqrt{3}+5\sqrt{11}-7i\sqrt{33}}{(\sqrt{3}-i)(\sqrt{33}-7)} \\ \frac{36\sqrt{11}-68\sqrt{3}}{(\sqrt{3}-3i)(\sqrt{33}-7)} \\ \frac{-7-25i\sqrt{3}+13i\sqrt{11}+\sqrt{33}}{2(\sqrt{33}-7)} \\ 1 \end{pmatrix} \quad (C.3)
 \end{aligned}$$

$$\begin{aligned}
 |6\rangle &= \begin{pmatrix} 1 \\ -\frac{1}{2}i(\sqrt{3}-i) \\ -\frac{1}{6}i(\sqrt{3}-3i) \\ 1 \\ 0 \\ \frac{1}{6}(3-i\sqrt{3}) \\ 0 \\ 1 \end{pmatrix} & \quad |7\rangle = \begin{pmatrix} 0 \\ \frac{1}{2}(1-i\sqrt{3}) \\ -\frac{2i}{\sqrt{3}} \\ \frac{1}{2}(1+i\sqrt{3}) \\ -\frac{1}{2}i(\sqrt{3}-i) \\ 1 + \frac{i}{\sqrt{3}} \\ 1 \\ 0 \end{pmatrix} \quad (C.4)
 \end{aligned}$$

C.2 Auxiliary Matrices $N = 5$ and Parallel Boundaries

$$m^{(1)} = \begin{pmatrix} 0 & 0 & 0 & 0 & 0 & 0 & 0 & 0. + 0.00534126i & 0. + 0.00732264i \\ 0 & 0 & 0 & 0 & 0 & 0 & 0 & 0. - 0.00732264i & 0. + 0.00534126i \\ 0 & 0 & 0 & 0 & 0 & 0 & 0 & 0. + 0.0567647i & 0. - 0.0558992i \\ 0 & 0 & 0 & 0 & 0 & 0 & 0 & 0. - 0.0558992i & 0. - 0.0567647i \\ 0 & 0 & 0 & 0 & 0 & 0 & 0 & 0. + 0.114749i & 0. - 0.182038i \\ 0 & 0 & 0 & 0 & 0 & 0 & 0 & 0. - 0.182038i & 0. - 0.114749i \\ 0. - 0.00534126i & 0. + 0.00732264i & 0. - 0.0567647i & 0. + 0.0558992i & 0. - 0.114749i & 0. + 0.182038i & 0 & 0 & 0 \\ 0. - 0.00732264i & 0. - 0.00534126i & 0. + 0.0558992i & 0. + 0.0567647i & 0. + 0.182038i & 0. + 0.114749i & 0 & 0 & 0 \end{pmatrix} \quad (C.5)$$

$$m^{(2)} = \begin{pmatrix} 0.0266253 & 0 & -0.000849078 & -0.00571391 & -0.00576078 & -0.0145006 & 0.042664 & 0.0584906 \\ 0 & 0.0266253 & -0.00571391 & 0.000849078 & -0.0145006 & 0.00576078 & -0.0584906 & 0.042664 \\ -0.000849078 & -0.00571391 & 0.100196 & 0 & 0.133516 & -0.0313518 & 0.239916 & -0.236258 \\ -0.00571391 & 0.000849078 & 0 & 0.100196 & 0.0313518 & 0.133516 & -0.236258 & -0.239916 \\ -0.00576078 & -0.0145006 & 0.133516 & 0.0313518 & 0.560679 & 0 & -0.184464 & 0.292635 \\ -0.0145006 & 0.00576078 & -0.0313518 & 0.133516 & 0 & 0.560679 & 0.292635 & 0.184464 \\ 0.042664 & -0.0584906 & 0.239916 & -0.236258 & -0.184464 & 0.292635 & -0.6875 & AM3 \\ 0.0584906 & 0.042664 & -0.236258 & -0.239916 & 0.292635 & 0.184464 & BM3 & -0.6875 \end{pmatrix} \quad (C.6)$$

List of Figures

2.1	Sketch of an open quantum system.	6
2.2	Sketch of the phase diagram of the XXZ chain.	10
2.3	Sketch of a boundary-driven spin chain in XY-plane.	11
2.4	Coordinate system in 3D.	11
2.5	Sketch of a boundary-driven spin chain in Zeno limit.	13
2.6	Sketch of a spin helix state in the XY-plane.	14
2.7	Illustration of spin helix states.	14
3.1	Exemplary spectrum of the Liouvillian.	21
5.1	Density profiles as function of anisotropy of a spin chain $N = 6$, $\theta_L = \theta_R = \frac{\pi}{2}$, $\phi_L = 0$, $\phi_R = \frac{\pi}{3}$ and $\Gamma = 1000$	49
5.2	Entropy and Current as function of the anisotropy for spin chain $N = 6$, $\theta_L = \theta_R = \frac{\pi}{2}$, $\phi_L = 0$, $\phi_R = \frac{\pi}{3}$ and $\Gamma = 1000$	50
5.3	Winding weights as function of the anisotropy for spin chain $N = 6$, $\theta_L = \theta_R = \frac{\pi}{2}$, $\phi_L = 0$, $\phi_R = \frac{\pi}{3}$ and $\Gamma = 1000$	51
5.4	Sketches of the expected steady state and the actual steady state found by numerics of a chain with $N = 6$, $\theta = \frac{\pi}{2}$, $\phi_L = 0$, $\phi_R = \frac{\pi}{3}$ and anisotropy $\Delta = 0.5$	51
5.5	Entropy as function of the incremental turning angle γ for a spin chain of length $N = 6$	52
5.6	Eigenvalues of the density matrix and winding weights as function of polar angle θ for a spin chain $N = 4$, $\gamma = \pi/3$, $\theta = \theta_L = \theta_R$, $\phi_L = 0$, $\phi_R = \pi$	56
5.7	Entropy and winding weights for the breakdown of the pure helix state descrip- tion for a spin chain $N = 4$ with changing boundary gradient Φ	59
5.8	Entropy and winding weights as function of the entropy for a spin chain $N = 6$ with dissipatively oriented ($\Gamma = 1000$) parallel boundary spins.	66

5.9	Comparison of analytics and numerics for the time evolution of diagonal and off-diagonal elements of the density matrix for $N = 4$ spins.	77
5.10	Winding weights and entropy for the time evolution of the density matrix for $N = 4$ spins.	78
5.11	Density profiles for the short time scale of the time evolution for $N = 4$ spins.	79
5.12	Density profiles for the long time scale of the time evolution for $N = 4$ spins.	80
5.13	Comparison of analytic stochastic time evolution of the occupation ρ_{ii} to the numerics for finite dissipation strength Γ for $N = 4$ spins.	81

List of Tables

3.1	Eigensystems of left and rightboundary spin space.	22
3.2	Scaling of matrix size and memory with system size.	26
4.1	Trace orthonormal bases for the left and right boundary spin space.	29
5.1	Summary of ranks for various spin chains $N \leq 9$	53
5.2	Density profile of the non-equilibrium steady state for $N = 5, \gamma = \pi/3, \theta = \theta_L = \theta_R = \pi/2, \phi_L = 0, \phi_R = 4\pi/3$	57
5.3	Exact eigenvalues and eigenvectors of $N = 5, \gamma = \pi/3, \theta = \theta_L = \theta_R = \pi/2, \phi_L = 0, \phi_R = 4\pi/3$	58
5.4	Coefficients for the overlap η for (a) even and (b) odd system size and a boundary gradient $\Phi = \pi$	65
5.5	Rank 2 conditions checked for $N = 13$	73
5.6	Degeneracy of dissipation-projected Hamiltonian for γ being a reducible fraction in system $N \leq 13$	73

Acknowledgements

I want to thank Prof. Dr. Corinna Kollath, for having me in her group, for our open discussions, sending me to conferences and summer schools and to open my mind for the interesting physics when I was lost in technical details. In particular, I want to thank Dr. Vladislav Popkov for being incredibly patient, excusing many silly mistakes and constantly transmitting his fascination of solving and understanding problems.

Thanks to Johannes, Karla, Catalin and Stefan, my office colleagues, who received me with open arms and supported me finishing my thesis. Many thanks to the whole group for many entertaining lunches in the Mensa.

I want to thank many physicists, who accompanied me during the studies and motivated me in many occasions. Special thanks go to my colleagues from the Bachelor's: Kathinka, Fabian, Klaus, Johannes and Christian!

I want to thank my family: Thanks to my parents, Elke and Stefan, for always being there for me and having great advice in any situation. Thanks to my brother, who always understands my struggles and who helped me in everything ranging from personal life questions to difficulties in the studies.

Finally, I want to thank Maria, who endured all my mood swings and crazy physics talks, for supporting me fantastically and even reading the thesis.